

**Evaluation of Metal Flow In Precision Forging of  
Axisymmetric Parts**

**M.Sc. Thesis**

**in**

**Mechanical Engineering  
University of Gaziantep**

**Supervisor**

**Prof. Dr. Ömer EYERCİOĞLU**

**By**

**Tunç UĞUR**

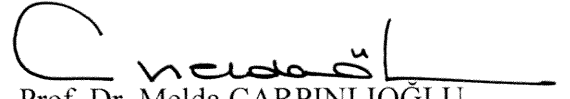
**September 2005**

Approval of the Graduate School Natural and Applied Sciences

Prof. Dr. Sadettin ÖZYAZICI

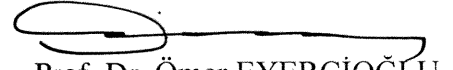
**Director**

I certify that this thesis satisfies all the requirements as a thesis for the degree of Master of Sciences.

  
Prof. Dr. Melda ÇARPINLIOĞLU

**Chairman of the Department**

I certify that I read this thesis and that in my opinion it is fully adequate, in scope and quality, as a thesis for the degree of Master of Sciences.

  
Prof. Dr. Ömer EYERCİOĞLU

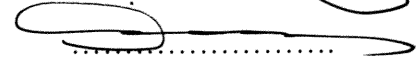
**Supervisor**

**Examining Committee in Charge**

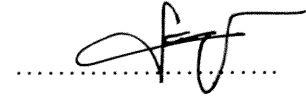
Prof. Dr. I. Hüseyin FİLİZ



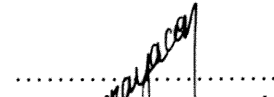
Prof. Dr. Ömer EYERCİOĞLU



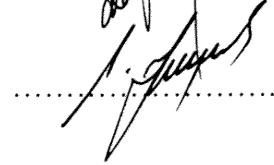
Assoc. Prof. Dr. Cengiz DOĞAN



Assist. Prof. Dr. M. Cengiz KAYACAN



Assist. Prof. Dr. N. Fazıl YILMAZ



## ABSTRACT

### EVALUATION OF METAL FLOW IN PRECISION FORGING OF AXISYMMETRIC PARTS

UĞUR, Tunç

M. Sc. In Mechanical Engineering

Supervisor: Prof. Dr. Ömer EYERCİOĞLU

September 2005, 148 Pages

The purpose of the study is to obtain the optimum pre-form geometry by investigating the metal flow of axisymmetric parts in net-shape forging process. For this reason metal-shaping process, which is required for the U-shapes, T-shapes and H-shapes, the shapes accepted as axisymmetric parts, metal flow direction and forging load are determined. To obtain the product net-geometry is proposed by decreasing the forging load and energy with the help of theoretical and experimental study.

The experiments are carried-out by using different aluminum and lead performs for optimising the net-shape forging process of the main shapes (U, T and H-Shapes) and simulating the hot and cold forging processes. In addition, metal flow is investigated by using finite-element method in computer. Moreover, the effects of vibrated die and re-lubrication in stepwise processes are investigated.

Optimum perform geometry is obtained with low forging load and energy. The experiments, carried out with different performs, and simulations show that the required forging load and energy are different although, the product is same. In addition, vibrating of die and re-lubricating in steps decreases the forging load and energy required for net-shape forging.

**Key Words:** Axisymmetric Forging, Metal Flow, Precision Forging

## ÖZET

### EKSENELSİMETRİK PARÇALARIN NET-ŞEKİL DÖVMECİLİĞİNDE METAL AKIŞININ DEĞERLENDİRİLMESİ

UĞUR, Tunç

Yüksek Lisans Tezi, Makina Mühendisliği Bölümü

Tez Yöneticisi : Prof. Dr. Ömer EYERCİOĞLU

Eylül 2005, 148 Sayfa

Bu çalışmanın amacı aksel simetrik parçaların net şekil dövme işleminde metal akışını inceleyerek en iyi numune geometrisini elde etmektir. Bu amaçla temel aksel simetrik geometri olarak kabul edilen U-şekli, H-şekli ve T-şekli için gerekli olan metal şekillendirme işlemini, metal akış yönü ve dövme yükü belirlenmeye çalışılmıştır. Yapılan teorik ve deneysel çalışmalarla dövme yükünün ve enerjisinin düşürülerek, son ürünün boyutlarının hassas (net) olarak elde edilmesi amaçlanmıştır.

Temel geometrilerin (U, H ve T-Şekiller) net-şekil dövme işlemini en iyilemek için soğuk ve sıcak şekil dövmeciliğini bilgisayar ortamında yapan bir program kullanılarak alüminyum ve kurşun malzemelerden yapılmış değişik numuneler ile deneyler yapılmıştır. Buna ek olarak metal akışı sonlu eleman yöntemi ile de bilgisayar ortamında gözlemlenmiştir. Ayrıca, titreşimli kalıbın ve ara basamaklarla yeniden yağlamanın dövme yükü üzerindeki etkileri incelenmiştir.

Düşük dövme yükü ve enerjisi ile en iyi numune geometrisi elde edilmiştir. Farklı numunelerle yapılan deneyler ve bilgisayar ortamında yapılan gösterimler son şekil aynı olsa bile gerekli olan dövme yükü ve enerjisinin değiştiğini göstermiştir. Buna ek olarak, kalıp titreşimi ve ara basmakta yağlama yapılması hassas(net)-şekil dövme için gerekli olan enerjiyi ve yükü düşürmüştür.

**Anahtar Kelimeler:** Eksenel-Simetrik Dövmecilik, Malzeme Akışı, Hassas Dövmecilik

## ACKNOWLEDGEMENT

I would like to express my sincere gratitude to my supervisor, Prof. Dr. Ömer EYERCİOĞLU for the encouragement, guidance, suggestions and help in making this thesis understandable.

I also wish many thanks to Research Assist. Kürşad GÖV for his valuable criticism, suggestions and helps throughout the experiments.

I am very thankful to my valuable parents for their supports and motivation in this study. I am also very thankful to my cousins Kaan ÜNAL and Kadir ÜNAL for their supports in writing this manuscript.

Particular thanks are due to personnel of the ÇİLTUĞ Heavy Machinery and Heat Industry and ŞİRİNPUL Ltd. for their guidance and helps in preparing the work-pieces.

I am also very grateful to workshop personnel of Mechanical Engineering Department of Gaziantep University for their valuable guidance, criticisms, suggestions and help throughout this study.

# TABLE OF CONTENTS

	<u>PAGE</u>
<b>ABSTRACT</b>	iii
<b>ÖZET</b>	iv
<b>ACKNOWLEDGMENT</b>	vi
<b>TABLE OF CONTENTS</b>	vii
<b>LIST OF TABLES</b>	xi
<b>LIST OF FIGURES</b>	xii
<b>LIST OF SYMBOLS</b>	xvii
<b>1. INTRODUCTION</b>	1
<b>1.1. Introduction</b>	1
<b>2. LITERATURE SURVEY</b>	4
<b>2.1. Introduction</b>	4
<b>2.2. Literature Survey</b>	4
<b>3. METAL FORMING, FLOW RULE AND FORGING</b>	9
<b>3.1. Metal Forming</b>	9
<b>3.2. Flow Stress in Tension</b>	10
<b>3.3. Flow Stress in Compression</b>	15
<b>3.4. Discontinous Yielding</b>	16
<b>3.4.1. Yield Point Elongation</b>	16
<b>3.4.2. Serrated Yielding</b>	17
<b>3.5. Effects of Cold Working</b>	17

<b>3.6. Recrystallization</b>	19
<b>3.7. Hot Working</b>	21
3.7.1. Mechanisms of Hot Working	21
3.7.2. Flow Stress in Hot Working	22
<b>3.8. Warm Working</b>	24
3.8.1. Superplasticity	25
<b>3.9. Mechanics of Deformation Processing</b>	25
3.9.1. Yield Criteria	26
3.9.2. The Relevant Flow Stress	30
3.9.3. Effects of Friction	31
<b>3.10. Measurement of Friction</b>	32
3.10.1. Purposes of Friction Measurement	32
3.10.2. Upsetting of Cylinders	33
3.10.3. Upsetting of Slabs	36
3.10.4. Ring Upsetting	37
3.10.5. Plane-Strain Compression	38
<b>3.11. Lubrication</b>	39
<b>3.12. Inhomogenous Deformation</b>	40
<b>3.13. Bulk Workability</b>	42
<b>3.14. Temperature of Deformation</b>	43
3.14.1. Hotworking	44
3.14.2. Cold Working	45
3.14.3. Warm Working	45
<b>3.15. Steady State Processes</b>	46
<b>3.16. Non-Steady State Processes</b>	47
<b>3.17. Forging</b>	48
<b>3.18. Forging Equipments</b>	
3.18.1. Hammers and Presses for Forging	51
3.18.2. Closed Die Forging Hammers	
3.18.2.1. Board Drop Hammers	51
3.18.2.2. Air-Lift Gravity Drop Hammers	51
3.18.2.3. Power Drop Hammers (Steam Hammers)	51
3.18.2.4. Counterblow Hammers	51



3.18.3.	Open Die Forging Hammers	52
3.18.4.	Closed Die Forging Presses	53
3.18.4.1.	Mechanical Presses	54
3.18.4.2.	Hydraulic Presses	56
3.18.5.	Open Die Forging Presses	56
3.19.	General Criteria for Forging Die Design	58
3.19.1.	Strength	60
3.19.2.	Wear resistance	61
3.19.3.	Kinematics	61
3.19.4.	Accuracy	61
3.19.5.	Performance	62
3.19.6.	Shrink Rings	62
3.20.	Factors in the Selection of Die Material	62
		62
4.	EXPERIMENTAL SET UP AND DIE DESIGN	63
4.1.	Introduction	65
4.2.	Press Used For Experiments	65
4.3.	Product and Preform Geometry	65
4.4.	Die Design	67
4.5.	Die Geometry	76
		79
5.	EXPERIMENTAL STUDY	
		81
5.1.	Introduction	
5.2.	Preparation of Dies	81
5.3.	Preparation of Billets	80
5.4.	Lubrication	80
5.5.	Experimental Procedure	81
		83
6.	RESULTS AND DISCUSSION	
6.1.	Introduction	83
6.2.	Results and Discussion	83

6.2.1.	U-Shape Aluminum Forgings	83
6.2.2.	T- Shape Aluminum Forgings	91
6.2.3.	H- Shape Aluminum Forgings	98
6.2.4.	U- Shape Lead Forgings	106
6.2.5.	T- Shape Lead Forgings	114
6.2.6.	H-Shape Lead Forgings	123
6.2.7.	Reducing Load and Energy	130
<b>7.</b>	<b>CONCLUSION AND RECOMMENDATIONS FOR FUTURE STUDIES</b>	<b>133</b>
7.1.	Introduction	133
7.2.	Conclusion	133
7.2.1.	U- Shape Forgings	133
7.2.2.	T- Shape Forgings	134
7.2.3.	H- Shape Forgings	134
7.2.4.	Vibrating Tool	134
7.2.5.	Two-Step Forging	135
7.3.	Recommendations for Future Studies	135
	<b>LIST OF REFERENCES</b>	<b>136</b>
	<b>APPENDICES</b>	<b>140</b>

## LIST OF TABLES

	<b><u>PAGE</u></b>
Table 4.1. Dimensions of Preform for U, T and H-Shapes	71
Table 4.2. Calculated Values of Strain, Flow Stress and Load	71
Table 4.3. Specifications Of The Die Material	76
Table 5.1. Deformation Modes of the Forging Processes	81
Table D.1. Mechanical Properties of Al 1050	145
Table D.2. Mechanical properties of pure lead	145
Table E.1. Manufacturing Properties of Steels	146
Table E.2. Manufacturing Properties Various Non-Ferrous Alloys	147
Table F.1. Typical Lubricants and Friction In Plastic Deformation	148
Table G.1. Multiplying Forces For Estimating Forces $Q_c$ and $Q_{fe}$ In Impression Die Forging	149

## LIST OF FIGURES

		<u>PAGE</u>
Fig.3.1	Engineering Stress-Strain Curve	11
Fig.3.2.	Tensile Stress-Displacement Curve	12
Fig.3.3.	Logarithmic Plot of Flow Stress-True Strain	13
Fig.3.4a.	Material with High Strain Hardening Rate	14
Fig.3.4b.	Material with Low Strain Hardening Rate	14
Fig.3.5.	Dimensional Changes in Upsetting of a Cube	15
Fig.3.6a.	Yield Point Elongation of a Mild-Steel	17
Fig.3.6b.	Serrated Yielding of Solid-Solution Alloys	17
Fig.3.7.	Tension Tests Conducted on Previously Worked Material	18
Fig.3.8.	The Effects of Prior Cold Work	19
Fig.3.9.	Prior Cold Work-Grain Size-Annealing Temperature Curve	20
Fig.3.10.	Flow Stress-Strain Rate	23
Fig.3.11.	Flow Stress-Strain Rate in Logarithmic Scale	23
Fig.3.12.	Flow Stress-Strain Rate	25
Fig.3.13.	Pure Tension Specimen	26
Fig.3.14a.	Pure Bending Specimen	27
Fig.3.14b.	Pure Bending Specimen	27
Fig.3.15.	Maximum Distortion Energy-Maximum Shear Stress Theorem	29
Fig.3.16.	Methods of Measuring Friction Effects in Upsetting and Indenting	32
Fig.3.17.	Calibration Curves for Decrease in Internal Diameter of Standard Rings	37
Fig.3.18.	Inhomogenous Deformation	40
Fig.3.19.	Workability of Materials	43

Fig.3.20a.	Steady State Cold Working, Material Subjected to Strain Hardening During Passaging Through Die	46
Fig.3.20b.	The Mean Flow Stres from the True Stres-True Strain Curve	47
Fig.3.21.	Non-Steady State Processes	47
Fig.3.22.	Impression Die Forging	48
Fig.3.23.	Principal Components of a Board Drop Hammer	51
Fig.3.24.	Principal Components of a Power Drop Hammer	53
Fig.3.25.	Components of a Vertical Counter Blow Hammer with a Steam Hydraulic Actuating System	54
Fig.3.26.	Single Frame Power Hammer used For Open-Die Forging	55
Fig.3.27.	Double Frame Power Hammer Used for Open-Die Forging	56
Fig.3.28.	Components of Mechanical Forging Press	57
Fig.3.29.	Components of a Four Post Hydraulic Pres for Closed-Die Forging	59
Fig.3.30.	Shrink Rings of Dies	62
Fig.3.31.	Theoretical Stres Distribution in a Thick-Walled Cylinder	63
Fig.4.1.	Press used for Experimental Studies	66
Fig.4.2.	Graphic Drawing Unit of the Pres	66
Fig.4.3.	Schematical Graphic Drawing Unit	67
Fig.4.4.	Forging Products	68
Fig.4.5.	Dimensions of Forging Products	71
Fig.4.6.	Preforms for U-Shaped Forging Products	73
Fig.4.7.	Preforms for T-Shaped Product	74
Fig.4.8.	Preforms for H-Shaped Product	74
Fig.4.9.	Used Dies in Experiments	75
Fig.4.10.	Presure Distribution in Dies	75
Fig.4.11.	Dimensions of the Forging Dies and Punches	78
Fig.4.12.	Photo of the lower dies and Punches	78
Fig.4.13.	Photo of the Cover Die	78
Fig.6.1.	Flow Simulation of U1-Al Forging	84
Fig.6.2.	Experimental Load-Stroke characteristics of U1-Al forging	85
Fig.6.3.	Photo of U1-Al Forging	85
Fig.6.4.	Flow Simulation of U2-Al Forging	86

Fig.6.5.	Experimental Load-Stroke characteristics of U2-Al Forging	86
Fig.6.6.	Photo of U2-Al Forging	87
Fig.6.7.	Flow Simulation of U3-Al Forging	88
Fig.6.8.	Experimental Load-Stroke characteristics of U3-Al Forging	88
Fig.6.9.	Photo of U3-Al Forging	88
Fig.6.10.	Flow Simulation of U4-Al Forging	89
Fig.6.11.	Experimental Load-Stroke characteristics of U4-Al Forging	90
Fig.6.12.	Photo of U4-Al Forging	90
Fig.6.13.	Experimental Load-Stroke Curve of U-Shape Aliminum	91
Fig.6.14.	Flow Simulation of T1-Al Forging	92
Fig.6.15.	Experimental Load-Stroke characteristics of T1-Al Forging	92
Fig.6.16.	Photo of T1-Al Forging	93
Fig.6.17.	Flow Simulation of T2-Al Forging	94
Fig.6.18.	Exprimental Load-Stroke characteristics of T2-Al Forging Flow	94
Fig.6.19.	Simulation of T3-Al Forging	97
Fig.6.20.	Experimental Load-Stroke characteristics of T3-Al Forging	95
Fig.6.21.	Flow Simulation of T4-Al Forging	97
Fig.6.22.	Experimental Load-Stroke characteristics of T4-Al Forging	97
Fig.6.23.	Experimental Load Stoke Curve of T-Shape Aliminum	98
Fig.6.24.	Flow Simulation of H1-Al Forging	99
Fig.6.25.	Experimental Load-Stroke characteristics of H1-Al Forging	99
Fig.6.26.	Photo of H1-Al Forging	100
Fig.6.27.	Flow Simulation of H2-Al Forging	101
Fig.6.28.	Experimental Load-Stroke characteristics of H2-Al Forging	101
Fig.6.29.	Photo of H2-Al Forging	102
Fig.6.30.	Flow Simulation of H3-Al Forging	102
Fig.6.31.	Experimental Load-Stroke characteristics of H3-Al Forging	103
Fig.6.32.	Photo of H3-Al Forging	103
Fig.6.33.	Experimental Load-Stroke characteristics of H4-Al Forging	104
Fig.6.34.	Photo of H4-Al Forging (Failed Specimen)	104
Fig.6.35.	Photo of H4-Al Forging	104
Fig.6.36.	Figure 6.36. Flow Simulation of H4-Al Forging, if the specmen would be fit to the die guide diameter	105

Fig.6.37.	Experimental Load Stoke Curve of H-Shape Aliminum	106
Fig.6.38.	Flow Simulation of U1-Pb Forging	107
Fig.6.39.	Experimental Load-Stroke characteristics of U1-Pb Forging	108
Fig.6.40.	Photo of U1-Pb Forging	108
Fig.6.41.	Flow Simulation of U2-Pb Forging	109
Fig.6.42.	Expermental Load-Stroke characteristics of U2-Pb Forging	110
Fig.6.43.	Photo of U2-Pb Forging	110
Fig.6.44.	Flow Simulation of U3-Pb Forging	111
Fig.6.45.	Experimental Load-Stroke Characteristics of U3-Pb Forging	111
Fig.6.46.	Photo of U3-Pb Forging	112
Fig.6.47.	Flow Simlation of U4-Pb Forging Specimen	113
Fig.6.48.	Experimental Load-Stroke characteristics of U4-Pb Forging	113
Fig.6.49.	Photo of U4-Pb Forging	113
Fig.6.50.	Experimental Load Stoke Curve of U-Shape Lead	114
Fig.6.51.	Flow Simulation of T1-Pb Forging	115
Fig.6.52.	Experimental Load-Stroke characteristics of T1-Pb Forging	115
Fig.6.53.	Photo of T1-Pb Forging	116
Fig.6.54.	Flow Simulation of T2-Pb Forging	117
Fig.6.55.	Experimental Load-Stroke characteristics of T2-Pb Forging	118
Fig.6.56.	Photo of T2-Pb Forging	118
Fig.6.57.	Flow Simulation of T3-Pb Forging Specimen	119
Fig.6.58.	Experimental Load-Stroke characteristics of T3-Pb Forging	119
Fig.6.59.	Photo of T3-Pb Forging	120
Fig.6.60.	Flow Simulation of T4-Pb Forging	121
Fig.6.61.	Experimental Load-Stroke characteristics of T4-Pb Forging	121
Fig.6.62.	Photo of T4-Pb Forging	122
Fig.6.63.	Experimental Load Stoke Curve of T-Shape Lead	122
Fig.6.64.	Flow Simulation of H1-Pb Forging	124
Fig.6.65.	Experimental Load-Stroke characteristics of H1-Pb Forging	124
Fig.6.66.	Photo of H1-Pb Forging	124
Fig.6.67.	Flow Simulation of H2-Pb Forging	125
Fig.6.68.	Experimental Load-Stroke characteristics of H2-Pb Forging	126
Fig.6.69.	Photo of H2-Pb Forging	126

Fig.6.70.	Flow Simulation of H3-Pb Forging	127
Fig.6.71.	Experimental Load-Stroke characteristics of H3-Pb Forging	128
Fig.6.72.	Photo of H3-Pb Forging	128
Fig.6.73.	Experimental Load-Stroke characteristics of H4-Pb Forging	129
Fig.6.74.	Photo of H4-Pb Forging	129
Fig.6.75.	Experimental Load Stoke Curve of H-Shape Lead	130
Fig.6.76.	Experimental Load-Stroke characteristics of Single Step Ring Upsetting	131
Fig.6.77.	Experimental Load-Stroke characteristics of Double Step Ring Upsetting	132
Fig.6.78.	Experimental Load-Stroke characteristics of Ring Upsetting in Vibrated Die	132



## LIST OF SYMBOLS

$\sigma_f$	Flow Stress
$\sigma$	Stress
$\sigma_{fm}$	Mean Flow Stress
$\sigma_{eng}$	Engineering Stress
$V$	Final Volume
$V_0$	Initial Volume
$v$	Velocity
$\varepsilon_t$	Engineering Strain
$\varepsilon$	Logarithmic Strain
$\dot{\varepsilon}$	Strain Rate
$\mu$	Coefficient of Friction
$\tau_i$	Interface Shear Stress
$\tau_f$	Shear Flow Stress
$P$	Interface Pressure
$p$	Pressure Acting on Unit Area
$F_n$	Normal Force
$\sigma_{max}$	Maximum Stress
$\sigma_{min}$	Minimum Stress
$A$	Deformed Crosssectional Area
$A_0$	Initial Crosssectional Area
$l$	Final Length
$l_0$	Initial Length
$K$	Strength Coefficient
$n$	Strain-Hardening Exponent
$h$	Final Height
$h_0$	Initial Height

$v$	Velocity
$C$	Strength Coefficient in Hot-Working
$F$	Force
$P$	Force Required for filling of Die
$m^*$	Frictional Shear Factor
$r_c$	Radius of Edge of Sticking Zone
$\sigma_v$	Internal Pressure
$\sigma_r$	Radial Stress
$\sigma_t$	Tangential Stress
$Q_c$	Multiplying Factor for Forging
$P_i$	Internal Pressure
$A_t$	Crosssectional Area
$\epsilon_{ave}$	Average Strain
$h_{ave}$	Average Height
$d_0$	Initial Diameter

# CHAPTER 1

## 1.1. INTRODUCTION

The development in metal forming area brings new technologies together and forces the existing methods to become more efficient. In this manner forging, although the oldest metal forming process, has become one of the competitive technologies in the manufacturing field. Material costs of forging and any reduction in material waste during operation has a direct effect on the price of the finished product. In order to improve the productivity of forging at low production cost, an integrated system approach is necessary in handling the material preparation and the optimum process design considering the forming machines, tooling and operation. [1-2]

The forging process is fundamentally the deformation of metal under pressure or impact to produce a desired shape. This controlled deformation assures the elimination of internal gas pockets or voids and results in greater metallurgical behaviours and improvement of mechanical properties[3].

Forging is better suited for many applications than cast materials, due to change in state or volume as are casting during solidification. Forged components are more reliable than parts machined from bar stock or plate; because properly developed grain flow in forging closely the outline of components[4].

Today's trend toward higher speeds and greater loads in many types of mechanical equipment is leading to the recognition by designers and mechanical engineers of the increasing importance to impact and fatigue, as a portion of total component reliability. Forged products meet those requirements and they are specified where the strength, reliability, economy and resistance to shock and fatigue are vital

considerations. The optimisation criteria may vary depending on the product requirements, but establishing an appropriate criterion requires true understanding of manufacturing process. In metal forming technology, proper design and control requires the determination deformation mechanics involved in the processes.

Precision forging does not specify a distinct forging process but rather describes a philosophical approach to forging. The goal of this approach is to produce a near net shape in the as-forged condition [5, 6].

In the precision forging, a given material of a simple geometry is transformed under controlled application of energy into useful component. The precision forged components may only need little or no finishing, thus reducing the manufacturing cost.

Forging operation comprises all the process input variables such as billet material, dies, the conditions at the die-work interface, the mechanics of shape change in the workzone, and the characteristics of the equipment.

The design, control and optimization of forging processes require knowledge regarding metal flow, stresses and heat transfer, as well as technological information related to lubrication, heating and cooling techniques, material handling, die design and manufacturing and forging equipment.

Complete filling of die with relatively low forging load and energy, i.e. lower die stresses, can be obtained by proper design of preforms[7]. To design a preform, material flow during forging should be known in advance. In precision forging operation, if other factors such as forging temperature, interface friction and billet volume remain unchanged, for a given load the extent of the filling is determined by the pattern of material flow. There has been many studies on the subject of metal flow and preform design for specific parts, however, there is a lack of knowledge generalized for axisymmetric parts[8-17].

The purpose of this study is to evaluate metal flow in precision forging of axisymmetric parts. To evaluate metal flow, a series experiments were carried out. Aluminum billets were used for cold forging and lead for hot forging. Forging dies for T-shape, U-shape and H-shape geometries were designed and manufactured. The evaluation process may lead to optimum design of preform geometry. So that, precision forging of axisymmetric parts with higher accuracy and lower load, energy and stresses could be achieved.

## **CHAPTER 2**

### **LITERATURE SURVEY**

#### **2.1. INTRODUCTION**

There has been some studies about preform design but the optimum preform is studied by benefitting FEM solution. Although there have been enormous amount of studies, there is no generated rules. The summaries of the very related studies carried on are as follows:

#### **2.2. STUDIES IN THIS SCOPE**

Parikh H. and Bhavin M. [18] developed optimizing the forging process and reduce the required force to forge the final product. A complex 3- dimensional part has been studied. Simulation results predicted that the complex 3D part could be forged in one step, using at least a 900 ton capacity press or higher. Solid Edge was used to model the dies while MSC Super Forge was used to simulate the forging process. Several different preforms were designed and analyzed to obtain the final product in two stages with a maximum load of less than 750 tons.

Badrinarayanan S., Constantinescu A., and Zabarar N. [19] studied preform and of the process parameters (e.g. the die shape) that lead to a final product with desired geometry and material properties. The solutions to inverse problems were usually obtained by trial and error methods using the results of direct analysis or each set of

preforms and process parameters. Sensitivity analysis facilitated a rigorous mathematical formulation and solution of preform and process design problems. In an earlier work, a sensitivity analysis were presented for determining an optimal shape of extrusion dies that leads to a desired material state in the final product. In the work, it was concentrated on the formulation and the finite element solution of preform design problems. The objective was to design the initial shape of the workpiece that when it deforms under the action of a given die, results in a final product with a desired material state and geometry. Shape sensitivities was defined in a rigorous sense and the entire analysis was performed in a fully infinite dimensional setting. An example problem was solved in axisymmetric disk forging where the preform was designed such that, after forging with a flat die, a product with a minimum barreling effect was achieved.

Qingbin L., Shichun W. And Sheng S. [20] presented a preform design method which combines the FEM-based forward simulation and the UBET-based reverse simulation techniques. The billet designed using the new technique was achieved a final forging with minimum flash. A gear blank forging was used as an example to demonstrate the preform design.

Yilmaz, N. F. [21] studied the application of rule base expert system to the near net shape axisymmetric forging die design, and development of a knowledge base for it. The developed system is aimed to cover the design of forging dies for axisymmetric parts and meet them with the power of expert system. The drawing file of a final product, taken from AutoCAD, was converted into a format and it was integrated with the system by means of feature recognition module. After the recognition of input geometry of the product, checking that whether it was forgeable in closed die or not forms the second step. The required forging load was calculated so as to fill the die cavity completely. The power and energy requirements for making the finished forging were also determined. Die stress calculation and die shape determination were also investigated. The main contribution of study was the realisation of forging die design for not only specific industrial parts but also all axisymmetric components. For this purpose, an expert system application was developed for product geometry, forging load and the die dimensions.

Almohaileb M., Gunasekera J. S. [22] developed mathematical models based on modified UBET for forging processes as well as forging preform design of axisymmetric parts. The velocity fields was derived based on volume mapping approach and evaluated by minimizing the total energy rate of UBET. The model was developed for forging processes based on MUBET (modified UBET) using forward simulations. FEM (finite element method) simulations was conducted in order to validate the developed models. The significance of various process parameters such as the intermediate/preform geometry, the optimum aspect ratio of billet, and forming load was determined.

Srikanth A., Zabaras N. [8] developed for the computation of the shape sensitivity of finite hyperelastic-viscoplastic deformations involving contact with friction using a direct differentiation method. Weak shape sensitivity equations was developed that were consistent with the kinematic analysis, constitutive sub-problem as well as the analysis of the contact/friction sub-problem was used in the solution of the direct deformation problem. The shape sensitivities were defined in a rigorous sense and a linear sensitivity analysis was performed in an infinite-dimensional continuum framework. The direct deformation and the sensitivity deformation problems was implemented using the finite element method. The shape sensitivity analysis was validated by a comparison of the results with those obtained from solution of the perturbed direct deformation problem (i.e. using finite differences). Finite-dimensional gradients of objective functions were computed using results of the shape sensitivity analysis for the purpose of preform design and shape optimization in metal forming.

Li Q. and Hu Z. [23] studied a number of recent advances towards the development of a robust computational design Lagrangian FEM simulator for multi-stage metal forming processes. A continuum parameter and shape sensitivity analysis were developed for metal forming processes using an updated Lagrangian framework suitable for very large deformations when remeshing operations were performed during the analysis. In addition to exploring the issue of transfer of variables between meshes for finite deformation analysis, the complex problem of transfer of design sensitivities between meshes for large deformation inelastic analyses would be



discussed. A method was proposed to give accurate estimates of design sensitivities when remeshing operations were performed during analysis. In particular, the performance of quadrilateral elements for the sensitivity analysis of large deformations was studied. The results of the continuum sensitivity analysis were validated by a comparison with obtained by finite difference approximations (i.e. using the solution of a perturbed deformation problem).

Balendra R. and Qin Y. [24] were studied the development of high-precision material-conversion processes: the focus was on development of experimental and numerical simulation techniques, new forming-configurations and the development of industrial applications. The study was concentrated on conventional forging, injection forging, precision-blanking, vibration-assisted forging and micro-forming.

Rasgado M. T. A. and Davey K. [25] concerned with an investigation into the feasibility of applying die vibration to commercial dies and processes. Boundary element models was utilised to simulate the complex vibrational behaviour of arbitrary shaped dies. Numerical simulations was used to establish the conditions that prevail at the die surface by varying the position and the number of sources of vibration, that conditions required for polishing were approached.

Huang Z., Lucas M. and Adams M. J. [26] described a finite element study of the effect of wall boundary conditions on the upsetting of plasticine as a model for hot metal. The wall boundary and intrinsic flow characteristics for the model material were used to investigate the effects of introducing a vibration assisted tooling method. The aim was to modify the wall boundary conditions in a way that reduced the forming force.

Hung J. C. and Hung C. [27] established an ultrasonic-vibration hot upsetting system. A cooling mechanism was used to solve the problem of high temperature. The effects of temperature and strain rate during ultrasonic-vibration on the upsetting of aluminum alloy were explored. Hung J. C. and Hung C. indicated that ultrasonic-vibration could considerably reduce the compressive forces during hot upsetting. The study indicated that reducing effect on compressive forces decreased

while increasing temperature and the strain rate did not significantly effect the reducing effect on compressive forces.

## CHAPTER 3

### METAL FORMING, FLOW RULE AND FORGING

#### 3.1. METAL FORMING

Metallic materials may be shaped by applying external forces to them without reducing their structural cohesion. This property is known as the formability of metal. Deformation or flow occurs when the rows of atoms within the individual crystalline grains are able, when stressed beyond a certain limit, to slide against one another and cohesion between the rows of atoms takes place at the following atomic lattice. This sliding occurs along planes and directions determined by the crystalline structure and is only made possible by, for example, dislocations (faults in the arrangement of the atomic lattice). Other flow mechanisms such as twin crystal formation, in which a permanent deformation is caused by a rotation of the lattice from one position to another, play only a minor role in metal forming technology. Flow commences at the moment when the principle stress difference ( $\sigma_{\max}-\sigma_{\min}$ ) reaches the value of the flow stress  $\sigma_f$ , or when the shear strain caused by a purely shearing stress is equal to half the flow stress, given by:

$$\sigma_f = \sigma_{\max} - \sigma_{\min} \quad (3-1)$$

The value of the flow stress depends on the material, the temperature, the deformation or strain,  $\epsilon$ , and the speed at which deformation or strain rate is carried out,  $\dot{\epsilon}$ . Below the recrystallisation temperature, the flow stress generally rises with increasing deformation, while the temperature and deformation rate exert only a

minimal influence. Exceptions to this rule are forming techniques such as rolling and forging, in which extremely high deformation rates are used. Above the recrystallisation temperature, the flow stress is generally subject to the temperature and deformation rate, while a previous deformation history has only minimal influence. The flow stress generally drops with increasing temperature and decreasing deformation rate .

The process is carried out without heating named as cold forming and after the application of heat named as hot forming. These terms simply specify whether heating devices are necessary. Unlike their former meaning, these terms are not physically related to the material concerned. The flow stress of the individual materials is determined by experiments in function of deformation (or strain) and deformation rate (or strain rate) at the various temperature ranges, and described in flow curves. One of the uses of flow curves is to aid the calculation of possible deformation, force, energy and performance.[28]

For metalworking calculations, yield strength and tensile strength-the properties of primary interest for the design of products- are of secondary importance. First concern is the stress required to deform the workpiece material.

### **3.2. FLOW STRESS IN TENSION**

The engineering stress conventionally calculated from the tension test is of little value for computations, although it is widely used in communication. By definition, stress is force acting on unit area (Eq. 3-2). We need a true stress which, by definition, is force  $P$  divided by instantaneous area  $A$  (Eq. 3-3). We could measure the instantaneous cross-sectional area, but most of time we compute it using the principle of constancy of volume (Eq 3-4). As long as elongation is uniform over the gage length (Fig. 3-1),

$$\sigma_{eng} = \frac{P}{A_0} \quad (3-2)$$

$$\sigma = \frac{P}{A} \quad (3-3)$$

$$\begin{aligned} V_0 = V &\Rightarrow A_0 \cdot l_0 = A \cdot l \\ \Rightarrow A &= A_0 \frac{l_0}{l} = \frac{V}{l} \end{aligned} \quad (3-4)$$

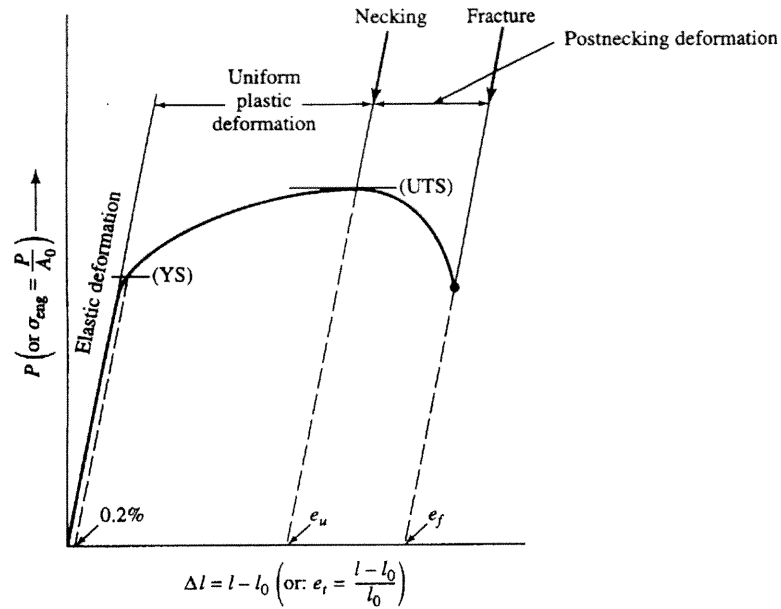


Fig. 3-1 Engineering Stress Strain Curve

Since our interest is in permanent deformation which begins at the point of yielding, the true stress is usually calculated from initial yielding to necking. Each calculated point defines the stress that must be applied to keep the material deforming, flowing; hence, we call it the flow stress,  $\sigma_f$  (Eq.3-5).

$$\sigma_f = \frac{P}{A} \quad (3-5)$$

where  $P$  is the instantaneous force, Flow stress is plotted as a function of engineering tensile strain  $\epsilon_t$  (Eq. 3-6), but for computational purposes the true strain  $\epsilon$  (also called

natural or logarithmic strain) is needed. By definition, it is obtained as the natural logarithm of the ratio of instantaneous length,  $l$ , to original length,  $l_0$  (Eq. 3-7).

$$\varepsilon_t = \frac{l - l_0}{l_0} \quad (3-6)$$

$$\varepsilon = \ln \frac{l}{l_0} \quad (3-7)$$

The data derived from the tensile stress-strain curve may now be plotted to define the true stress-true strain curve (Fig. 3-2). For comparison, the engineering stress-true strain curve is also shown in Fig. 3-2 in broken lines. There is one point that can be calculated beyond necking: The fracture force  $P_f$  is available, and the corresponding minimum cross-sectional area  $A_f$  (area measured after fracturing) can be measured on the broken specimen. As a result, the true stress calculated is somewhat high.

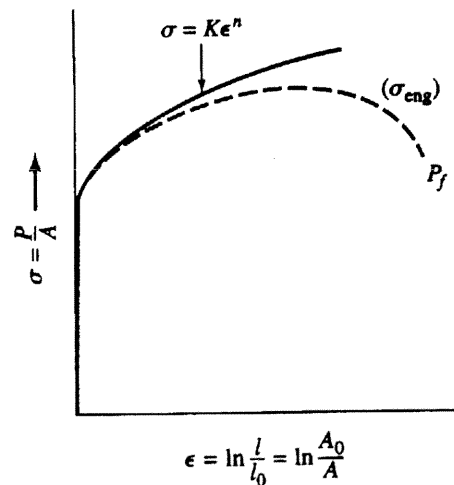


Fig. 3-2 Tensile Stress-Strain Curve

Flow stress curves of many materials have been determined, and an atlas of such curves has been built up. However, a more condensed and more convenient record can be kept. When  $\sigma_f$  is replotted against  $\epsilon$  on logarithmic paper, a straight line frequently results, indicating that  $\sigma_f$  is a power function of  $\epsilon$  (Fig. 3-3). So we can formulate the flow stress as a powerful function of true strain (Eq. 3-8).

$$\sigma_f = K \cdot \epsilon^n \quad (3-8)$$

K is the strength coefficient and n is the strain-hardening exponent. From the log-log plot, K is the stress at a strain of unity, and n is the slope of the line, measured on a linear scale.

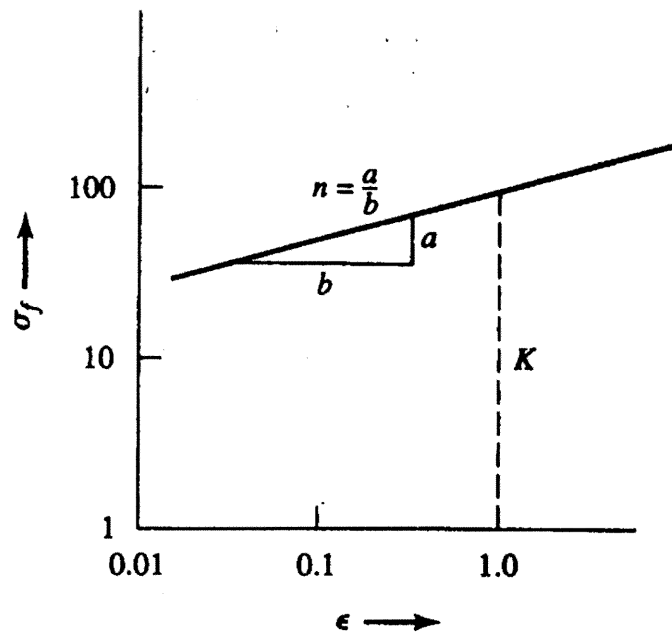


Fig. 3-3 Logarithmic Plot of Flow Stress-True Strain

**Effect of Strain Hardening on Necking** When metals are plastically deformed, they *strain harden*. They become harder and stronger, and this change is progressive one. If a stress is producing plastic deformation, an even greater stress will be required to induce further flow. Various materials strain harden at different rates, for a given amount of deformation, different materials will exhibit different increases in strength, as described in Eq. 3-8. The strain hardening slows down the onset of necking. This may be understood by considering the events involved in the formation of a neck. In the course of extension, an incipient neck may form anywhere along the gage length, generally at a point of inhomogeneity, i.e., where the material is, for any reason, weaker (because of a surface irregularity, an inclusion or a large grain of

weak orientation). If the  $n$  value is high, localized deformation in the incipient neck raises  $\sigma_f$  at this point. Deformation will now continue in other, less strain-hardened parts of the specimen, until hardening can no longer keep up with the loss of load-bearing capacity due to reduced cross section; at this time, one of the necks stabilizes and continues to neck (Fig. 3-4a) while the applied force drops. It can be shown that, for a material that obeys the power law of strain hardening (Eq. 3-8), the  $n$  value is numerically identical to the uniform (prenecking) strain expressed as true strain  $\epsilon_u$ ; therefore, a material of low  $n$  necks soon after initial yielding (Figs. 3-4a and 3-4b) [29].

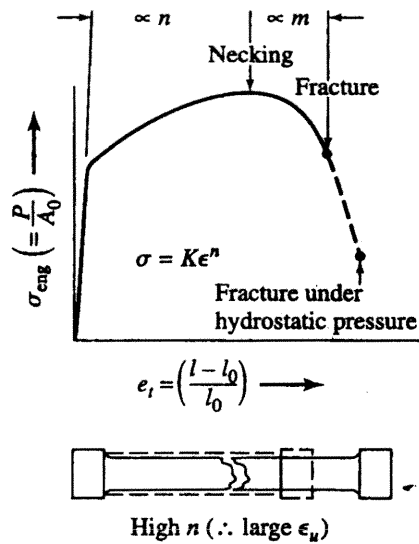


Fig. 3-4a Material with High-Strain Hardening Rate

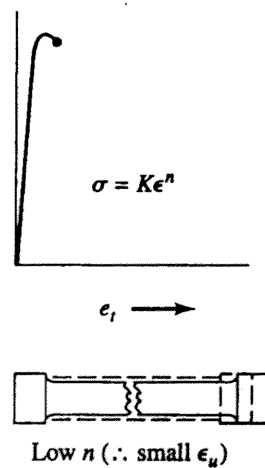


Fig. 3-4b Material with Low-Strain Hardening Rate



### 3.3. FLOW STRESS IN COMPRESSION

A problem with the tension test is that necking limits strain that can be obtained, and the development of flow stress at higher strains is uncertain. Yet, many metalworking processes involve heavy deformation, and the compression test is more useful. The instantaneous cross-sectional area is again calculated from constancy of volume (Eq. 3-4) but now the length is more descriptively called the height  $h$  (Fig. 3-5). The true strain  $\epsilon$  is, by definition,

$$\epsilon = \ln \frac{h}{h_0} = \ln \frac{A_0}{A} \quad (3-9)$$

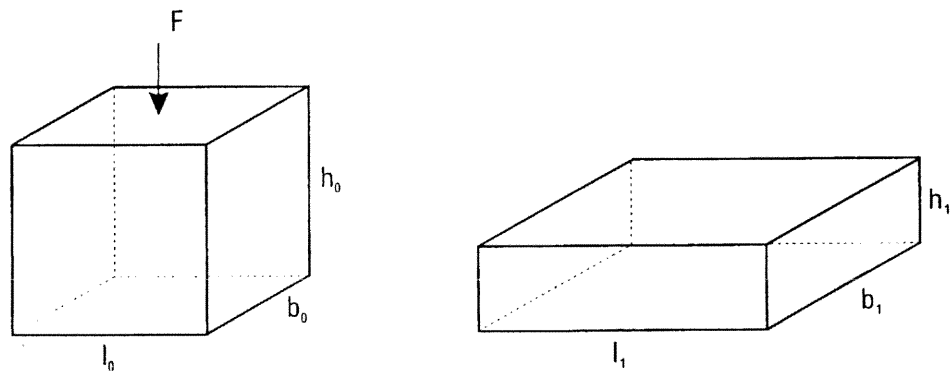


Fig. 3-5 Dimensional Changes in Upsetting of a Cube

$$\begin{aligned} V_0 = V &\Rightarrow A_0 \cdot h_0 = A \cdot h \\ \Rightarrow A &= A_0 \frac{h_0}{h} = \frac{V}{h} \end{aligned} \quad (3-10)$$

The calculation yields a negative number. As far as the material is concerned, compressive and tensile deformations cause the same metallurgical changes. Hence the convention is usually ignored and, to obtain a positive value, true strain is taken as the natural logarithm of the ratio of the larger value to the smaller value.

$$\varepsilon = \ln \frac{h_0}{h} = \ln \frac{A}{A_0} \quad (3-11)$$

The true stress is calculated from the Eq. 3-5. This is an interface pressure between the work material and the tool but also the surface conditions between two materials should be accepted as frictionless. And from the logarithmic plot of flow stress-true strain curve, the strength coefficient, K, and the strain hardening exponent, n, can be extracted. Although the K and the n values of some of the material are given in Table E.1 and Table E.2 in Appendix E [28].

### **3.4. DISCONTINUOUS YIELDING**

Not all metals and alloys show the smooth transition from elastic to plastic deformation and not all of them strain-harden in a continuous fashion. Such anomalies in plastic flow behavior have structural reasons [29].

#### **3.4.1. Yield-Point Elongation**

The possibility of forming interstitial solid solutions in which solute atoms, much smaller than the solvent atoms, fit into the spaces existing between atoms in the basic lattice. These solute atoms often seek more comfortable sites where lattice defects have created voids in the structure. Most markedly, this is found with carbon and nitrogen in iron. Their atoms are small enough to fit into the lattice; nevertheless, they tend to migrate to dislocations where distortion of the lattice provides more room. In a sense, the solute atoms form a condensed atmosphere that completes the lattice and immobilizes, pins the dislocations.

In the course of deformation, a larger stress must be applied before dislocations can break away from the condensed atmosphere of carbon or nitrogen atoms. This leads to the appearance of a yield point on the stress-strain curve of low-carbon steels (Fig. 3-6a). After the dislocations have broken away from the pinning atoms, they multiply and move in large groups in the direction of maximum shear stress (very approximately, at 45° to the applied force).

### 3.4.2. Serrated Yielding

Discontinuous yielding during strain hardening is observed in some materials for causes related to negative strain-rate sensitivity rather than to dislocation pinning. When tested on a "soft" machine (of low spring constant), yielding is stepwise; on a hard machine, the force drops erratically and rapidly (serrated yielding) (Fig. 3-6b). Such behavior can be particularly troublesome with some substitutional aluminum alloys, because it again leads to the development of visible and objectionable marks on the surface .

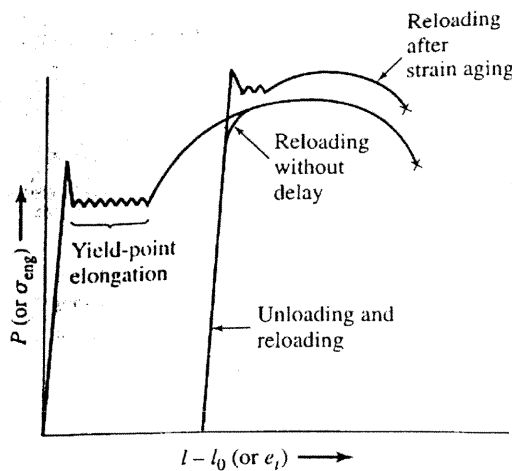


Fig. 3-6a Yield Point Elongation of Mild Steel

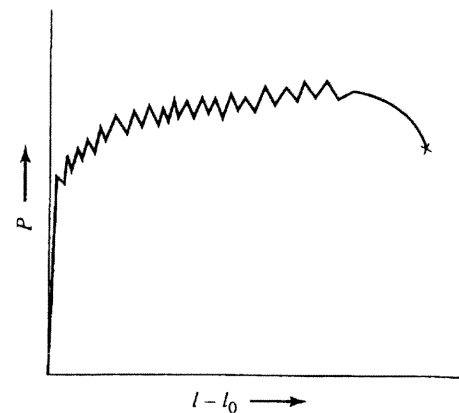


Fig. 3-6b Serrated Yielding of Solid-Solution Alloys

### 3.5. EFFECTS OF COLD WORKING

It is obvious from Fig. 3-2 and Fig. 3-3 that an ever-increasing true stress is needed for the continuing deformation of a metal. Because this is a direct consequence of working or straining, namely work hardening or strain hardening. The reason for it is to be found in the mechanism of plastic deformation.

Crystalline metals deform by slip and, on the atomic scale, by the propagation and multiplication of dislocations. As deformation proceeds, dislocations may begin to move on several systems. It takes a higher stress to move a succession of dislocations on the same plane, and a yet higher stress is needed to move them once dislocations propagating on different planes become entangled. This higher stress is the cause of the increase in flow stress. Distortion of the crystal lattice by foreign atoms further inhibits the free movement of dislocations and increases strain hardening; therefore, solid solutions have a higher  $n$  value. Since this gives a larger prenecking strain, solid solutions have high ductility.

A material subjected to cold working, for example, by rolling or drawing, strain-hardens too. Dislocation density increases and, when a tension test is performed on this strain-hardened material, a higher stress will be needed to initiate and maintain plastic deformation; thus, the YS rises. The tensile strength, TS, rises too, although not as rapidly as the yield strength, YS, and the TS/YS ratio approaches unity (Fig.3-7).

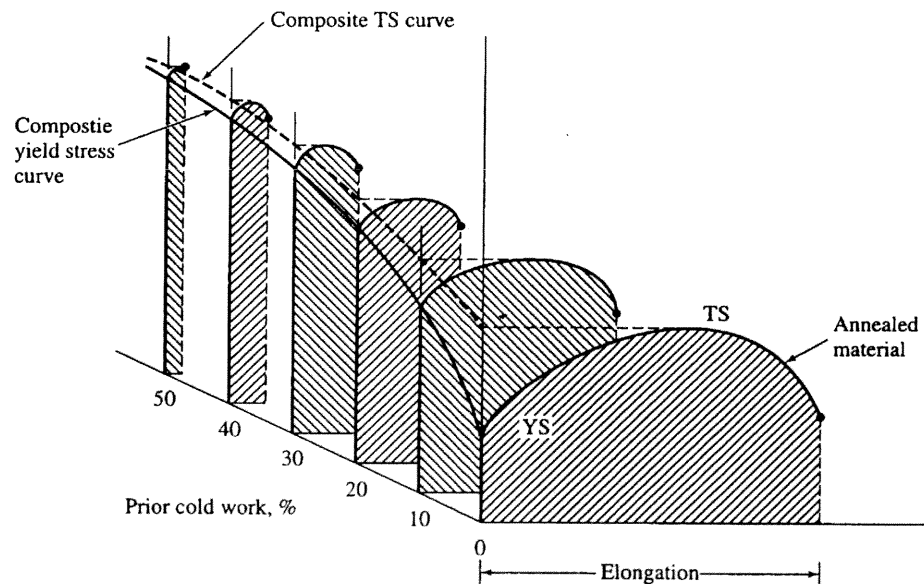


Fig. 3-7 Tension Tests Conducted on Previously Worked Material

However, the ductility of the material as expressed by total elongation and reduction of area drops because of the higher initial dislocation density. Similarly,  $K$  rises and

n drops. The microstructure changes too: Crystals (grains) become elongated in the direction of major deformation. These changes are summarized in Fig. 3-8.

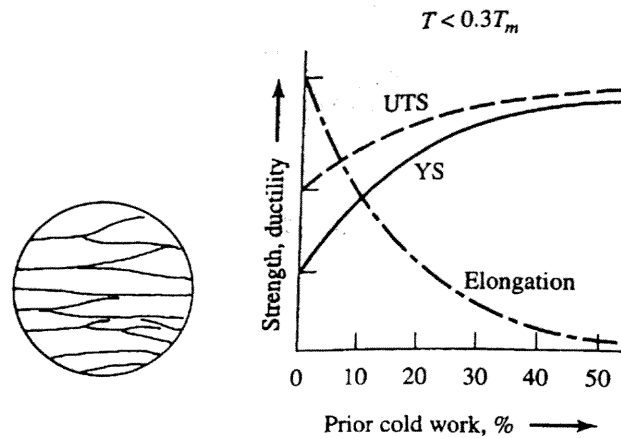


Fig. 3-8 The Effects of Prior Cold Work

Strain hardening is important for several reasons. Since many cold-worked materials retain a reasonable level of ductility, cold working offers the designer a low-cost method of obtaining higher-strength materials. There is, however, a price to pay: the increased flow stress can generate excessive tool pressures and the reduced ductility may lead to fracture of the workpiece. This can become a major problem when heavy reductions are to be taken or when the manufacture of products involves a succession of cold-working steps. It is then necessary to remove the effects of cold working by annealing [29].

### 3.6. RECRYSTALLIZATION

Above half of melting temperature,  $T_m$ , atoms move relatively dislocation-free nuclei which grow until all the cold-worked structure is recrystallized. Diffusion is greatly time- and temperature-dependent. The driving force for recrystallization is provided by the increased energy content (stored energy) resulting from the higher dislocation density induced by cold working [30].

Therefore, recrystallization begins at a lower temperature with increasing prior cold work (Fig. 3-9). Coarse-grained material has low strength, so the aim is generally that of producing finer grain. This can be achieved with increasing cold work

because, for any given temperature, more nuclei form and grain size diminishes. Strength increases with little loss in ductility. There is no recrystallization possible if cold work is zero, and the original grain size is retained. The low dislocation densities induced by very light, i.e. 2-4%, cold work results in the formation of only a few nuclei which can then grow to a large size. Such critical cold work is usually undesirable because of the poor mechanical properties of coarse-grained structures. On the other hand, very fine grain obtained by annealing a heavily cold-worked metal gives high strength yet reasonable ductility [29].

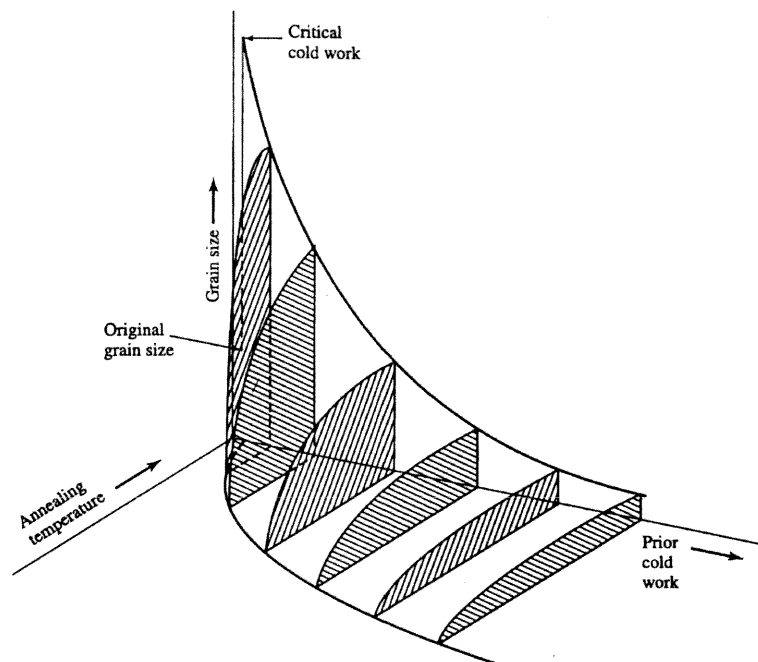


Fig. 3-9 Prior Cold Work (%)-Grain Size-Annealing Temperature Curve

The temperature of  $0.5T_m$ , melting temperature, is a very rough guide, since even minor amounts of alloying elements can substantially delay the formation of new grains and thus raise the recrystallization temperature. In alloys specifically designed for high-temperature service, such as the superalloys, heavy alloying pushes the onset of recrystallization to around  $0.8T_m$ .

When a metal is held at temperature for a prolonged time, larger grains—which have a smaller surface area per unit volume and hence a lower surface energy—grow at the

expense of smaller grains. Such grain growth is undesirable because strength and, if excessive grain growth occurs, even ductility suffers [29].

### **3.7. HOT WORKING**

We have noted that temperatures above  $0.5T_m$  greatly facilitate the diffusion of atoms. This means that an arrested dislocation has the option of climbing, and can thus move into another, unobstructed, atomic plane. If, therefore, deformation itself takes place at such elevated temperatures, many dislocations can immediately disappear; in fact, one finds that softening processes work simultaneously with dislocation propagation. Material resulting from such hot working has a much lower dislocation density and, therefore, is less strain-hardened than cold-worked material. In practice, hot working is conducted at higher temperatures, where softening processes are fast, but not at such high temperatures that there would be danger of incipient melting (typically between  $0.7T_m$  and  $0.9T_m$ ) [29].

#### **3.7.1. Mechanisms of Hot Working:**

Since  $0.5 T_m$  is also the temperature of recrystallization, it is often said that hot working is conducted above the recrystallization temperature. Recrystallization may still occur on holding at or cooling from the hot-working temperature. Therefore, the distinctive mark of hot working is not a recrystallized structure, but the simultaneous occurrence of dislocation propagation and softening processes, with or without recrystallization during working. The dominant mechanism depends on temperature, strain rate, and grain size, and may be conveniently shown on deformation mechanism maps. In general, the recrystallized structure becomes finer with lower deformation temperature and faster cooling rates, and material of superior properties is often obtained by controlling the finishing temperature.

#### **3.7.2. Flow Stress in Hot Working:**

Since all softening processes require the movement of atoms, the time available for these processes is critical. This means that in hot working there is substantial strain-

rate sensitivity. In its simplest definition, strain rate is the instantaneous deformation velocity divided by the instantaneous length or height of the workpiece ( Eq. 3-12) [30]. For compressive deformation:

$$\dot{\epsilon} = \frac{v}{h} \quad (3-12)$$

Where the strain rate,  $\dot{\epsilon}$  is expressed as  $s^{-1}$ .

From recordings of force versus displacement, stress-strain curves are plotted which may show a number of trends (Fig. 3-10):

1. After an initial peak, flow stress drops with increasing strain. Such strain softening is usually a sign of dynamic recrystallization.
2. The stress-strain curve may be fairly flat after initial yielding, indicating that strain hardening and softening processes roughly balance each other.
3. At yet higher strain rates, stresses increase with increasing strain, indicating that softening processes could not keep pace with strain hardening.

To a first approximation, hot working can be regarded as though it were governed purely by strain rate. Then flow stress values for a given strain may be extracted from the true stress-true strain curves (Fig. 3-10) and replotted as a function of strain rate on a log-log scale (Fig. 3-11). In the majority of instances, the line thus defined will be straight, indicating that hot-working flow-stress is a power function of strain rate  $\dot{\epsilon}$ :

$$\sigma_f = C \cdot \dot{\epsilon}^m \quad (3-13)$$

where  $C$  is a strength coefficient, and  $m$  is the strain-rate-sensitivity exponent. The value of  $C$  is found at a strain rate of unity, and  $m$  is the slope of the line, again measured on a linear scale (Fig. 3-11). Alternatively, a power-law function is fitted to the data points. It is evident from Fig. 3-10 that different  $C$  and  $m$  values will be found for different strains. Both  $C$  and  $m$  also change with temperature. Increasing temperature usually increases strain-rate sensitivity and thus  $m$ , but always decreases the flow stress and thus  $C$ .



For computational purposes, experimentally determined  $C$  and  $m$  values (for example, from Tables 3-1 and 3-2) or flow stress curves must be used.

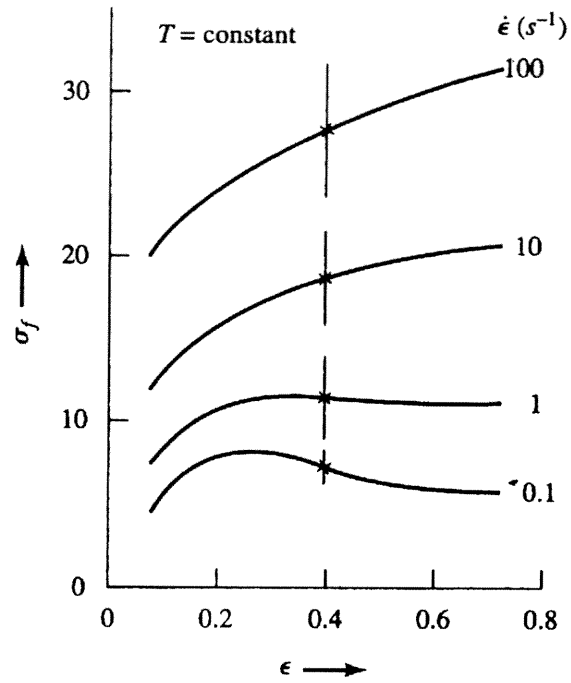


Fig. 3-10 Flow Stress- Strain Rate

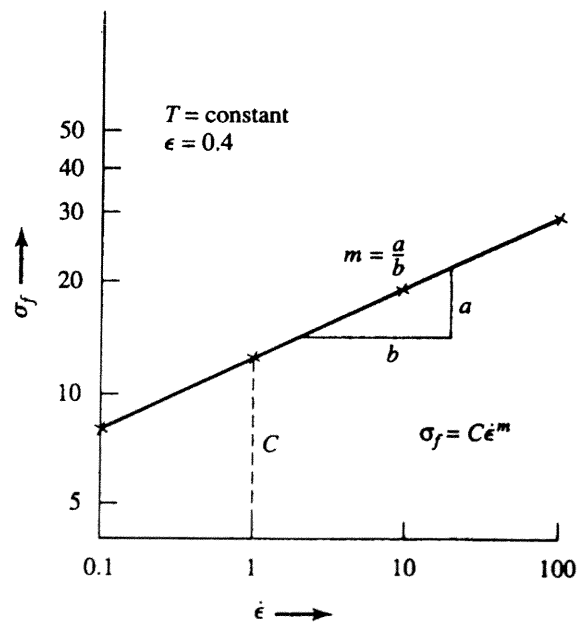


Fig. 3-11 Flow Stress-Strain Rate in Logarithmic Scale

### 3.8. WARM WORKING

Deformation at  $0.3 T_m$  to  $0.5 T_m$  is often denoted as warm working, and is characterized by reduced strain hardening, increased strain-rate sensitivity, and a somewhat lower flow stress relative to cold working [29].

**Ductility:** A high  $m$  value means that higher forces are needed to deform the material at higher strain rates.

When a neck begins to form, this incipient neck is the smallest cross section of the specimen. In a non-strain-rate-sensitive material, it would also be the weakest part and it would thin out and fracture. Since deformation is concentrated in the neck, the instantaneous deforming length in Eq. (3-12) suddenly drops. Strain rate in the neck becomes much higher than it was before necking, whereas it drops to zero outside the necked zone. Consequently, the flow stress of the material in the neck increases, and the neck resists further deformation. Instead, adjacent material deforms and further locations neck until the entire gage length is deformed. Thus, we find that total elongation increases with higher  $n$  (strain-hardening exponent) which governs prenecking strain and a higher  $m$  (strain-rate sensitivity exponent) which governs postnecking strain (Fig. 3-4a).

#### 3.8.1. Superplasticity:

In some extremely fine-grained materials high-temperature deformation takes place by extensive grain-boundary sliding and accompanying diffusion or by mass diffusion which reshapes entire grains. Deforming forces can be very low and, as long as strain rates are kept within the limits that allow these deformation mechanisms to prevail (Fig. 3-12), the superplastic behavior is maintained and very large elongation values (up to several hundred and even thousand percent) are readily obtained.

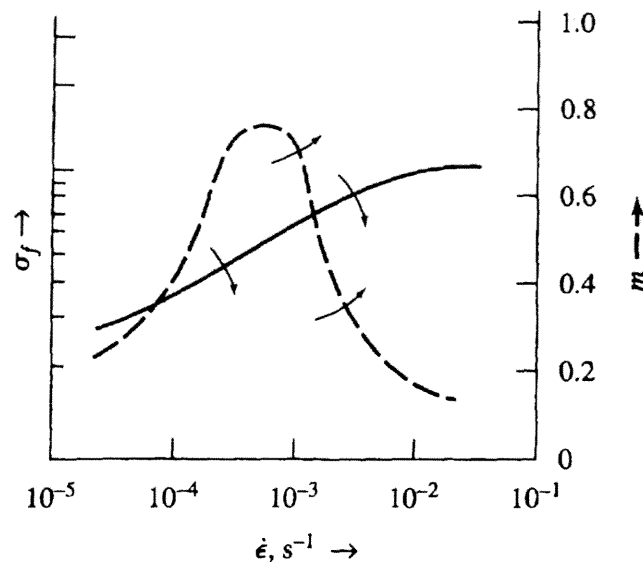


Fig. 3-12 Flow Stress-Strain Rate

### 3.9. MECHANICS OF DEFORMATION PROCESSING

There is a great variety of plastic deformation processes but some principles can be applied to all of them.

Plastic deformation is conducted with the aid of tools (dies). All die materials have limited strength; therefore, the magnitude of pressure developed in the course of deformation should be concerned. If pressure is too large, the process is not feasible and the total deformation force may be too high for available equipment. Consequently, computation of pressures and forces is our primary job on deformation processes. In order to get a reasonable estimate of pressure, four points are analyzed [29];

- 1) the stress state must be analyzed;
- 2) a relevant flow stress must be found;
- 3) the effects of friction must be judged;
- 4) inhomogeneous deformation must be taken into account,

### 3.9.1. Yield Criteria

The stress state is stresses act in all directions. Analysis is simplified if the coordinate system is oriented in such a way that shear stresses disappear and only three normal stresses act. These are then called principal stresses and are denoted  $\sigma_1$ ,  $\sigma_2$  and  $\sigma_3$ .

Structural elements and machine components made of a ductile material are usually designed so that the material will not yield under the expected loading conditions. When the element or component is under uniaxial stress, as Fig.3-13, the value of the normal stress  $\sigma_1$ , which will cause the material to yield may be obtained readily from a tensile test conducted on a specimen of the same material, since the test specimen and the structural element or machine component are in the same state of stress. Thus, regardless of the actual mechanism which causes the material to yield, we may state that the element or component will be safe as long as  $\sigma_1 < \sigma_y$ .

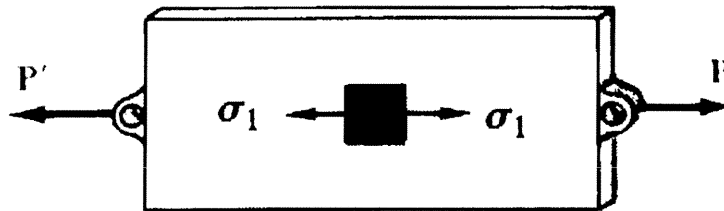


Fig. 3-13 Pure Tension Specimen

On the other hand, when a structural element or machine component is in a state of plane stress, as Fig. 3-14a, it is convenient to use the principal stresses  $\sigma_1$ , and  $\sigma_2$ , as Fig. 3-14b. The material may then be regarded as being in a state of biaxial stress. Since this state is different from the state of uniaxial stress found in a specimen subjected to a tensile test, it is clearly not possible to predict directly from such a test whether or not the structural element or machine component under investigation will fail. A yield criterion regarding the actual mechanism of failure of the material must first be established, which will make it possible to compare the effects of both states of stress on the material [29].

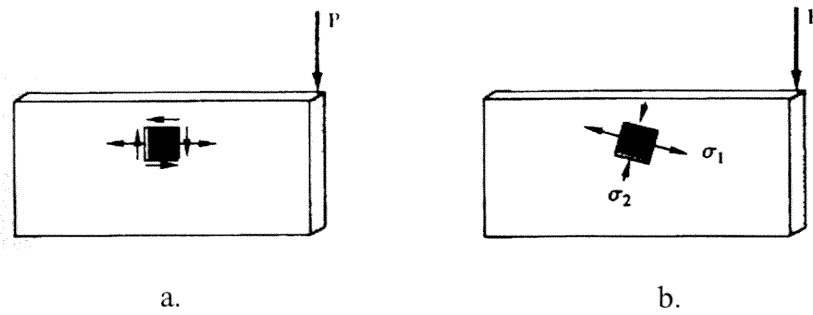


Fig. 3.14 Pure Bending Specimens

For plastic flow to occur, the combination of stresses must satisfy the yield criterion. Yield criteria have been formulated to describe the beginning of plastic deformation by relating the principal stresses to the tensile or compressive yield strength of the material. Our concern is with large plastic deformations; therefore, we will use the flow stress  $\sigma_f$ . For metals, two criteria are frequently used; Tresca Theorem and The Von Misses Theorem.

**Tresca Theorem:** This criterion is based on the observation that yield in ductile materials is caused by slippage of the material along oblique surfaces and is due to shearing stresses. According to this criterion, a given structural component is safe as long as the maximum value  $\tau_{\max}$  of the shearing stress in that component remains smaller than the corresponding value of the shearing stress in a tensile-test specimen of the same material as the specimen starts to yield or flow. The maximum value of the shearing stress is equal to half the value of the corresponding normal stress, so that the maximum shearing stress is half of the shearing stress. But Here we use flow stress instead of yield for the next chapters, Eq. 3-14 [31].

$$\frac{\sigma_{\max} - \sigma_{\min}}{2} = \frac{\sigma_f}{2} \quad (3-14)$$

**Von Misses Theorem:** This criterion is based on the determination of the distortion energy in a given material. A given structural component is safe as long as the maximum value of the distortion energy per unit volume in that material remains

smaller than the distortion energy per unit volume required to cause yield in the material. So the yield criterion according to Von Mises is:

$$(\sigma_1 - \sigma_2)^2 + (\sigma_2 - \sigma_3)^2 + (\sigma_3 - \sigma_1)^2 = 2\sigma_f^2 \quad (3-15)$$

The significance of yield criteria is best illustrated by examining a simplified stress state in which  $\sigma_3=0$  (plane stress). For ease of visualization, one may think of a plate in which the rolling direction is arbitrarily taken as the  $\sigma_1$  direction and the width direction the  $\sigma_2$  direction (Fig. 3-15). Plastic flow can be initiated in many ways:

1. If a tensile specimen is cut in the rolling direction, flow occurs according to both Tresca and von Mises at the flow stress  $\sigma_f$  (points 1, corresponding to the two directions in the plane of the plate).
2. Shorter cylinders cut in the same directions can be tested in compression and will usually be found to flow at the same stress  $\sigma_f$  (points 2).
3. When the plate is bulged by a punch or a pressurized medium (as a balloon is blown up by air), the two principal stresses acting in the plane of the plate are equal (balanced biaxial tension) and must reach  $\sigma_f$  (point 3).
4. A technically very important condition is reached when deformation of the workpiece is prevented in one of the principal directions (plane strain) for one of two reasons:
  - a. A die element keeps one dimension constant .
  - b. Only one part of the workpiece is deformed, and adjacent nondeforming portions exert a restraining influence.

In either case, the restraint imposes a stress on the material in that principal direction; the stress is the arithmetic average of the other two principal stresses (corresponding to points 4 in Fig. 3-15). The stress required for deformation is still  $\sigma_f$  according to Tresca, who ignores the intermediate principal stress. However, according to Von-Mises, the stress required is higher,  $1.15 \sigma_f$ , which value is often denoted as  $2k$ . It is also called the plane-strain flow stress or constrained flow stress of the material. Plane strain may be imposed also in tension, point 4a.

5. If a cylinder is cut out and twisted (torsion), the two principal stresses on the surface of the cylinder are of equal magnitude but of opposing sign (points 5 in Fig. 3-15). This is a condition of pure shear, and flow occurs at the shear flow stress  $\tau_f$ ,

which is equal to  $0.5 \sigma_f$  according to Tresca and  $0.577 \sigma_f$  according to Von Mises. The shear flow stress according to Von-Misses is often denoted as  $k$ . The important point is that when, in the course of deformation by compression, a transverse stress of opposing sign (a tensile stress) is imposed, the stress required for compression will decrease. This offers a powerful mechanism for reducing die pressures.

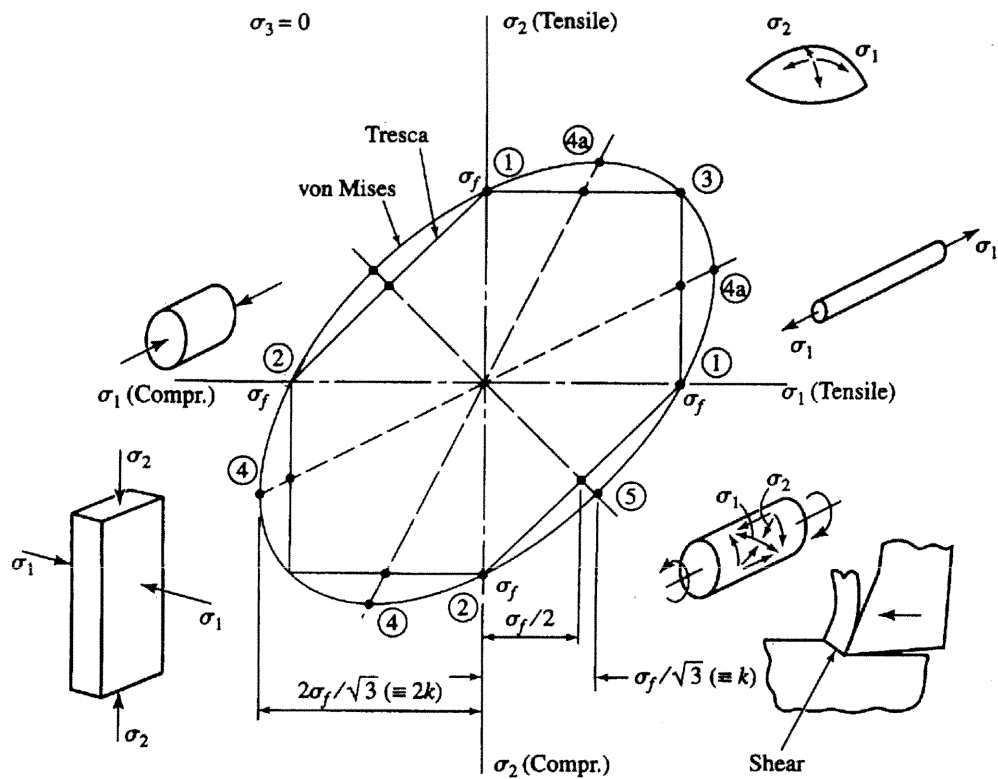


Fig. 3-15 Maximum Distortion Energy-Maximum Shear Stress Theorem

6. A special condition is reached when all three principal stresses are equal in magnitude (hydrostatic stress state). An inspection of the Yield Criteria [Eqs. (3-14) and (3-15)] will show that superimposition of a hydrostatic stress simply shifts all principal stresses by the same amount, thus there is no change in the yield criterion and flow still begins at  $\sigma_f$ .

### 3.9.2. The Relevant Flow Stress

In all calculations, the stress sufficient to maintain plastic deformation,  $\sigma_f$ , must be taken for the temperature, strain, and strain rate prevailing in the process. It cannot be sufficiently emphasized that our interest is not just in initiating but also in maintaining plastic flow. Thus, the yield strength found in many handbooks is of little use; the flow stress traverses the true stress-true strain curve (Fig. 3-2 or 3-10) within the strain limits defined by the condition of the starting material and the end strain [29].

1. In cold working it can be assumed that the power law, Eq. (3-8), holds and, whenever available, the  $K$  and  $n$  values should be used (a selection is given in Tables 3-1 and 3-2).
2. For hot working, the flow stress can be calculated from the power function, Eq. (8-11), with the appropriate  $C$  and  $m$  values (Tables 3-1 and 3-2). If these values are not available for various strains, one has to assume that the flow stress remains constant throughout deformation (as in the curve for a strain rate of  $1 \text{ s}^{-1}$  in Fig. 3-10; in Tables 3-1 and 3-2 the values are given for a strain of  $\epsilon = 0.5$ ). If no  $C$  and  $m$  data are available, one is obliged to make a compression test. It is quite inadmissible to use hot-strength values determined in conventional, slow tension tests, because they often represent only a fraction of the true flow stress prevailing at the much higher (typically,  $1-1000 \text{ s}^{-1}$ ) strain rates attained in deformation processes. Extrapolation from low strain rates to high strain rates is hazardous because  $m$  may also change with strain rate (see Fig. 3-12).

### 3.9.3. Effects of Friction

In most deformation the workpiece is brought in contact with a tool or die; therefore, friction between the two contacting bodies is unavoidable. With few exceptions, our aim will be to reduce friction by the application of a lubricant. Friction is examined or described by coefficient of friction,  $\mu$ ;



$$\mu = \frac{F}{P} = \frac{\tau_i}{p} \quad (3-16)$$

When the interface pressure  $p$  is low relative to the flow stress  $\sigma_f$  of the contacting materials with increasing pressure  $p$  the interface shear stress  $\tau_i$  increases linearly (Fig. 3-16a), and  $\mu$  could assume any constant value. In deformation processes one of the contacting materials (the workpiece) deforms and in doing so slides against the harder surface (the tool or die). A frictional stress  $\tau_i$  is again generated, but this time there is a limit to  $\mu$ , because the material will choose a deformation pattern that minimizes the energy of deformation. If friction is high, interface shear stress  $\tau_i$  will reach the shear flow stress  $\tau_f$  of the workpiece material (Fig.3-16a). At this point the workpiece refuses to slide on the tool surface; instead, it deforms by shearing inside the body (Fig. 3-16b). Since  $\tau_f = 0.5\sigma_f$  (Fig. 3-15), it is often said that the maximum value of  $\mu = 0.5$ . This is true only when  $p = \sigma_f$ , at higher  $p$ , the maximum value of  $\mu$  is lower (Fig. 3-16b). The coefficient of friction becomes meaningless when  $\tau_i = \tau_f$ , since there is no relative sliding at the interface. This is described as sticking friction, even though the workpiece does not actually stick to the die surface [29].

Because of some difficulties introduced by the coefficient of friction, it is often preferable to use the actual value of  $\tau_i$ , especially when interface pressures are very high. Alternatively,  $\tau_i$  can be denoted as a fraction of the shear flow stress

$$\tau_i = m^* \cdot \tau_f = m^* \cdot \frac{\sigma_f}{2} \quad (3-17)$$

where  $m^*$  is the frictional shear factor. For a perfect lubricant,  $m^*=0$ ; for sticking friction,  $m^*=1$ .

### 3.10. MEASUREMENT OF FRICTION

#### 3.10.1. Purposes of Friction Measurements

Friction determines forces and power requirements, and is responsible for a number of process limitations. Improved lubrication is immediately noticeable in reduced equipment loading, in greater reductions per pass and, frequently, in an increased

output from a given installation. Simple evaluation techniques or production observations are usually adequate for a semiquantitative ranking of lubricants. More sophisticated measurements and calculations are needed if the quality of the lubricant

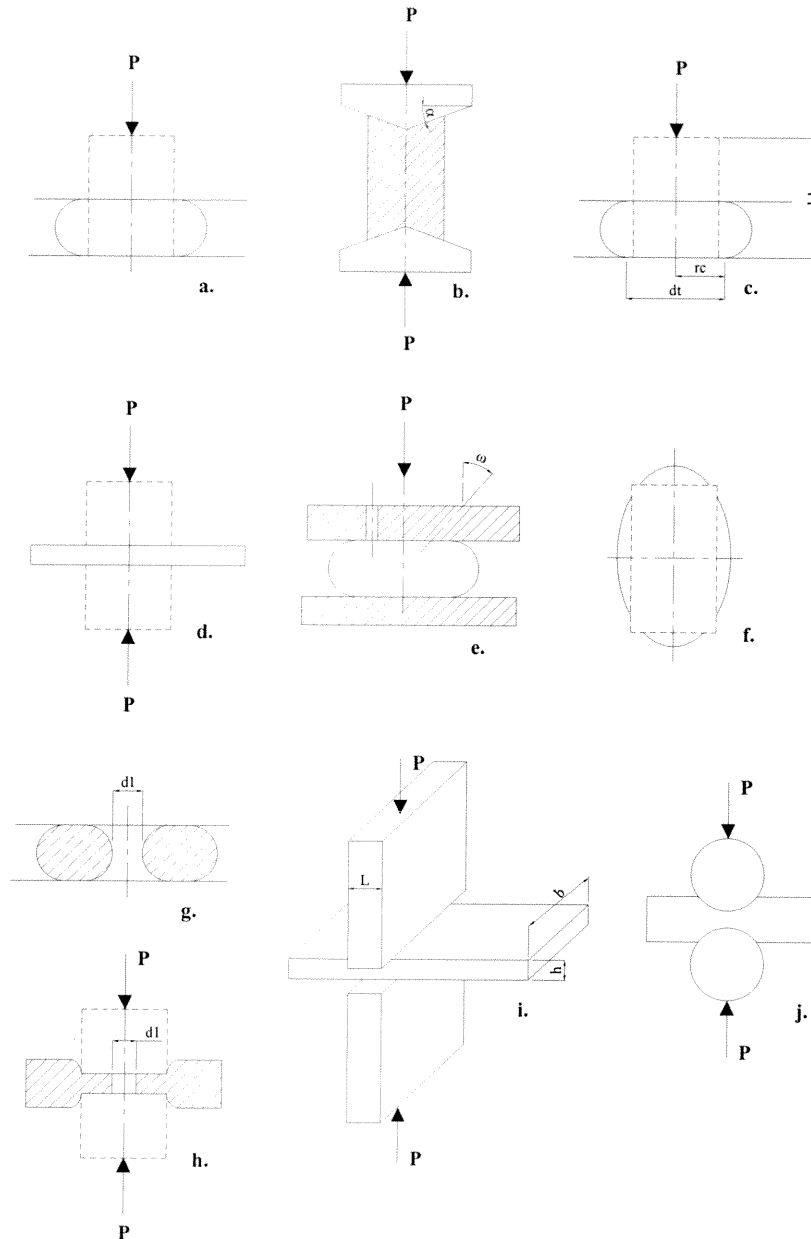


Fig. 3-16 Methods of Measuring Friction Effects in Upsetting and Indenting

is to be judged from a coefficient of friction value. In principle, this has advantages in that clues to the operative lubricating mechanism may be gleaned, generalized conclusions may be drawn for various production conditions, optimum production

sequences may be planned, and equipment may be designed on a more scientific basis. It must be recognized that friction values are, very frequently, specific to the given experimental conditions, and indiscriminate extension of "typical" values could lead to serious errors [32].

The first logical step is the evaluation of lubricants in the same deformation process as it is intended for, but on a smaller scale; the problem here is to determine how far dimensions, speeds, strain, and other process variables may be scaled down before the test loses its relevance. A further step toward simplification involves the selection of a simple metalworking process that can be performed at a low cost to evaluate lubricants for another, more costly, process. For example, wire drawing has been proposed and used for the evaluation of rolling lubricants. The question here arises as to whether one metalworking operation can be used to simulate lubricant performance in another. The final step, of course, is the development of a simulating technique that may be performed on a bench-type apparatus. Such tests may involve plastic flow or may be limited to elastic contact between tool and workpiece material. The task then remains to show the applicability of such test results to real metalworking processes. The main limitation is usually the absence of sufficient surface strain that would expose new surfaces at a rate comparable to deformation processing.

### **3.10.2. Upsetting of Cylinders**

The dependence of upsetting force on interface friction offers a simple way of ranking lubricants. The force required to upset specimens of constant size to a predetermined height may be noted or, conversely, a constant force may be applied and the resulting deformation measured (Fig. 3-16a). These techniques are suitable for an overall ranking of lubricants. But since friction is bound to vary from the center toward the edges and since partially sticking friction or complete sticking along with folding over of side surfaces is likely to occur. The validity of theoretical solutions is better for small deformations, but incremental upsetting would interfere with the natural development and breakdown of lubricant films and could invalidate the test. In general, specimens with a relatively large diameter-to-height ratio (at least

4) are preferable so as to encourage expansion of the original end face even when friction is high. These reservations apply even more to upsetting at elevated temperatures, since cooling at the interface restricts end face movement and indicates an apparently higher coefficient of friction. If a lubricant is used, the results may be indicative more of heat insulating than lubricating characteristics.

The coefficient of friction is determined in cylindrical upsetting by using conical compression platens (Fig. 3-16b). At the die-workpiece interface, a component of the normal force,  $P_2 = P_n \tan \alpha$ , acts to move the material in a radial direction. This force is opposed by the frictional force  $F = P_n \cdot \mu$ . When the frictional force balances the radial upsetting force component ( $P_2 = F$  or  $\mu = \tan \alpha$ ) the cylinder deforms uniformly; when the frictional force is higher, barreling occurs; whereas if the radial force component of the upsetting force prevails, the end faces spread. Even though the method is accurate--at least if the absence of barreling can be correctly judged--a large number of precise specimens and dies must be prepared. With high values of friction, a zone of sticking develops in the center of the interface. The extent of the sticking zone may be found by applying a measured grid onto the end faces of cylinders with heights  $h_1$  greater than their diameter  $d_1$ . After deformation, the radius of the edge of the sticking zone  $r_c$  is readily measured (Fig. 3.4c). A mean coefficient may then be determined for the sliding zone from the following equation:

$$\ln \frac{1}{2\mu} + \frac{2\mu}{h_1} \cdot \left( r_c - \frac{d_1}{2} \right) = 0 \quad (3-18)$$

Since this equation holds only at the moment of yielding, the coefficient of friction is underestimated unless the test is repeated at several reductions and the results are extrapolated to zero reduction. Such extrapolation does not pertain if the lubricating film changes during compression. The grid should be printed rather than engraved (otherwise, the trapped lubricant may falsify the results), and the surface topography must be very uniform.

The high interface pressures often obtained in practical metalworking processes may be reproduced on a small scale by upsetting cylinders of rather large diameter-to-

height ratio. A disk-shaped specimen is compressed between anvils of somewhat smaller diameter; thus the area of contact remains constant and calculations are simplified (Fig. 3-16d). In this respect, the test is similar to plane-strain compression; however, the annular overhang of the workpiece material exerts a restraint on the deforming portion and raises the apparent resistance to deformation. The lubricant effectiveness may be judged from forces generated without and with the lubricant, and an order of merit can be established, but a coefficient of friction is difficult if not impossible to calculate. Therefore, plane-strain compression remains preferable to this method.

For theoretical purposes, the variation of friction from point to point is of interest. The principle of measurement is shown in Fig. 3.4e. Two pins are embedded into the surface of the compression platen at the same radial distance on the specimen. The measured pressure is composed of the normal pressure acting on the interface and of the frictional force between pin and platen. If the local coefficient of interface friction  $\mu$  is defined as the friction-induced shear stress  $\tau_i$  divided by the normal pressure prevailing at the same point and if friction between pin and platen is,  $\mu_0$ , the pressure acting on the normal pin may be expressed as;

$$P_n = \sigma - \mu_0 \cdot \mu \cdot \sigma \quad 3-19$$

For the oblique pin, with  $y$  smaller than  $\tan\Phi$

$$\frac{P_\phi}{P_n} = 1 + \tan\phi(\mu - \mu_0) + \mu_0 \cdot \mu \quad 3-20$$

From these;

$$\frac{P_\phi}{P_n} = \frac{1 + \tan\phi(\mu - \mu_0) + \mu_0 \cdot \mu}{1 - \mu_0 \cdot \mu} \quad 3-21$$

from which the coefficient of friction may be derived if friction between pin and platen (bushing) is known.

Experiments conducted with this technique call for careful calibration. Possible binding or rotation of the pin in the platen and variations of pinplaten friction  $\mu_0$  with lubricants penetrating into the clearance must be considered. The clearance between the pin and the platen must be small enough to preclude penetration of specimen material into the gap, yet large enough to allow sliding of the pin without binding.

### **3.10.3. Upsetting of Slabs**

From a consideration of stresses and displacements in the compression of a thin sheet between overhanging platens, the friction coefficient may be determined if the lamina is rectangular, its length at least 10 times its width, and its height similar to its width. Under these conditions, the only stress components are the compressive stress, the interface pressure, and the friction, allowing a simplified analysis of the problem. The width change is measured in the middle length of the specimen; the ends deform less, giving a characteristic cigar-shape (Fig. 3-16f). The analysis shows that the test is sensitive to very small friction values but becomes inoperable at higher friction, and the test has found little use.

The variation of interface shear stresses along the width of a compressed, rectangular workpiece was measured Fig. 3-16j. A divided platen was sandwiched between two identical workpieces, which were then compressed between two overhanging platens. The separating force acting on the divided central platen was measured on load cells; this indicated the net frictional forces at a selected point of the interface. From a simultaneous measurement of the local interface pressure with a pin embedded in the outer platens, friction coefficients could also be determined.

### **3.10.4. Ring Upsetting**

This technique was originally developed for cold working and was later adapted for hot working. Since the position of the neutral zone is a function of friction, there is

no need to measure forces--it is sufficient to measure only the changes in internal diameter (Fig. 3-16g). If the specimen geometry is kept constant and the reduction can be exactly reproduced, no other variable needs to be considered. This simple procedure allows a ranking of lubricants.

As soon as a quantitative value of the coefficient of friction is sought, one of the theoretical treatments of the position of the neutral plane must be adopted. Both rings and cylinders are compressed under identical lubricating conditions, and calculated friction from the cylinder upsetting experiments. These friction values were then plotted against the changes in internal diameter of the ring and were used as a calibration (Fig. 3-17). Such procedure allows comparison of data obtained at different reductions, provided that lubricant breakdown does not occur.

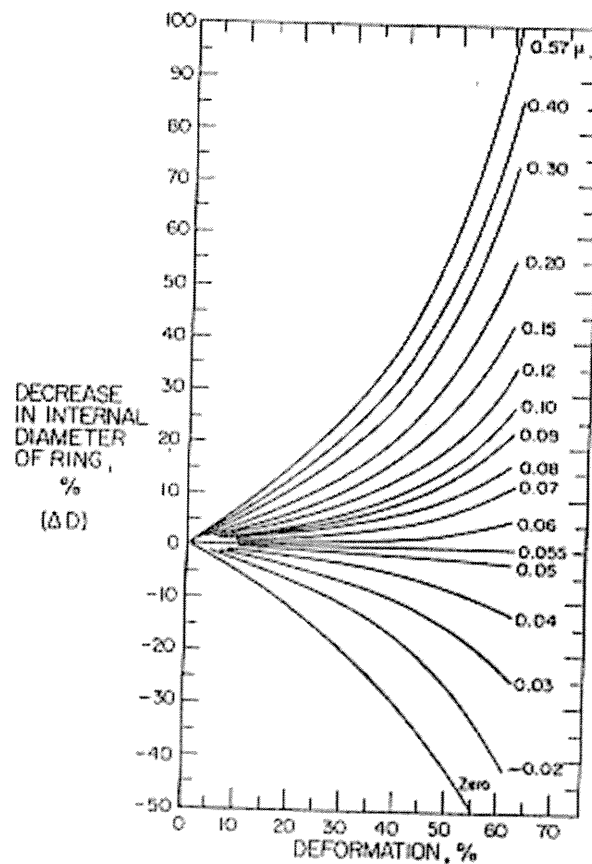


Fig. 3-17 Calibration Curves for the Decrease in Internal Diameter of Standard Rings  
(Outside Diameter:Inside Diameter:Height=6:3:2)

Some uncertainty enters into the evaluation when high friction causes severe barreling in the hole surface. The minimum diameter essentially represents the consequences of inhomogeneous deformation, the diameter measured at the surface is more typical of interface sliding. For most purposes, the minimum inner diameter seems to serve well.

A Variant of the ring compression test is described in which the specimen is upset between two punches, the diameter of which is smaller than the OD of the specimen but larger than the hole (Fig. 3-16h). Lubricant efficiency is again judged from the increase of the bore, but it would appear that the restraint provided by the overhanging, elastically strained material must interfere with evaluation; the test offers no visible benefit over the more generally accepted ring compression test.

### **3.10.5. Plane-Strain Compression**

Plane-strain compression (Fig. 3-16i), originally developed for the accurate determination of the compressive yield strength of materials, has been repeatedly applied for the measurement of friction. A coefficient of friction can be determined from measured compression pressures. Most experimental work has been conducted along one of two different lines.

First, a qualitative rating of lubricants may be obtained by presetting the compressing force and measuring the resulting thickness or, conversely, by compressing to a preset thickness and measuring the maximum force developed. If a coefficient of friction is to be derived, the plane-strain yield strength of the material needs to be known to a great accuracy. This may be achieved by plane-strain indentation with a lubricant that gives close to zero friction and, preferably, with the technique of incremental deformation, in which the surfaces are relubricated after small (2 to 5%) compressive increments. To assure plane strain, the strip width  $b$  should be at least 6-10 times the thickness  $h$ . Also, for the measurement of yield stress, the  $L/h$  ratio should be kept between 2 and 4. If the test is then repeated with the lubricant to be investigated, the coefficient of friction may be derived, for example, from Fig. 3.20b. The determination of  $\mu$  becomes less accurate as  $L/h$  becomes smaller and, in common



with most forging experiments, sensitivity is lost when the coefficient of friction is greater than 0.2. The yield strength of the material need not be known if the test is repeated with a constant reduction in height and with the same lubricant at two L/h ratios, because it can then be taken directly from Fig. 3.22b.

The second technique described may be regarded as a modification of the plane-strain indentation technique. A thick specimen is indented by two cylindrical anvils (Fig. 3-16j); since the indentation force is dependent on penetration, a constant penetration is standardized. From a slip-line field solution, the coefficient of friction may be determined if the indentation stress for zero friction is known. In practice, it is easier to determine the indentation stress in sticking friction with a roughened indenter. Repeating the test with a smooth indenter and the experimental lubricant, the indentation pressure is determined and a coefficient of friction may be obtained. It is not clear whether this test has any advantages over plane-strain compression; deformation and the generation of new surfaces is rather limited, and friction conditions are unlike most of those prevailing in practical deformation processes. Nevertheless, an essentially similar test using constant load instead of a constant indentation has been found useful for a fast and simple ranking of lubricants, particularly at elevated temperatures.

### **3.11. LUBRICATION**

The principle of supporting a sliding load on a friction-reducing film is known as lubrication. The substance of which the film is composed is a lubricant, and to apply it is to lubricate. These are not new concepts, nor, in their essence, particularly involved ones. Farmers lubricated the axles of their ox carts with animal fat centuries ago.

But modern machinery has become many times more complicated since the days of the ox cart, and the demands placed upon the lubricant have become proportionally more exacting. Though the basic principle still prevails—the prevention of metal-to-metal contact by means of an intervening layer of fluid or fluid-like material.

We already mentioned that lubricant is applied to reduce (or control) friction. A good lubricant accomplishes much more: It separates die and workpiece surfaces and thus prevents adhesion with its undesirable side effects of tool pickup, workpiece damage, and die wear; it reduces die wear due to abrasion and other mechanisms; it controls the surface finish of the part produced; and it cools the system in cold working and helps to prevent heat loss (or removes heat at a controlled rate) in hot working. The lubricant must not be toxic or allergenic, it must be easy to apply and remove, and residues must not interfere with subsequent operations or cause corrosion [32].

The most frequently used lubricants and  $\mu$  values are listed in Table 3-3.

### 3.12. INHOMOGENOUS DEFORMATION

There is an important source of high pressures and forces which has nothing to do with interface friction, and, therefore, is not affected by lubrication. It can be best understood from the example of indentation. Inspection of Fig. 3-18a suggests that a small tool cannot possibly deform the entire bulk of a large (semiinfinite) workpiece.

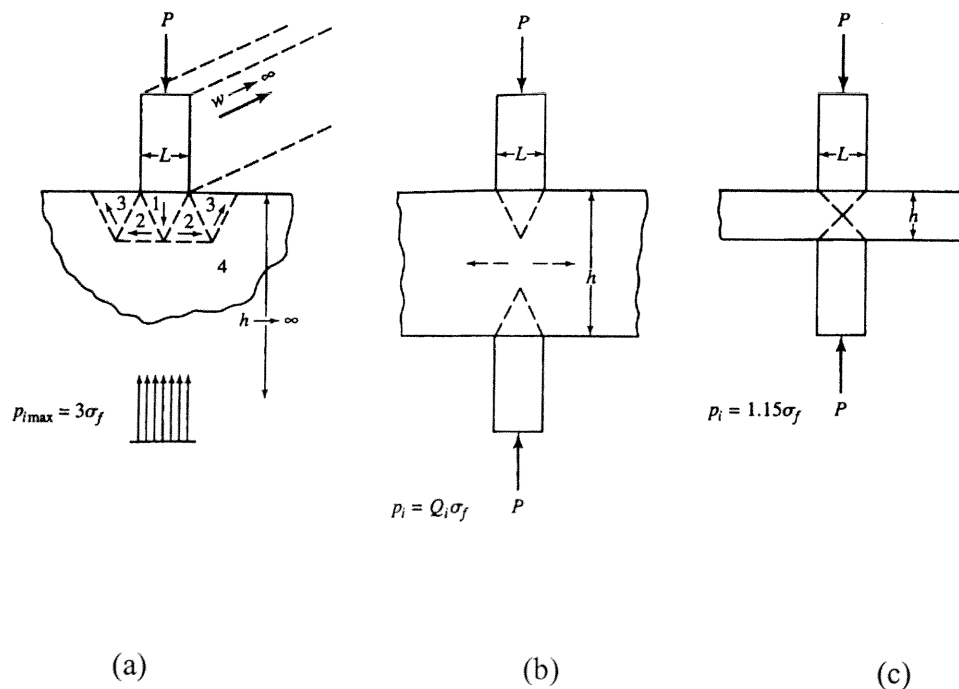


Fig. 3-18 Inhomogeneous Deformation

Indeed, experiments show that when the tool penetrates, highly inhomogeneous material flow takes place.

The mechanism is shown in Fig. 3-18a: a part of the workpiece (1) immediately under the indenter remains immobile relative to the indenter and moves with it as though it were an extension of the indenter itself. This rigid wedge then pushes two triangular wedges (2) beside, which in turn push up two outer wedges (3), thereby forming humps corresponding to the volume displaced by the indenter. The rest of the workpiece (4) is only elastically loaded. The difficulty of moving the material purely locally--against the restraint given by the surrounding elastic material--raises the required interface pressure. Compared to homogeneous deformation, the forging force now has to perform extra work, referred to as redundant work.

In some processes a workpiece of finite thickness is deformed simultaneously from two sides (Fig. 3-18b). Inhomogeneity of deformation then depends on how far the two deformation zones are separated, and this is most usefully expressed by the  $h/L$  ratio, that is, the ratio of height to contact length. It is found from both theory and experiment that when  $h/L > 8.7$ , the two deformation zones are entirely separated; the material between these zones is only elastically deformed and exerts the same restraining effect as though it were of infinite thickness. At lower  $h/L$  ratios the two wedges cooperate (Fig. 3-18b) and the pressure drops.

As might be expected, at a ratio of  $h/L = 1$  the two deformation zones fully cooperate (Fig. 3-18c) and the material flows at a minimum pressure. If the  $h/L$  ratio were to diminish further, deformation would be homogeneous, but friction would now increase die pressures.

Inspection of Fig. 3-18b indicates that the two wedges penetrating from top and bottom tend to tear the workpiece apart; in other words, inhomogeneous deformation generates secondary tensile stresses (i.e., stresses that are not externally imposed but are generated by the process of deformation itself). Several consequences are possible:

- Internal fracture may occur in the workpiece during deformation.
- A residual stress pattern (internal stresses) may be set up that may cause subsequent deformation (warping) of the workpiece, particularly on heating.
- Surface residual tensile stresses can combine with other effects to cause delayed failures (e.g., stress-corrosion cracking in the presence of a corrosive medium).

In general, therefore, the aim of process development is to make deformation as homogeneous as possible, unless internal fracture is intentionally induced. If harmful residual stresses remain, a stress-relief heat treatment is given [29].

### **3.13. BULK WORKABILITY**

Once we have determined that a process is feasible from the point of view of pressure and forces we will want to make sure that the workpiece will survive deformation without fracture. A material of given ductility may fare very differently in various processes, depending on the conditions imposed on it. Therefore, our main concern is not simply ductility, but a more complex property called formability in bulk metalworking operations [29].

Ductile fracture is induced by triaxial tensile stresses imposition of hydrostatic pressure delays fracture. Thus, workability has two components:

- The basic ductility of the material allows it to deform to some extent, without fracture, even in the presence of tensile stresses. Therefore, reduction in area measured in the tension test is a useful (but not universally applicable) measure of basic ductility; it is essentially a measure of resistance to void formation. Other possible measures are the number of turns to fracture in a torsion test, or the reduction in height in compression (upsetting) tests designed to generate high secondary tensile stresses. Upsetting with sticking friction at the end face causes severe barreling and thus surface cracking in a material of low ductility (Fig. 3-19a). Tensile stresses are higher on a collared specimen (Fig. 3-19b) or in a partial-width indentation test (Fig. 3-19c).

- The stress state induced by the process modifies ductility. If the process maintains compressive stresses in all parts of the deforming workpiece (if hydrostatic pressure prevails), cavity formation cannot begin and ductile fracture does not set in. (At very heavy deformations, ductility of the material may be exhausted and then brittle, shear-type fracture may occur.) If the process allows tensile stresses to develop, cavity formation can begin and finally, will lead to fracture.

### 3.14. TEMPERATURE OF DEFORMATION

As it mentioned before,  $0.5T_m$  is a roughly separating line of the hot and cold forming processes [29].

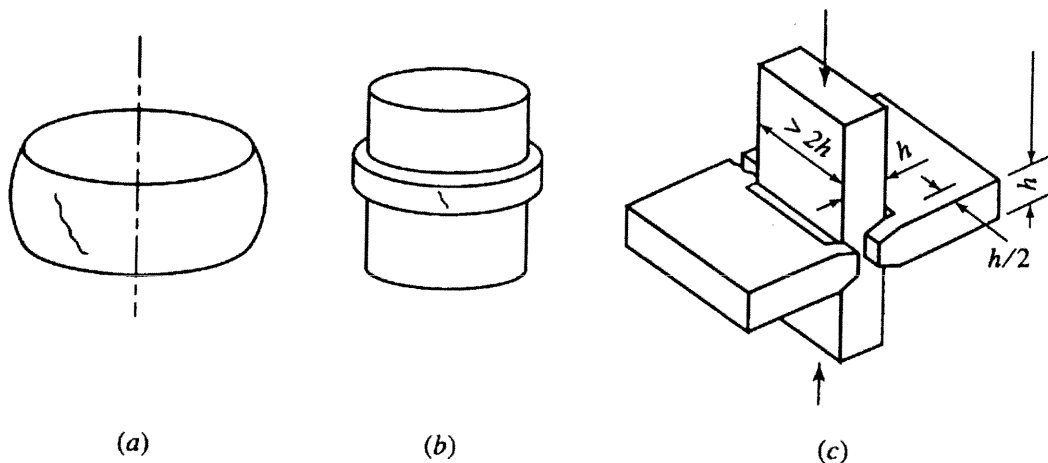


Fig. 3-19 Workability of Materials

#### 3.14.1. Hot Working:

In everyday usage, the term simply refers to the working of preheated material. Usual hot-working temperatures are given in Tables 3-1 and 3-2. Since for most technical materials (except tin and lead),  $0.5T_m$  is above room temperature, the everyday definition is correct also from a materials point of view.

Hot working offers several advantages: Flow stresses are low, hence forces and power requirements are relatively low, and even very large workpieces can be deformed with equipment of reasonable size. Ductility is high, hence large deformations (in excess of 99% reduction) can be taken (usually in a succession of passes) and complex part shapes can be generated. The cast structure can be destroyed by a deformation equivalent to 75% reduction in height or area, although reductions of 90% (10:1 ratio) may be needed if highest properties are to be attained.

There are also disadvantages. It takes energy to heat the workpiece to the elevated temperature. Most materials oxidize and the oxides of some metals (e.g., scale on steel) can impair surface finish. Variations in finishing temperatures can lead to fairly wide dimensional tolerances and also to a less well-defined set of properties in the as-hot-worked condition.

Hot working may be carried out by:

- 1. Nonisothermal forming:** The deforming tool must be several times stronger than the workpiece, and this usually means that the tool must be kept much colder. It is then necessary to minimize contact time to prevent excessive cooling. Cooling of the surface layers of the workpiece has several disadvantages: material flow is retarded; cooling of thin sections limits the minimum wall thickness attainable; die pressure and deformation force increase. Cooling affects the product too, because variable cooling introduces variations in properties. Furthermore, periodic contact with the hot workpiece exposes the tooling to thermal cycling which leads to thermal fatigue.
- 2. Isothermal forming:** Some of the above problems disappear when the tool is at the same temperature as the workpiece. Contact time ceases to be a problem since there is no cooling; however, it is more difficult to find an appropriate tool material and lubricant.

**3. Controlled hot working:** Usually conducted nonisothermally, controlled hot working is used to impart desirable properties.

### **3.14.2. Cold Working**

In the everyday sense, the term refers to working at room temperature, although the work of deformation can raise temperatures to 100-200°C. Cold working usually follows hot working, and scale and other surface films are normally removed by chemical etching (pickling) or shot blasting.

Cold working has several advantages. In the absence of cooling and oxidation, tighter tolerances and better surface finish can be obtained and thinner walls are also possible. The final properties of the workpiece can be closely controlled, and, if desired, the high strength obtained during cold working can be retained or, if high ductility is needed, grain size can be controlled to advantage in annealing. Lubrication is, in general, somewhat easier.

There are also drawbacks. For most technological materials, room temperature is below  $0.5T_m$ ; therefore, flow stresses are high and hence tool pressures, deformation forces, and power requirements are high too. The ductility of many materials is also limited, thus limiting the complexity of shapes that can be readily produced.

### **3.14.3. Warm Working**

This combines some of the advantages of hot and cold working, especially in the warm working of steel (typically between 650 and 700°C). Temperatures are low enough to avoid scaling, thus ensuring a good surface finish, yet they are high enough to reduce flow stress and thus allow the forming of parts that would generate excessive die pressures in cold working. The elevated temperature results in substantial strain-rate sensitivity, and the flow stress remains low only if strain rates are kept low.

### 3.15. STEADY-STATE PROCESSES

In these, all elements of the workpiece are subjected successively to the same mode of deformation. Thus, once the situation is analyzed for the deformation zone, the analysis remains valid for the duration of the process. Drawing of a sheet in plane strain can be taken as the generic case (Fig. 3-20a). The workpiece strain-hardens or suffers other changes as it passes through the deformation zone, and, to simplify computations, a mean flow stress  $\sigma_{fm}$  is used. For cold working, this is found by integrating Eq. (3-8) between the limits of strains:

$$\sigma_{fm} = \frac{K}{\varepsilon_2 - \varepsilon_1} \cdot \left[ \frac{\varepsilon_2^{n+1} - \varepsilon_1^{n+1}}{n+1} \right] \quad (3-22)$$

For annealed material,  $\varepsilon_1 = 0$ , so:

$$\sigma_{fm} = \frac{K}{\varepsilon} \cdot \left[ \frac{\varepsilon^{n+1}}{n+1} \right] \quad (3-23)$$

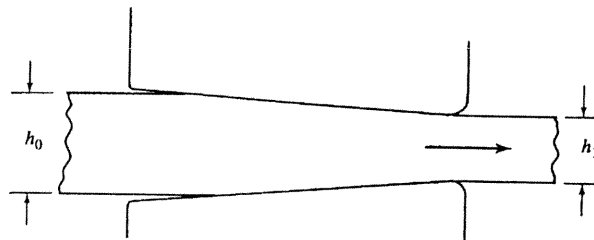


Fig. 3-20a Steady-State Cold Working, Material Subjected to Strain Hardening during passaging through Die

Alternatively, the flow stress curve is plotted and the mean is found by visual averaging (Fig. 3-20b). For hot working, a mean strain rate specific for the process is computed and the flow stress is taken from Eq. (3-13).



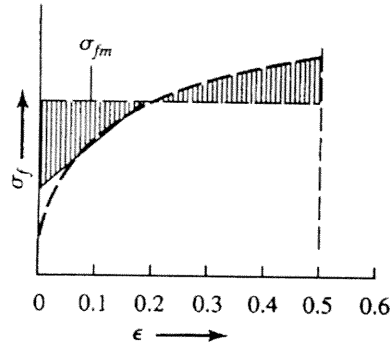


Fig. 3-20b The Mean Flow Stress from The True Stress-True Strain Curve

### 3.16. NON-STEADY STATE PROCESSES

In processes such as compression, the geometry of the part changes continually (Fig. 3-21a) and the analysis must be repeated for various points in time, from the starting condition to the end of the stroke. Thus, the instantaneous flow stress  $\sigma_f$  at the point of interest must be taken (Fig. 3-21b), from Eq. (3-8) for cold working and from Eq. (3-13) for hot working. It often happens that we are concerned only with the maximum force, developed at the end of deformation, and then the flow stress corresponding to the final strain is used.

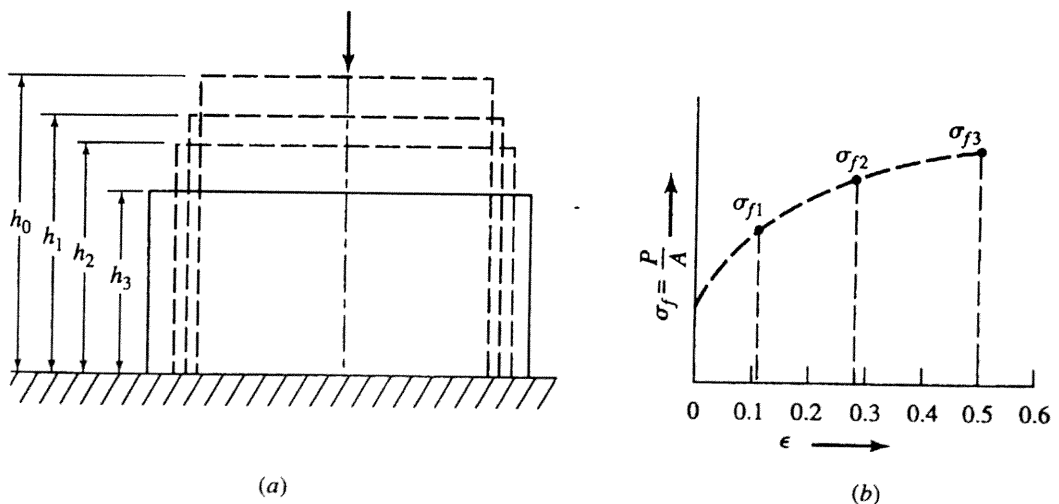


Fig. 3-21 Non-Steady State Processes

### 3.17. FORGING

Forging processes are among the most important manufacturing techniques. Three broad groups can be distinguished: open-die forging allows free deformation of at least some workpiece surfaces; deformation is much more constrained in impression-die forging and is fully constrained in closed-die forging. Because at least one of the workpiece surfaces deforms freely, open-die forging processes produce workpieces of lesser accuracy than impression or closed-die forging; however, tooling is usually simple, relatively inexpensive, and allows the production of a large variety of shapes. More complex shapes cannot be formed with great accuracy by open-die forging techniques. Specially prepared dies are required that contain the negative shape of the forging to be produced: The process is simplified to a sequence of simple compression strokes at the expense of a complex die shape [28].

In one variant of the process (Fig. 3-22) the shape is obtained by filling out the die cavity defined by the upper and lower die halves. Excess material is allowed to escape into the flash; since the die is not fully closed, it is properly called an impression die. The term closed-die is, nevertheless, sometimes applied, and the term drop forging has been used to denote forging conducted on a hammer; however, this distinction has no particular technical merit [29].

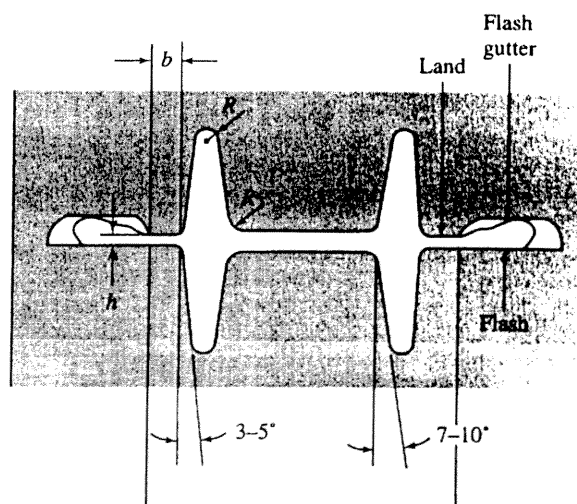


Fig. 3-22 Impression Die Forging

In true closed-die forging the workpiece is completely trapped in the die and no flash is generated. Economy of forging is thus increased, but die design and process variables must be very carefully controlled. At the end of the stroke the cavity is completely filled with an incompressible solid, and die pressures rise very steeply; this becomes a critical factor in setting up the equipment.

A special case of closed-die forging is coining, in which a three-dimensional surface detail is imparted to a preform. The largest application is, of course, to the minting of coins, but coining is useful for improving the dimensional accuracy, surface finish, or detail of other parts too. The forging pressure is at least  $p_i = 3\sigma_f$ , but filling of fine details calls for pressures of  $5\sigma_f$  or  $6\sigma_f$ .

Due to the fact that our concern is to investigation of the flow mechanism in closed-die forging, we are especially deal with the deformation in closed type process. So the upsetting procedure is as follows;

1. The volume of the work or billet is found,
2. Final dimensions of the work piece is calculated benefitting the constancy of the volume. As an aim, the final projected area and the final height of the finished part carrying separate importance for calculating the force or pressure and true strain or strain rate needed.
3. Flow stress for cold working or the strain rate for hot working is computed. For conversational purposes compressive engineering stress can be calculated.
4. The relevant flow stress for cold working is computed by using the Eq. 3-8 and strain rate for hot-working is computed from Eq. 3-13.
5. Now here is the most crucial points for caculating the die pressure we have to care about; a)stress state, b)friction, c)inhomogenity of the deformation.
  - The stress state is uniaxial, hence the flow stress or strain rate is  $\sigma_f$ .
  - Investigate the friction condition
  - For inhomogenity of deformation, investigate the indentation condition, benefitting the  $h/L$  ratio.
6. The press force is calculated by multiplying the interface pressure with the contact area.

## **3.18. FORGING EQUIPMENTS**

### **3.18.1. Hammers and Presses for Forging**

Hammers and Presses for forging may be considered in two groups: for closed-die forging and those open-die work. Some simple open-die forging can be done in a closed-die forging hammer, and occasionally an open-die forging hammer is used with closed dies; however, this is uncommon. Two or more pieces of equipment may be used to produce a specific forging; for instance, a power hammer using flat dies for pancaking and then another hammer or a press for forging in closed dies [6].

### **3.18.2. Closed-Die Forging Hammers**

With the exception of the counter-blow hammer, forging hammers have a weighted ram, which, when it moves vertically in a downward stroke, exerts a striking force against a stationary component of the anvil near the base of the hammer. The upper half of a pair of closed dies is fastened to the weighted ram, and the lower half to the anvil cap. The work metal (in the form of a heated bar, billet, bloom or ingot) is placed on the lower die, and striking force is imposed on the work metal by the upper die and ram, causing it to deform plastically with successive blow. Although all hammers operate on the principle of high impact depending on the method of actuation. Common types of hammers include gravity drop hammers (board or air-lift) and power drop hammers (steam or air-driven).

#### **3.18.2.1. Board Drop Hammers**

Board drop hammers are widely used especially for producing forgings weighing no more than a few pounds. In the board drop hammer, the ram is lifted by one or more boards keyed to it and passing between two friction rolls at the top of the hammer. The boards are rolled upward and are then mechanically released, permitting the ram to drop from the desired height. Power for lifting the ram is supplied by one or more motors. The hammers have a falling weight, or rated size, of 180 kg to 4.5 tons; standard sizes range from 455 kg to 2.3 tons, in increments of 230 and 455 kg. The

height of fall of the ram varies with hammer size, ranging from about 90 cm. for a 180 kg hammer to about 2 m for a 3.5 ton hammer. The height of fall, and thus the striking force, of the hammer is approximately constant for a given setting and cannot be altered without stopping the machine and adjusting the length of stroke. Anvils on board drop hammers are 20 to 25 times as heavy as the rams. Components of a typical board drop hammer are shown in Fig. 3.23.

In using the board drop hammer for closed-die forging, the heated metal for forging is placed over the cavity in the lower die, and the ram and top die drop when the operator releases the board clamp (usually by means of a foot treadle). When the treadle is depressed and released by the operator, the ram drops once and returns to its raised position, where it remains until it is again released. The operator can cause successive blows to be struck by keeping the treadle depressed. In practice especially in the production of small, simple closed die forgings, usually the hammer is allowed to strike successive blows while the operator moves the work piece from one impression to another without stopping the hammer. Since the stroke length is fixed, to provide the proper height of fall for the specific dies in the hammer, light and heavy blows to the workpiece can not be interspersed.

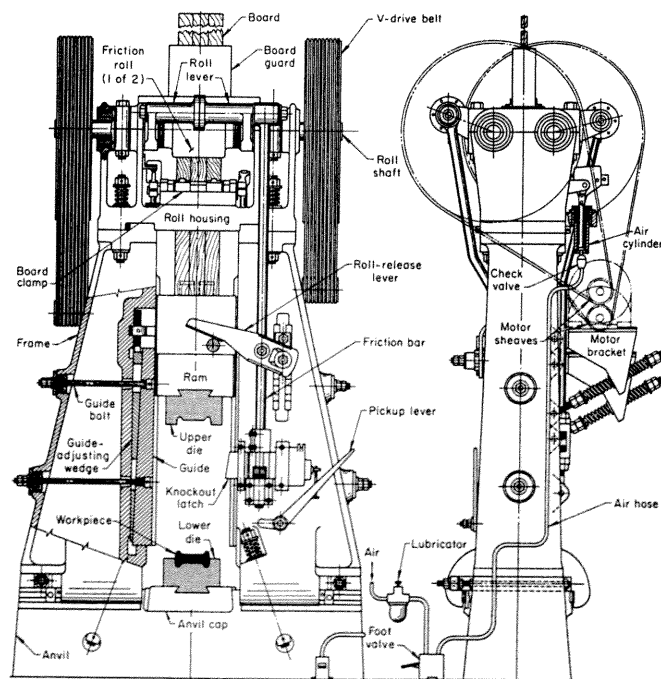


Fig. 3.23. Principal components of a Board Drop Hammer

### **3.18.2.2. Air-Lift Gravity Drop Hammers**

The air-lift gravity drop hammer is similar to the board hammer in that the forging force is derived from the weight of the falling ram assembly and upper die. It differs in that the ram is raised by air or steam power. Stroke-control dogs, preset on a rocker and actuated by the ram, control power to the ram cylinder. With the hammer shut down, the dogs can be reset on the rocker to adjust stroke length. A device that allows both a long stroke and a short stroke, in a variable sequence, is available.

The ram is held in the raised position by a piston-rod clamp, which is operated by its own cylinder using a separate compressed-air supply. When the clamp is oblique, the piston rod is clamped. When the operator's treadle is depressed, air enters the cylinder and raises the clamp horizontally, and the ram cycles. Cycling will continue until the treadle is released causing the rod clamp to drop obliquely and grip the rod. The treadle should not be released on the downstroke of the ram, because this will produce excessive strain in the rod and clamp parts.

The range of sizes generally available in air-lift hammers is 225 kg to 5 tons. The weight of forging that can be produced in an air-lift hammer of any size is about the same as can be produced in its board hammer counterpart.

### **3.18.2.3. Power Drop Hammers (Steam Hammers)**

The term "power drop hammer" has come into use because "steam hammer" is no longer adequately descriptive. Many hammers of this general type are actuated by air rather than steam. Components of a steam or air-actuated power drop hammer are shown in Fig. 3.24. This equipment is used almost exclusively for closed-die forging.

Power drop hammers differ in principle from air-lift gravity hammers in that steam (or air) under pressure of 65 to 90 tons/m<sup>2</sup> supplements the force of gravity in the downward stroke. The steam or air-powered drop hammer is the most powerful machine in general use for the production of closed-die forgings by impact pressure. In a power drop hammer, a heavy anvilblock supports two frame members that

accurately guide a vertically moving ram; the frame also supports a steam cylinder that, through a piston and piston rod, motivates the ram. In its lower face, the ram carries an upper die, which contains one part of the impression that shapes the forging. The lower die, which contains the remainder of the impression, is keyed into an anvil cap that is firmly wedged in place on the anvil. The motion of the piston is controlled by a valve, which admits steam to the upper or to the lower side of the piston. The valve in turn is controlled by a foot treadle or a hand lever.

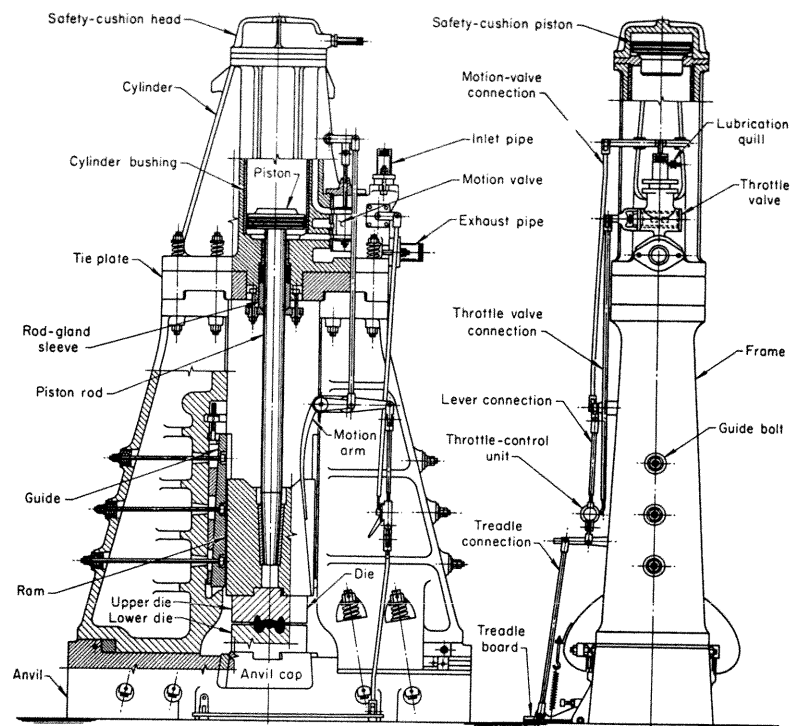


Fig. 3.24. Principal Components of a Power Drop Hammer with Foot Control to Regulate the Force of the Blow

Power drop hammers are rated by the weight of the striking mass, not including the upper die. Hammer ratings range commonly from 230 kg to, 15.5 tons, and occasionally to 23 tons.

#### 3.18.2.4. Counterblow Hammers

These hammers develop striking force by the movement of two rams, simultaneously approaching from opposite directions and meeting at a midway point. Some

hammers are pneumatically or hydraulically actuated; others incorporate a mechanical-hydraulic or a mechanical-pneumatic system.

A vertical counterblow hammer with a steam-hydraulic system is shown schematically in Fig. 3.25.

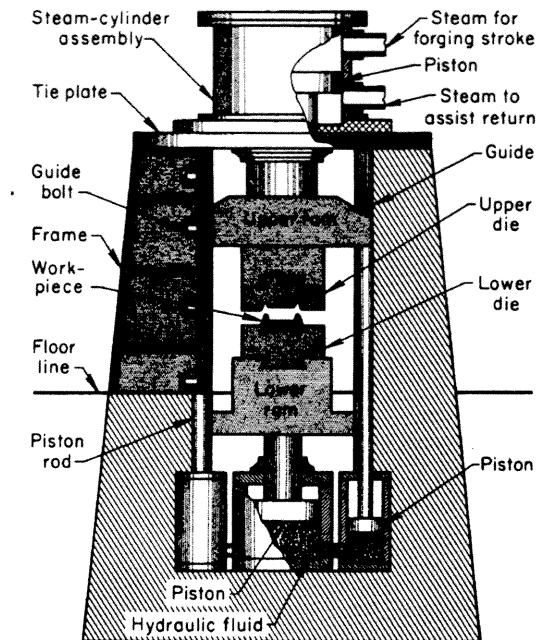


Fig. 3.25. Components of a Vertical Counterblow Hammer with a Steam Hydraulic Actuating System

### 3.18.3. Open Die Forging Hammers

A general forging hammer is operated by steam or compressed air, usually at pressures of 70 tons/m<sup>2</sup> to 85 tons/m<sup>2</sup> for steam and 65 tons/m<sup>2</sup> to 70 tons/m<sup>2</sup> for compressed air. These conditions are similar to those of the power drop hammer used for closed-die forging.

Open-die forging hammers are made either with a single frame (these are often known as C-frame or single-arch hammers) or with a double frame (often called double-arch hammers).



Single-frame hammers (Fig. 3.26) have rated sizes of about 500 kg to 3 tons. (Ratings for all hammers are based on the weight of their striking parts, which are the ram, piston, piston rod and top die.) A single-frame hammer is designed so that the hot metal can be placed between the dies from either side of the hammer as well as from the front. The front face of the anvil usually is set at an angle of about  $35^\circ$  to the front line of the hammer, to permit forging of long bars without frame interference. Ability to forge at almost any position around the anvil is advantageous for many open-die forgings, particularly if they have unusual combinations of length, width and twist.

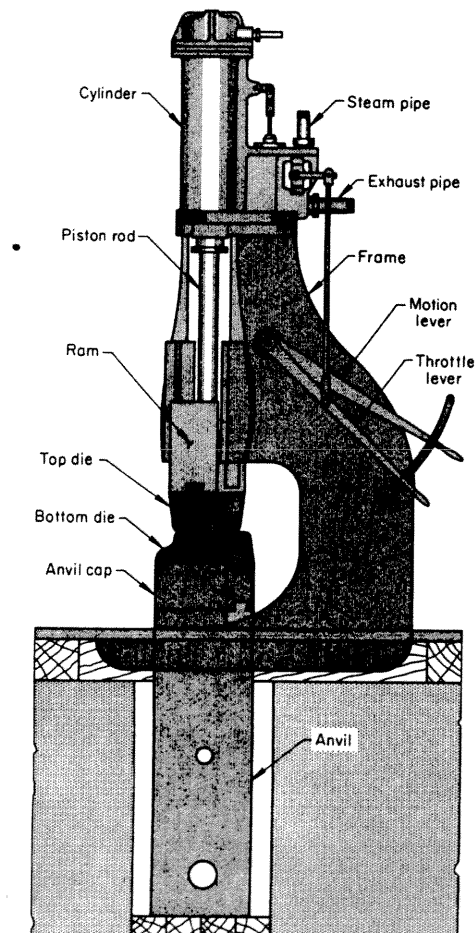


Fig. 3.26. Single Frame Power Hammer used for Open-Die Forging

A double-frame general forging hammer (Fig. 3.27.) usually has rated sizes of 2.5 tons to 11 tons. An advantage of a double-frame hammer is that the ram is rigidly guided. This makes it desirable for production work and general forging where

rigidity is needed, and for forging of high-strength steels, heat-resisting alloys, or other high strength metals.

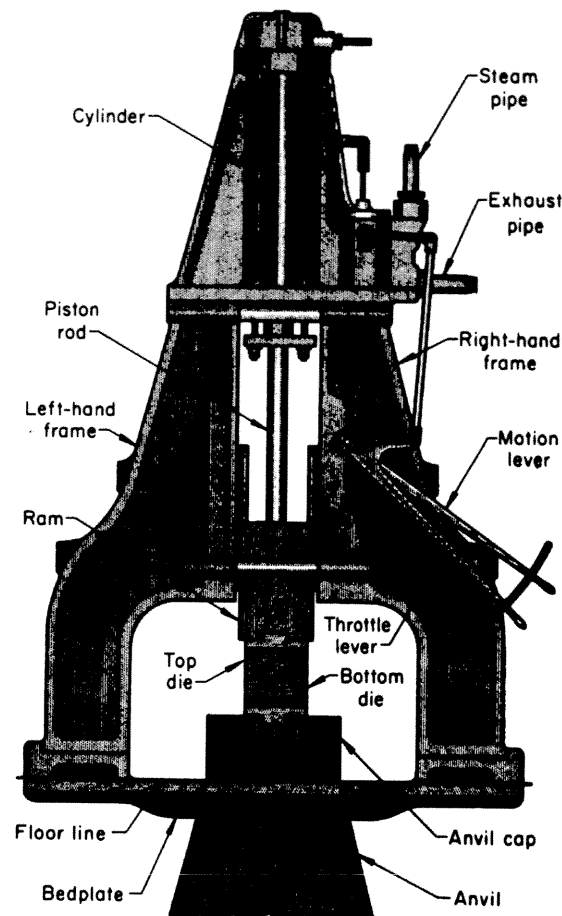


Fig. 3.27. Double-Frame Power Hammer used for Open-Die Forging

#### 3.18.4. Closed Die Forging Presses

Forging presses generally incorporate a ram that moves in a vertical direction to exert a squeezing action on the workpiece, in contrast with the repeated blows characteristic of hammer forging. Depending on their source of power, forging presses are classified as mechanical or hydraulic. Maximum capacities exceeding those of the largest power drop hammers are developed by hydraulic presses. In general, presses can produce all of the types of forgings produced by hammers and, in addition, can forge some alloys of moderate ductility that would shatter under the blows of a hammer.

### 3.18.4.1. Mechanical Presses

Driven by a motor and controlled by an air clutch, mechanical presses have a full-eccentric type of drive shaft that imparts a constant-length stroke to a vertically operating ram (Fig. 3.28). The ram carries the top (or moving) die, whereas the bottom (or stationary) die is clamped to the die seat of the main frame. The ram stroke is shorter than that of a forging hammer or a hydraulic press. Ram speed is greatest at the center of the stroke, but force is greatest at the bottom of the stroke. Because of the short stroke, mechanical presses are best suited for low-profile forgings. Capacities of these forging presses are rated on the maximum force they can apply, and range from about 300 to 8000 tons.

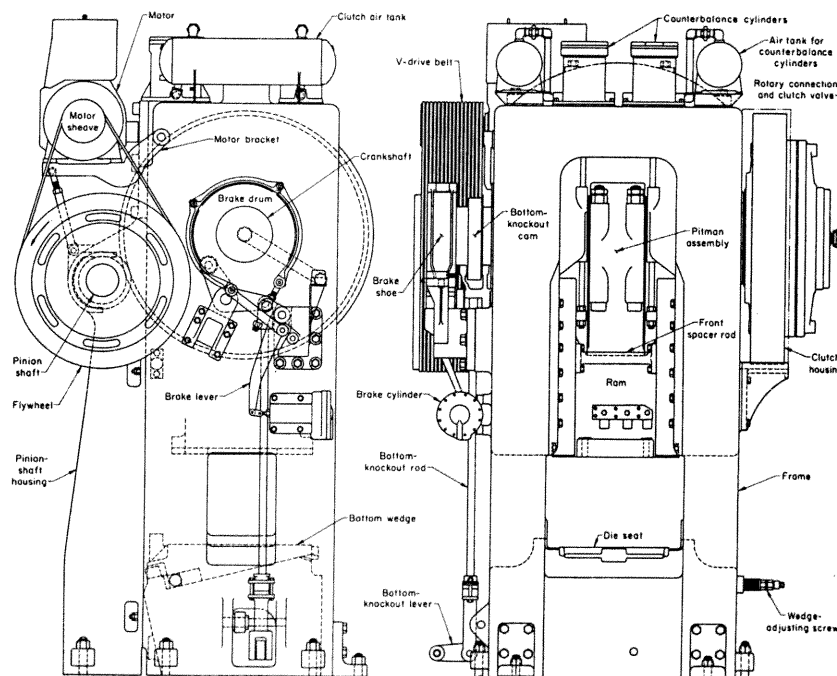


Fig. 3.28. Components of a Mechanical Forging Press

Some-advantages of mechanical forging presses are:

1. Higher production rates are possible with presses than with hammers. Many forging presses can deliver up to 70 strokes per minute.
2. Because the impact is less in presses than in hammers, dies can be less massive, thus requiring less tool steel to make the dies. If desired, cast dies can be used.

Also because presses deliver a less severe impact blow, can be operated at higher hardness, which prolongs die life.

3. Presses require less operator skill than is required for hammers.

Some disadvantages of mechanical forging presses are:

1. Initial cost is high as much as three times the cost of a hammer that will produce the same forging.
2. A press delivers consecutive strokes of equal force, and therefore is less suitable for preliminary shaping operations such as fullering or rollering.
3. Presses are generally less suitable for forging unsymmetrical workpieces than are hammers.

#### **3.18.4.2. Hydraulic Presses**

The ram of a hydraulic press is driven by hydraulic cylinders and pistons, which are part of a high-pressure hydraulic or hydropneumatic system. Following a rapid approach speed, the ram (with upper die attached) moves at a low speed while exerting a squeezing action on the work metal, which is retained in the lower die. Pressing speeds can be accurately controlled, thus permitting control of metal-flow velocities. This feature is particularly advantageous in producing close-tolerance forgings. Principal components of a hydraulic press are shown in Fig. 3.29. Capacities for hydraulic presses range from 300 to 50,000 tons.

The principal advantages of hydraulic presses are:

1. Pressure can be changed, as desired, at any point in the stroke by adjusting the pressure control valve.
2. Rates of deformation can be controlled, and even varied during the stroke if required. This is especially important in the forging of metals that will rupture if subjected to high deformation rates.
3. By the use of split dies, many parts are made with offset flanges, projections, back draft, and other design features that are extremely difficult, if not impossible, to incorporate in hammer forgings.

4. When excessive heat transfer (from the hot workpiece to the dies) is not a problem, or can be eliminated, the gentle squeezing action of a hydraulic press results in lower maintenance cost and increased die life because of less shock compared with other types of forging equipment.

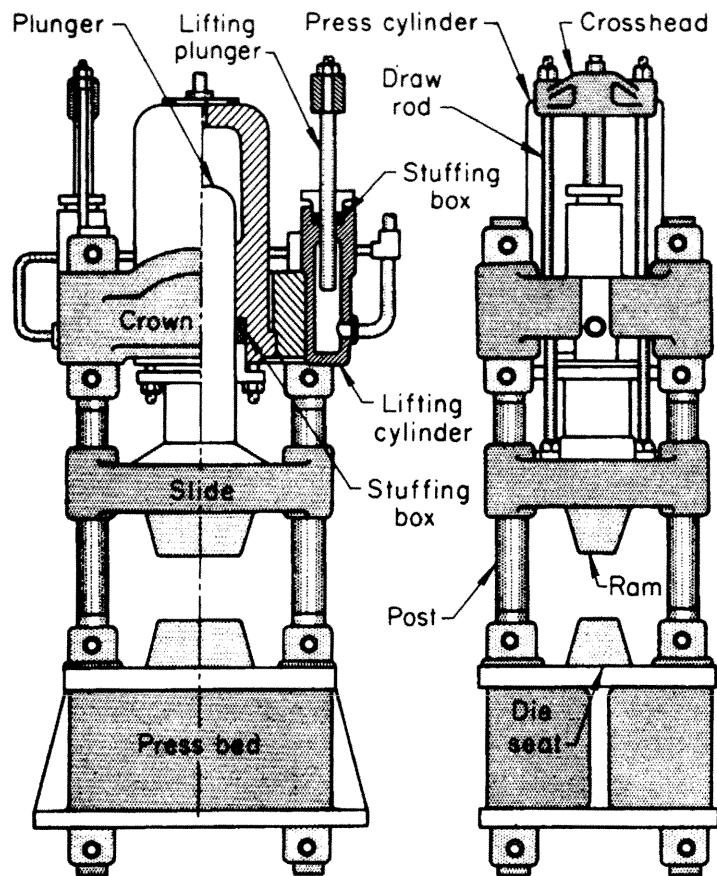


Fig. 3.29. Components of four-post Hydraulic Press for Closed-Die Forging

Some of the disadvantages of hydraulic presses are:

1. The initial cost of a hydraulic press is higher than that of a mechanical press of equivalent capacity.
2. The action of a hydraulic press is slower than that of a mechanical press.
3. The slower action of a hydraulic press permits longer contact between the dies and the workpiece; thus die life is sometimes shortened because of heat transfer from the hot workpiece to the dies.

### **3.18.5. Open Die Forging Presses**

Hydraulic forging presses designed for open-die forging work are used for medium-size and large open-die forgings made from almost any metal. Capacity of these presses ranges from 1900 to 20,000.tons of force.

The basic difference between the hydraulic forging presses used mainly for closed-die forging and those used for open-die forging is the same as between general open-die forging hammers and the closed-die power hammers.

## **3.19. GENERAL CRITERIA FOR FORGING DIE-DESIGN**

### **4.19.1 Strength**

In precision forging, die components are subjected to high loads in a very short period of time. Components must withstand high static and impact pressures, friction between the workpiece and die surfaces, and both mechanical and thermal fatigue. Although the workpiece is plastically deformed under compression, the working stresses in the dies are a complex combination of tension, compression and shear. Actually the stresses on the die insert change from a built-in compressive stress (as a result of shrink ring assembly) to a high tensile stress condition with every stroke of the press. Both punch and ejector are subjected to a change from zero stress to extremely high compressive loads in a fraction of a second, which can lead to early fatigue failure. This is particularly critical when the punch is subjected to bending stress in addition to the compressive loads. The die must withstand these fatigue stresses.

### **4.19.2. Wear resistance**

According to permitted post-forging machining of stock on the precision forged parts, there is very little or no wear allowance made for the die members. The service life of a precision forging die is therefore, mostly dependent on wear. The number of die components subjected to wear and maximum working stresses should be kept to a

minimum. Good design allowing for easy lubrication and hardening of parts reduces wear.

#### **4.19.3. Kinematics**

The kinematics of a die must be so chosen as to minimise loads by obtaining the correct sequence of filling in the die cavity. Good alignment must be maintained between the punch and die insert to avoid deflection, bending and premature failure of the punch. This can be accomplished by adequate guiding of the press itself, and proper design of the die.

#### **4.19.4. Accuracy**

Accuracy of forged parts depends mostly on the accuracy of the die, especially for complex parts like gears. Production of precision parts requires design and manufacture of dies with consistent accuracy. Dimensional changes to the die member, due to load and temperature changes, should be calculated.

#### **4.19.5. Performance**

Proper design of the precision forging die should allow easy loading and removal of the workpiece without distorting it. It should eliminate direct clashing of the punch and the die insert. Scale and lubricant deposits must be easily removable from the die cavity and sticking of the workpiece to die members has to be eliminated.

#### **4.19.6. Shrink Rings**

In Fig. 3.30, various shrink ring designs are illustrated. cylindrical shrink fits are simpler to produce, but can only be used up to interferences which can be achieved by warm shrink fitting, in order to avoid cold welds during assembly [28]. Tapered shrink fits permit simpler, scratch-free disassembly. A drawback of this method are the high production costs. The tapered shrink fit exhibits different levels of radial pre-stress, which can lead in case of very long containers to dimensional

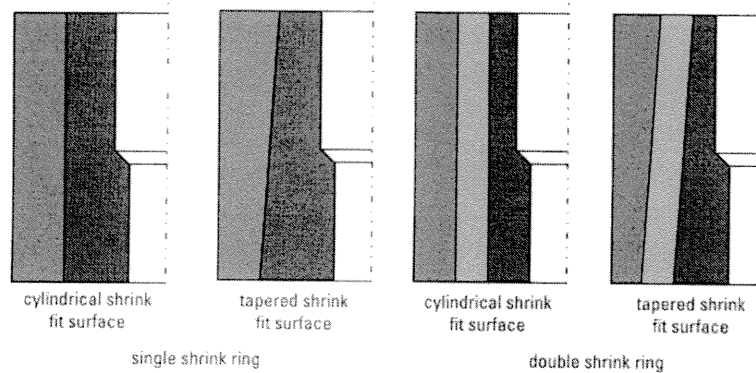


Fig. 3.30. Shrink Rings of Dies

differences on the forged part. Usual taper angles are 0.5 and 1°; if the height to diameter ratio of the container is below 0.8, taper angles of 2 to 3° are used in order to avoid disassembly of the shrink rings during part ejection. These assume an ideal loading situation where an infinitely long thick-walled cylinder is subjected to a constant hydrostatic pressure over its entire length. Using Tresca's yield condition, which can be applied in this case, the stress distribution can be calculated. It is found that the maximum values are at the internal wall of the container and correspond approximately to the value of the internal pressure  $P_i$ , for radial stress  $\sigma_r$  and tangential stress  $\sigma_t$  (Fig. 3.31.a). The internal pressure ;

$$\sigma_v = \sigma_r + \sigma_t = 2 \cdot P_i \quad (\text{Eq. 3.24})$$

If, in the case of thick-walled pipes subjected to internal pressure, the effective stress exceeds the yield strength of a material with sufficient toughness, then plastic flow occurs at the inside wall of the container. If the ultimate strength is reached in containers or inserts from brittle materials, cracks occur.

As a result of adding compressive stress, the tangential stress and thus also the effective stress status at the inside wall of the extrusion container (or insert) are reduced (Fig. 3.31.b/c). The radial pre-stress is generated by means of shrink rings. A



shrink ring has an internal diameter that is smaller than the outer diameter of the corresponding inner ring by a selected dimension (interference). By maintaining the outer diameter unchanged, the permissible internal pressure can be increased by up to 100 % as a result of the shrink ring compared to a container without a shrink ring. For a given permissible internal pressure, the outside diameter of the container, using shrink rings, can be reduced by about 60%. In multiple-station forming machines this results in a substantial reduction of die diameters, the distances between stations, the dimensions of the die holder and thus also the machine bed size [28].

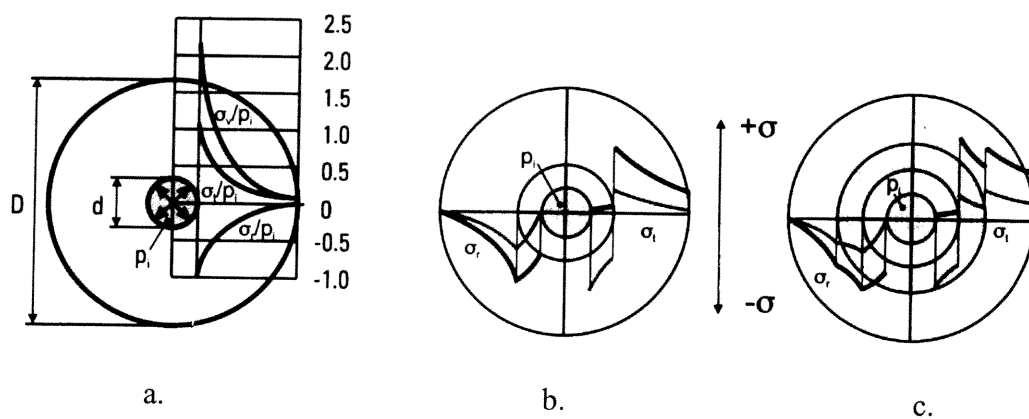


Fig. 3.31. Theoretical Stress Distribution in a Thick-Walled Cylinder

#### 4.20. FACTORS IN THE SELECTION OF DIE MATERIAL

Die steels are selected on the basis of the following characteristics [28]:

1. Ability to harden uniformly
2. Ability to resist the abrasive action of the hot metal while it is being forged
3. Ability to withstand high pressure and heavy shock loads
4. Ability to resist cracking and checking caused by heat.

Selection of the most suitable combination of steel and hardness for die blocks and die inserts is influenced by [28]:

1. Shape, size and weight of the forging
2. Composition of the metal to be forged
3. Temperature at which the work metal is to be forged

4. Number of forgings to be made
5. Type of forging equipment (hammer or preas)
6. Cost of the die steel
7. Sequence of machining the die impressions (before or after hardening)
8. Forging tolerances (including those specified for draft angles)
9. Established plant practice and previous experience with similar applications
10. Availability of auxiliary equipment.

## **CHAPTER 4**

### **EXPERIMENTAL SET-UP AND DIE DESIGN**

#### **4.1. INTRODUCTION**

In this chapter, the press used for experiments and its working principle is explained. Then the product and preform geometries are determined and the die and the punches are designed.

#### **4.2. PRESS USED FOR EXPERIMENTS:**

The hydraulic press and its graphic unit was used through out experiments (Fig. 4.1 and Fig. 4.2). As being shown in Fig. 4.1, single piston press was used in experimental study which has a capacity of 60 tons. The upper ram is stationary. However, the lower ram, also the die seat, moves upward and downward directions. The velocity of the die seat is controlled by means of the velocity control handle (Fig. 4.1). As the die seat of the press goes upward or downward (loading or unloading directions respectively), the drum rotates by means of the pulleys. Force – distance graphic is obtained on the scaled (milimetric) paper rolled on the drum. Rising and lowering the press bed is carried out by the loading and unloading arm. As the loading/unloading is carrying on, the force is read on the screen. The pulleys transmit the movement of the die seat to the drum by means of the rope rolled on pulleys and drum, Fig. 4.3 balancing weight is used for providing friction between the rope and the drum as well as keeping the rope in stretched form. As the

die seat moves up/down, pulley 1, that is fixed to the press body, transmits the motion to the pulley 2. Pulley 3 rotates the pulley 5 as a result, the rotation of drum is carried out as seen in Fig. 4.3, which illustrates the mechanism schematically.

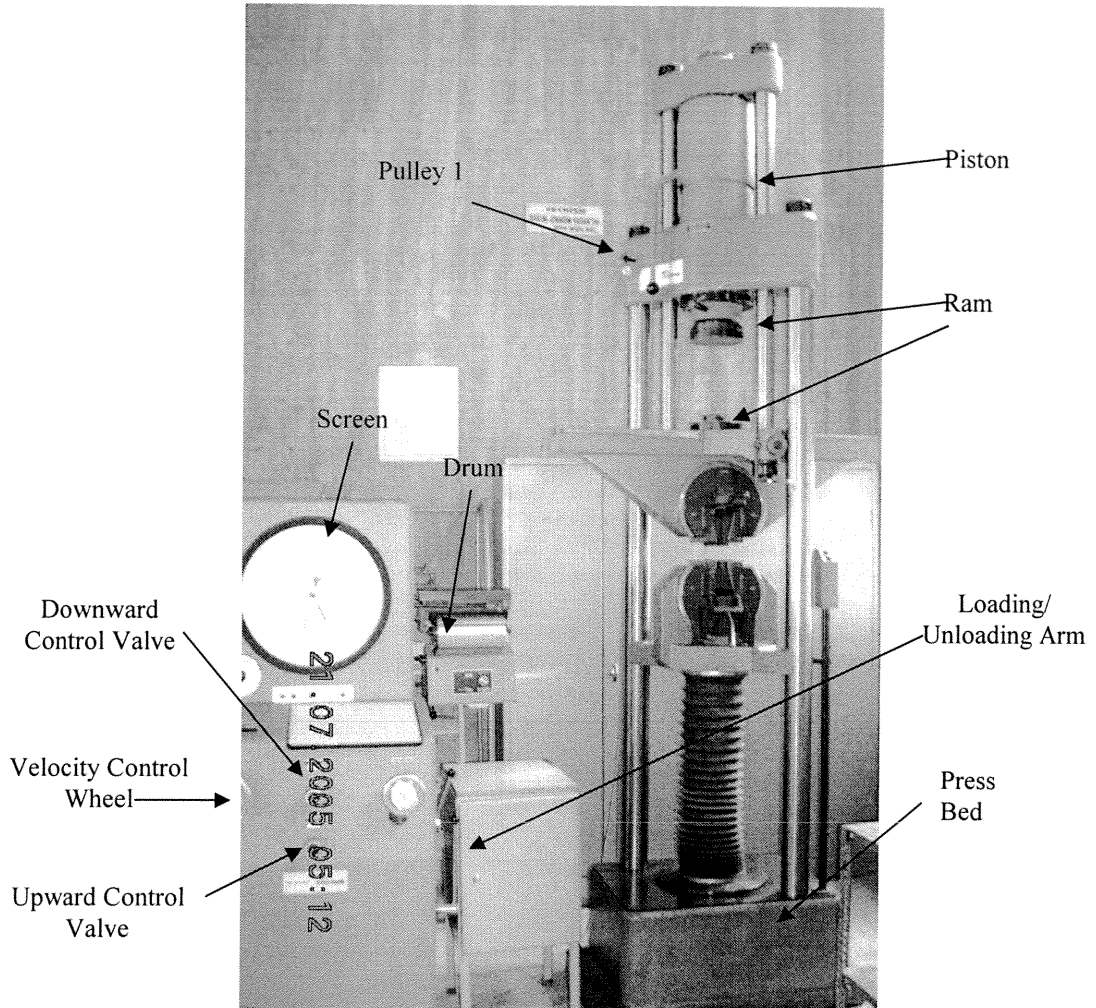


Fig. 4.1. Press Used for Experimental Studies

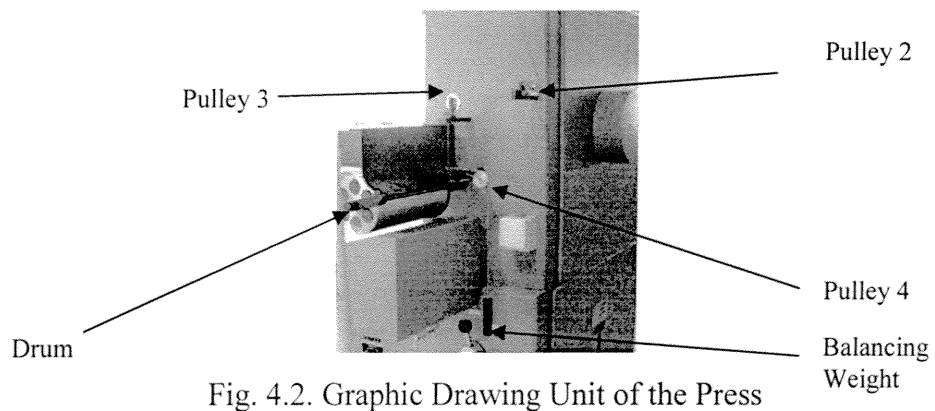


Fig. 4.2. Graphic Drawing Unit of the Press

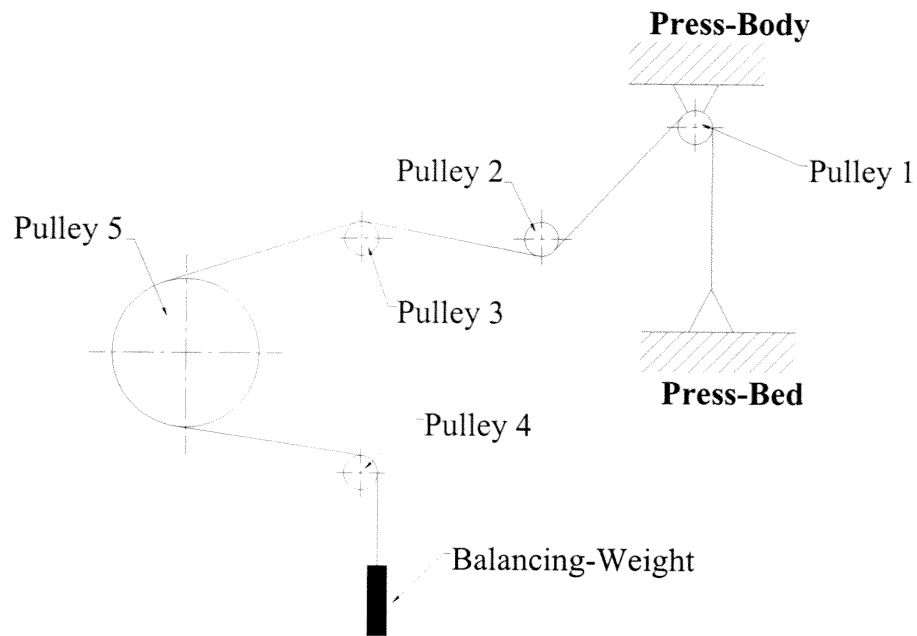


Fig. 4.3. Schematical Graphic Drawing Unit

#### 4.3. PRODUCT AND PREFORM GEOMETRY

In order to investigate the flow structure, the flow directions should be identified. Two main flow directions should be considered which are upset and extrusion. Extrusion is the flow of material in the direction parallel to the axis of motion of punch. But, upsetting is the flow of material in the direction perpendicular to the movement axis of the punch. Billets are so designed concerning the flow directions defined as follows;

- only extruded mode,
- only upsetting mode (flow to the central and/or from central directions),
- both extruded and upsetting modes.

Firstly, the geometries of the finished products will be obtained, then the billets will be identified concerning the volume constancy and flow directions.

At the end of the forging process, it is desired to obtain U-shape, T-shape and H-shape products, Fig. 4.4.

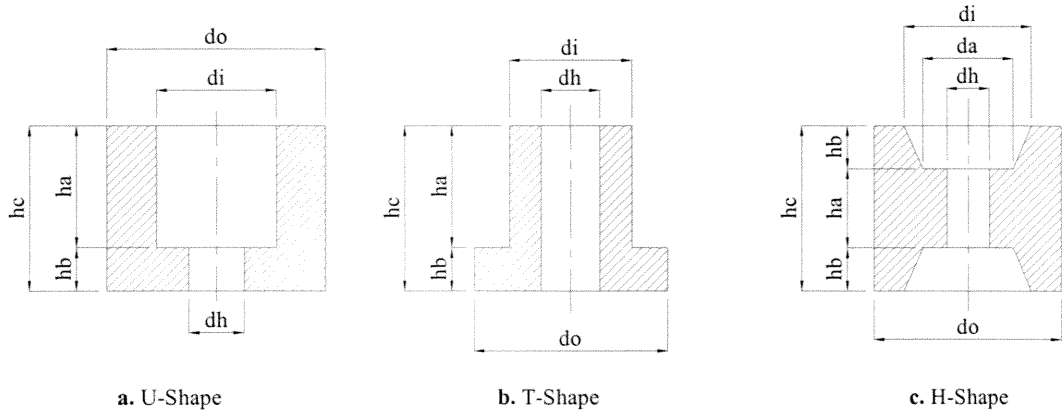


Fig. 4.4. Forging Products

**Product Geometries :** It is shown the dimensionless drawings of the U-shape, T-shape and H-shape as finished workpieces (Fig. 4.4). The dimensions of the parts are chosen according to the loading capacity of the press. So, the maximum load is assumed as 50 tons for calculating the dimensions of the finished parts.

For calculating the dimensions, firstly U-shape shall be taken into account then the maximum diameter, calculated for U-Shape, is benefitted for T and H-Shapes' designs.

$$F \leq 50 \text{ tons} \quad (\text{Eq. 4.2.})$$

$$P \leq F \quad (\text{Eq. 4.3.})$$

$$P = \sigma_f \cdot Q_c \cdot A_t \quad (\text{Eq. 4.4.})$$

$$Q_c = 5 \text{ (Table G.1/Appendix G)} \quad (\text{Eq. 4.5.})$$

$$A_t = \frac{\pi}{4} \cdot (d_o^2 - d_h^2) \quad (\text{Eq. 4.6.})$$

$$\sigma_f = K \cdot \varepsilon_{ave}^n \quad (\text{Eq. 4.7.})$$

Materials used in experiments are Al 1050 for cold forging and Pb for hot forging. But the designs should be carried out according to the cold forging process, due to the fact that force suffered in cold forging process is to be higher than the force needed in hot forging process for the same workpieces. So; for Al 1050 the strength

coefficient and the strain hardening exponent are 140 and 0.25 respectively, see Table E.1, Appendix E.

$$\varepsilon_{ave} = \ln \frac{h_o}{h_{ave}} \quad (\text{Eq. 4.8.})$$

$$h_{ave} = \frac{V}{A_t} \quad (\text{Eq. 4.9.})$$

$$V = \frac{\pi}{4} \cdot (d_o^2 h_c - d_h^2 h_b - d_i^2 h_a) \quad (\text{Eq. 4.10.})$$

$$\Rightarrow h_{ave} = \frac{d_o^2 h_c - d_h^2 h_b - d_i^2 h_a}{d_o^2 - d_h^2} \quad (\text{Eq. 4.11.})$$

$$\varepsilon_{ave} = \ln \frac{h_o \cdot (d_o^2 - d_h^2)}{d_o^2 h_c - d_h^2 h_b - d_i^2 h_a} \quad (\text{Eq. 4.12.})$$

As the  $\varepsilon_{ave}$  gets greater, the value of flow stress increases. This means that the required force increases to finish the process. Namely, the assumption of the dimensions of finished work should be chosen so that the finishing force is to be below or equal to 50 tons. As seen in the Eq. 4.12, the average strain  $\varepsilon_{ave}$ , does not only depend on the finished work dimensions but also on the initial height,  $h_o$ , of the billet. As a result, the flow stress and the maximum required force depend on the initial height too, see Eq. 4.13 & Eq. 4.14;

$$\Rightarrow \sigma_f = 140 \cdot \left[ \ln \frac{h_o (d_o^2 - d_h^2)}{d_o^2 h_c - d_h^2 h_b - d_i^2 h_a} \right]^{0.25} \quad (\text{Eq. 4.13.})$$

$$\Rightarrow P = \left[ 140 \left( \ln \frac{h_o (d_o^2 - d_h^2)}{d_o^2 h_c - d_h^2 h_b - d_i^2 h_a} \right)^{0.25} \right] \cdot 5 \cdot \left[ \frac{\pi}{4} \cdot (d_o^2 - d_h^2) \right] \quad (\text{Eq. 4.14.})$$

Fig. 4.5. illustrates the finished product of the T-Shape forging. The needed force and the flow stress, for finishing the T-Shape, depend on the outside diameter,  $d_o$ , hole diameter,  $d_h$ , and the diameter  $d_i$ , as well as the heights  $h_a$ ,  $h_b$  and  $h_c$ , Eq. 4.15, Eq. 4.16 and Eq. 4.17.

$$\varepsilon_{ave} = \ln \frac{h_o \cdot (d_o^2 - d_h^2)}{d_o^2 h_b - d_i^2 h_a - d_h^2 h_c} \quad (\text{Eq. 4.15.})$$

$$\Rightarrow \sigma_f = 140 \cdot \left[ \ln \frac{h_o (d_o^2 - d_h^2)}{d_o^2 h_b - d_i^2 h_a - d_h^2 h_c} \right]^{0.25} \quad (\text{Eq. 4.16.})$$

$$\Rightarrow P = \left[ 140 \left( \ln \frac{h_o (d_o^2 - d_h^2)}{d_o^2 h_b - d_i^2 h_a - d_h^2 h_c} \right)^{0.25} \right] \cdot 5 \cdot \left[ \frac{\pi}{4} \cdot (d_o^2 - d_h^2) \right] \quad (\text{Eq. 4.17.})$$

H-Shape geometry is more complicated than the U and T-Shape, because as seen in Fig. 4.6, diameter,  $d_a$ , is included in the Eq. 4.4. As seen in Eq. 4.20, the required load, flow stress and average strain values depend on the diameters  $d_o$ ,  $d_h$ ,  $d_a$ , and  $d_i$ , and the heights  $h_a$ ,  $h_b$ , and  $h_c$ , Eq. 4.18, 4.19 & 4.20.

$$\varepsilon_{ave} = \ln \frac{h_o \cdot (d_o^2 - d_h^2)}{d_o^2 h_b - d_h^2 h_a - 2 \cdot h_b \cdot (d_i^2 + d_i \cdot d_a + d_a^2)} \quad (\text{Eq. 4.18.})$$

$$\Rightarrow \sigma_f = 140 \cdot \left[ \ln \frac{h_a \cdot (d_o^2 - d_h^2)}{d_o^2 h_b - d_h^2 h_a - 2 \cdot h_b \cdot (d_i^2 + d_i d_a + d_a^2)} \right]^{0.25} \quad (\text{Eq. 4.19.})$$

$$\Rightarrow P = \left[ 140 \cdot \left[ \ln \frac{h_a \cdot (d_o^2 - d_h^2)}{d_o^2 h_b - d_h^2 h_a - 2 \cdot h_b \cdot (d_i^2 + d_i d_a + d_a^2)} \right]^{0.25} \right] \cdot 5 \cdot \left[ \frac{\pi}{4} \cdot (d_o^2 - d_h^2) \right] \quad (\text{Eq. 4.20.})$$

The maximum load needed to finish the U, T and H-shapes are as through Eqs. 4.12 to Eqs. 4.20. The parameters assumed, the strain values, flow stresses and the required loads are indicated in Table 4.1 and Table 4.2.



Process	$d_o$ (mm)	$d_i$ (mm)	$d_h$ (mm)	$d_a$ (mm)	$h_a$ (mm)	$h_b$ (mm)	$h_c$ (mm)	$h_o$ (mm)
U-Shape Forging	30	20	10	-	15	15	3	39
T-Shape Forging	30	20	10	-	15	10	25	42
H-Shape Forging	30	20	10	15	10	5	20	28

Table 4.1. Dimensions of Preform for U, T and H- Shapes

Process	$\epsilon_{ave}$	$\sigma_f$ (Mpa)	P (Tons)
U-Shape Forging	0.47	115.92	37.12
T-Shape Forging	0.99	139.61	45
H-Shape Forging	1.061	142.1	45.5

Table 4.2. Calculate Values of Strain, Flow Stress and Load

As a result the tabulated dimensions of the U, T and H-Shapes workpieces are illustrated in Fig. 4.5.

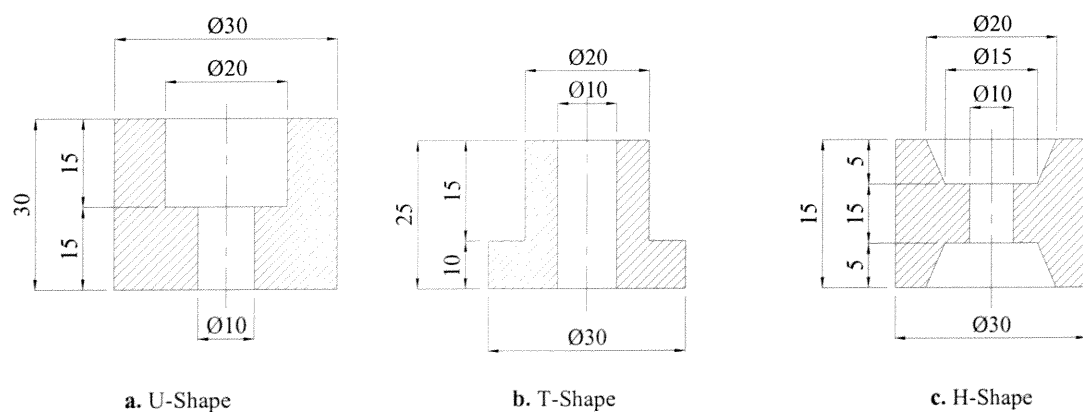
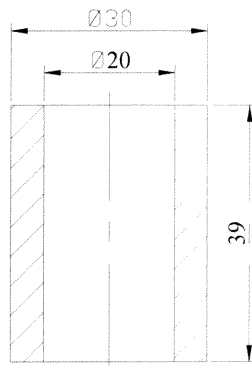


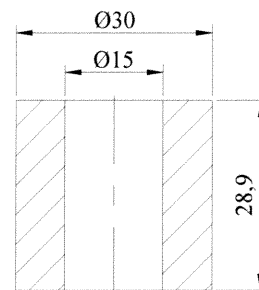
Fig. 4.5. Dimensions of Forging Products

By considering the volume constancy of the finished products, the dimensions of preforms are specified but the initial height,  $h_0$ , of the preforms can not be greater than the values tabulated in Table 4.1. In addition, the flow directions should be included before identifying the dimensions. Namely, the billets should have so different dimensions that the flow would be different for each forging of the specimens.

For U-Shapes; the billets are considered as in Fig. 4.6. As the preform, Fig. 4.6.a, is forged, the flow direction would be upsetting through inward direction. The billet, in Fig. 6.b, flows inward direction as well as extrudes parallel to the axis. The specimen, Fig. 4.6.c, is the uniquely extruding billet. The preform, Fig. 4.6.d, is upset inward and outward directions at same time extrudes.



a.



b.

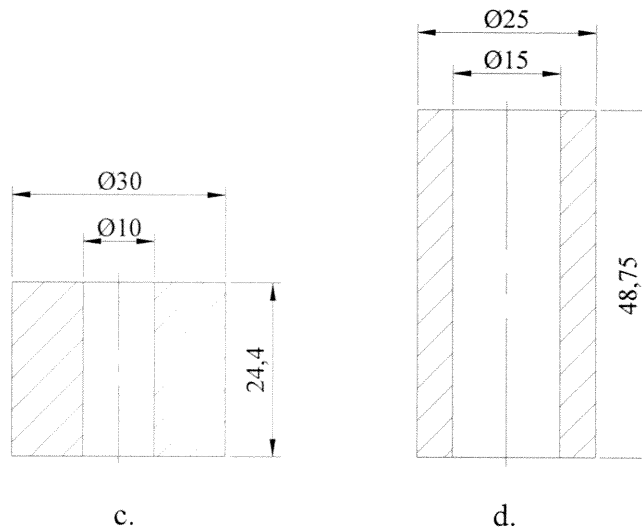
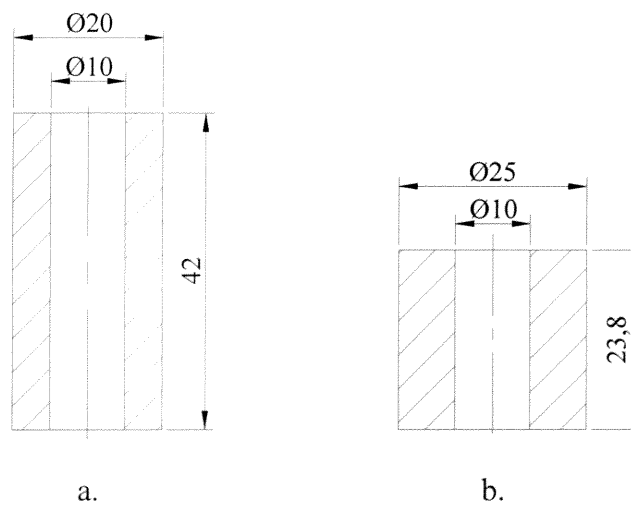


Fig. 4.6. Preforms for U-Shaped Product

T-Shape preforms are shown in Fig. 4.7. The preform, Fig. 4.7.a, is an upset billet to the outward direction. The preform, Fig. 4.7.b, flows through outward direction as well as extrudes while being formed. However, the preform, Fig. 4.7.c, is only an extruding billet while the billet, Fig. 4.7.d, flows through inward and outward directions, at the same time extrudes.



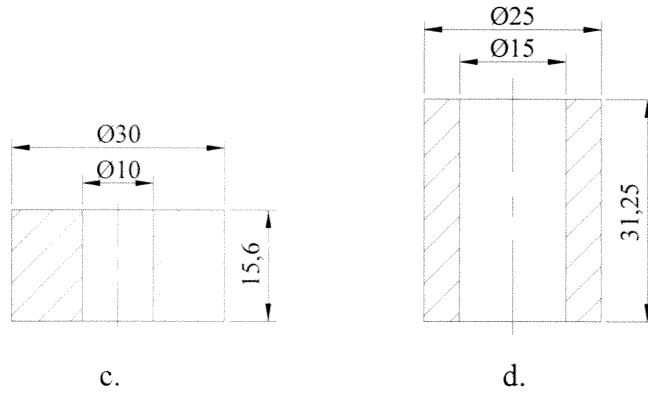


Fig. 4.7. Preforms for T-Shaped Product

The billets of H-Shaped products are shown in Fig. 4.8. The billet in Fig.4.8.a is upsets through inward direction but the preform, Fig. 4.8.b flows through inward direction as well as extrudes. However, the preform, Fig. 4.8.c, extrudes as being forged. The preform, Fig. 4.8.d, upsets inward and outward directions at the same time extrudes.

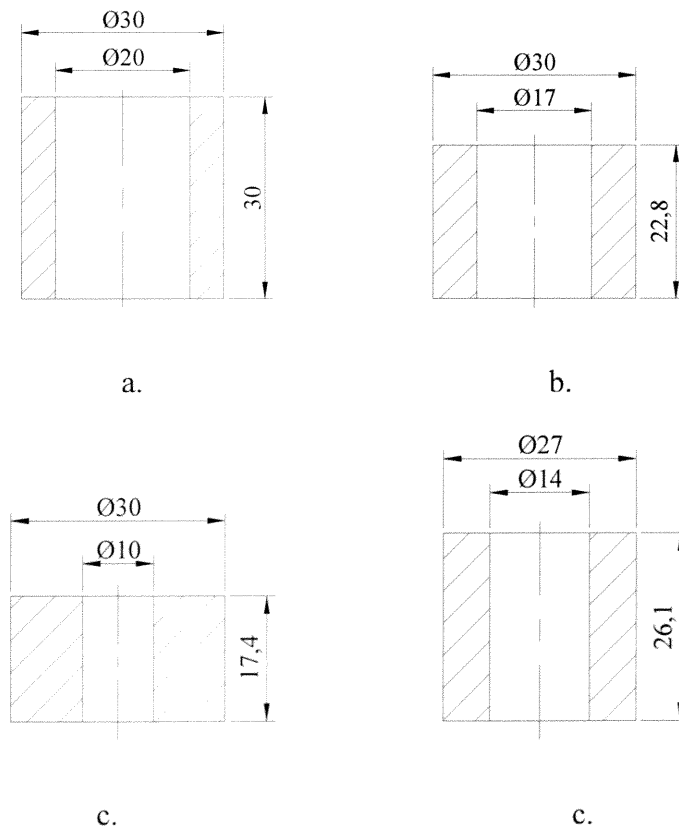


Fig. 4.8. Preforms for H-Shaped Product

#### 4.4. DIE DESIGN

As seen in Fig. 4.9, the tool used in experiments is made of two parts, which are dies and the punches. The cover die should be withstand the pressure of the metal flow. The maximum flow stress is 142.1 MPa, Table 4.2. So the design criteria for dies is accepted as 142.1 MPa. The flow stress effects the cover die in radial and the tangential directions, Fig. 4.10.

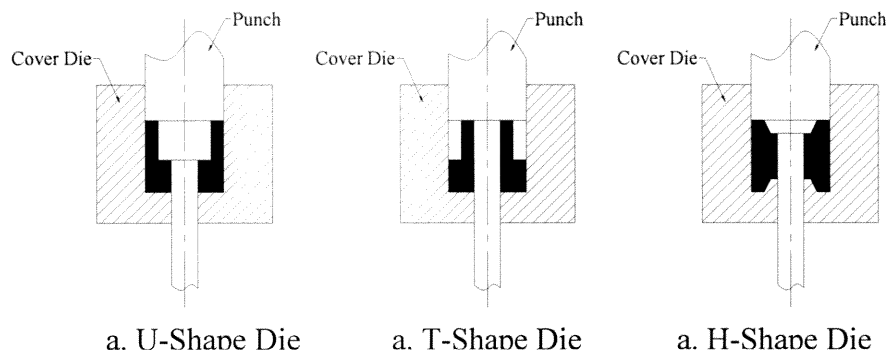


Fig. 4.9. Used Dies in Experiments

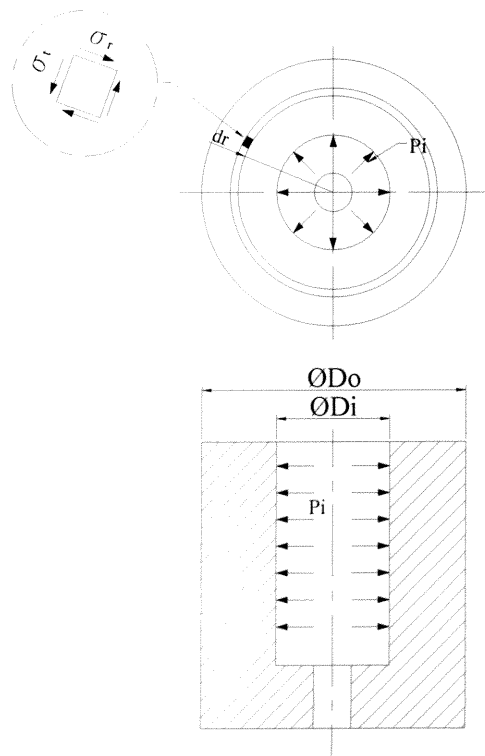


Fig. 4.10. Pressure Distribution in Dies

$$\sigma_{t \max} = P_i \cdot \left( \frac{D_i^2 + D_o^2}{D_o^2 - D_i^2} \right) \quad (\text{Eq. 4.21.})$$

$$\sigma_{r \max} = -P_i \quad (\text{Eq. 4.22.})$$

Assume the factor of safety as 1.5, so the maximum tangential stress should be 1.5 times of the inlet pressure, Eq.4.23. The inner diameter of die, 30 mm, is specified from the finished work pieces diameters, due to the fact that all the finished work pieces have same diameters of 30 mm, but the outer diameter is calculated from Eq. 4.21. As seen Eq. 4.25, the outer diameter of the die is to be higher than 67 mm. So, for easiness of processing the outlet diameter can be considered 70 mm.

$$\Rightarrow \sigma_{t \max} = 213.15 \text{ MPa} \quad (\text{Eq. 4.23.})$$

$$\Rightarrow P_i \cdot \left( \frac{D_i^2 + D_o^2}{D_o^2 - D_i^2} \right) = 213.5 \text{ MPa} \quad (\text{Eq. 4.24.})$$

$$\Rightarrow D_o = 67 \text{ mm} \quad (\text{Eq. 4.25.})$$

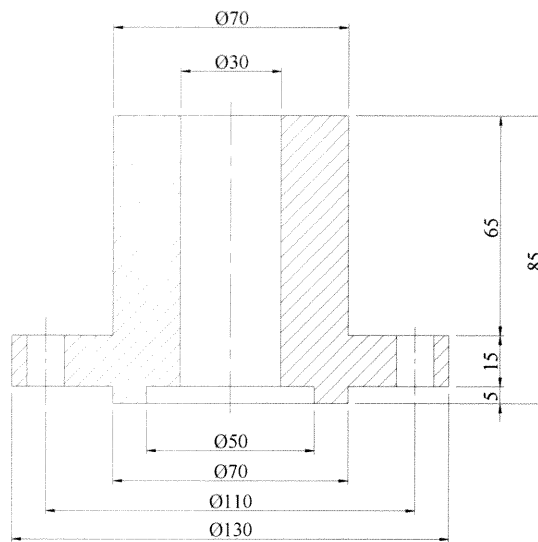
The material norm of the die is SAE 4140 which have the properties as follows;

Yield Stress	650 Mpa
Tensile Strength	90-110 Mpa
Maximum Elongation	%12
Reduction of Ruptured Area (minimum)	%50
Hardening Temperature for Quenching in Water	820-860 °C
Hardening Temperature for Quenching in Oil	820-860 °C
Hot Working Temperature	850-1050 °C
Normalizing Temperature	840-860 °C
Brinell Hardness 30 (minimum)	241 HB
Rockwell Hardness	53-61 Rockwell C
Vickers Hardness (minimum)	560 HV
Tempering	540-680 °C

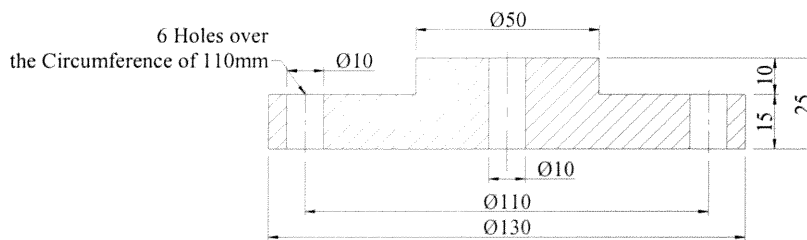
Table 4.3. Specifications of the Die Material (SAE 4140) [33]

#### 4.5. DIE GEOMETRY:

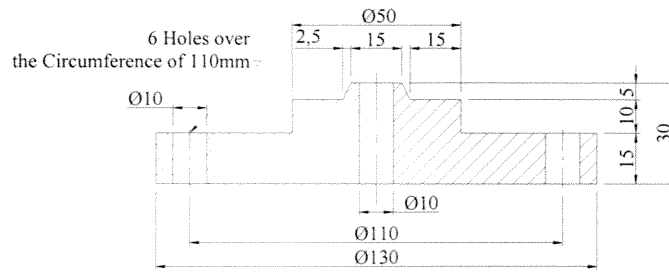
The dies were designed that the only punches should be changed for easiness of handling and removing the finished products. So, the cover die is kept constant, and the punches and lower dies are changed according to the process, Figs. 4.11.a, b, c and d Fig. 4.12 and Fig. 4.13.



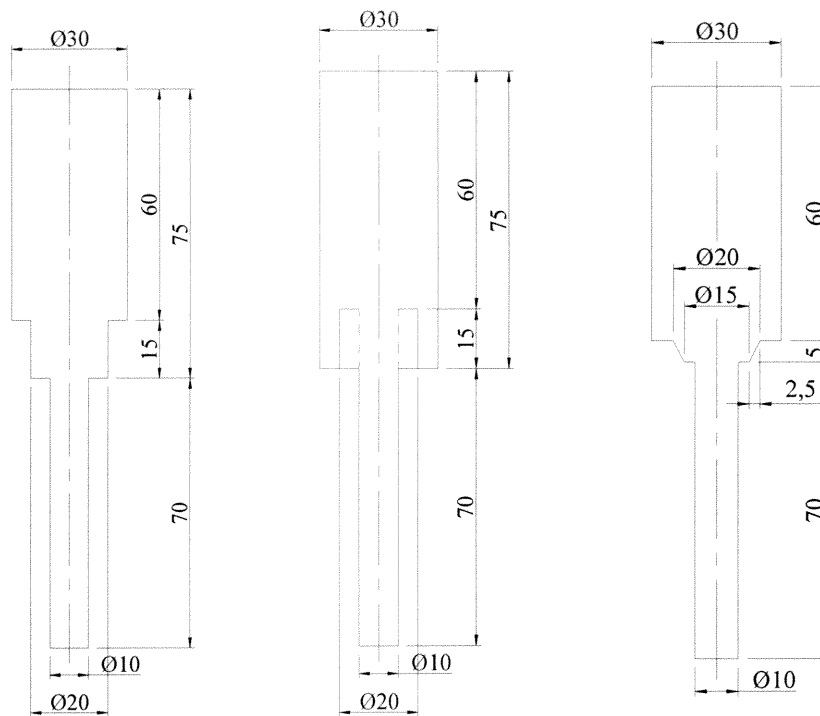
a. Die



b. Lower Die For U and T-Shapes Forging



c. Lower Die For H-Shape Forging



d. Punches for U, T and H-Shape Forgings

Fig. 4.11. Dimensions of the Forging Dies and Punches

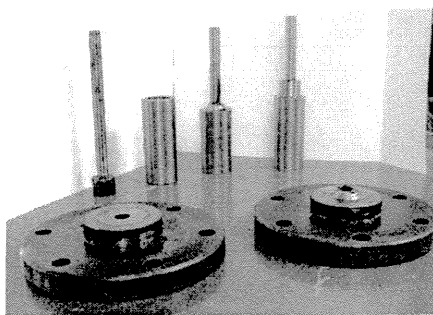


Fig. 4.12. Photo of the lower dies and Punches

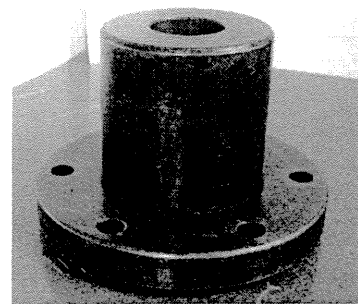


Fig. 4.13. Photo of the Cover Die



## CHAPTER 5

### EXPERIMENTAL STUDY

#### 5.1. INTRODUCTION

The experiments were carried out by using three different axisymmetric shapes, like U-Shape, T-Shape and H-Shape. In this chapter, the preparation of dies and billets are presented. As well, lubrication and the experimental studies were given.

#### 5.2. PREPARATION OF DIES

SAE 4140 material is used for all die components. The working part of the punch hole is turned to  $\Phi$  29.5 mm. Because it would be increased to  $\Phi$  30 mm. The lower die surfaces are turned by using the same billet of SAE 4140 material. The outer diameter is reduced to  $\Phi$  130 mm and the top surface of lower die is machined to  $\Phi$  50 mm net diameter, because the side surface does not interfere with the workpieces. The punches, shown in Fig. 4.24.d. (Chapter 3), are turned from  $\Phi$  35 mm billet of SAE 4140 material. All the diameters are machined with 0.5 mm larger tolerances, due to the fact that these surfaces contact with the workpieces. The surfaces contact with the workpieces would be ground. After rough processing of the dies, the die are heat treated for preventing deformation elastically. The heat treatment operation is carried out at 1000 °C for over 1 hours at the furnace and quenched in water. The hardness of the dies vary between the values of 45 HRC and 55 HRC. Then the surfaces of the punches, inner diameter of the cover die and the plane surfaces of the

lower dies which are in contact with the workpieces are ground to the design dimensions, see Figures 4.24, in universal grinding machines.

### **5.3. PREPARATION OF BILLETS**

For aluminum billets, material Al 1050 was used as mentioned in Chapter 4. Because of the fact that Al 1050 is a very relatively material. Al 1050 does not does not available commercially in circular shape. It is found as thin plates so the billets are prepared by casting into molds which has the dimensions of  $\Phi 30 \times 50$  mm then turned to final sizes mentioned in Section 4.4.4. The properties of the Al 1050 are as in Table D.1./Appendix D. According to test results, the ultimate tensile stress is 102.42 Mpa and the maximum elongation is % 16 before rupture. Yield stress is about 70 Mpa. The mechanical properties of the cast workpiece of aluminum are obtained by tensile test.

For lead billets, the material, which has purity over %98, was used as mentioned. Because of the fact that the pure lead is very soft material, pure lead exists in the shape of ingots. So the billets are prepared by casting in to molds which has the dimensions of  $\Phi 30 \times 50$  mm then turned to final sizes. The mechanical properties of the cast workpiece of the lead are obtained by tensile test. The properties of the pure-lead used in experiments are as in Table D.2./Appendix D. According to test results, the ultimate tensile stress is 15 Mpa and the maximum elongation is % 80 before rupture. Yield stress is about 8 Mpa.

### **5.4. LUBRICATION**

In the experiments the lubricant which contains molybdenum disulphide was used. The trade name of the lubricant is Molykote, which is in the form of grease. The working temperature lubricant is between  $-25$  °C and  $110$  °C, as well  $130$  °C for short periods. Especially, lubricant was used in high pressurized parts. The lubricant was applied by hand blastering to the surfaces of contacts between dies and the billets. These surfaces are especially the inner walls of the dies and the whole surfaces of the billets. The friction value of the lubricated surface was measured by

ring tests and denoted in Appendix C. According to test results the friction factor,  $\mu$ , is 0.125.

### 5.5. EXPERIMENTAL PROCEDURE:

The geometries of the preforms were identified in Chapter 4. They were designed to show the various effects of the main deformation modes which are upsetting or extrusion or both of the deformation modes. The modes of deformation of each preform prepared for U-Shape, T-Shape and H-Shape forgings are presented in Table 5.1.

Preforms	Deformation Mode		
	Upsetting		Extrusion
	Inner Flow	Outer Flow	
U1	X	-	-
U2	X	-	X
U3	-	-	X
U4	X	X	X
T1	-	X	-
T2	-	X	X
T3	-	-	X
T4	X	X	X
H1	X	-	-
H2	X	-	X
H3	-	-	X
H4	X	X	X

Table 5.1. Deformation Modes of the Forging Processes

After aluminum forging processes, experiments were carried out with lead specimens of the same type preforms as stated modes in Table 5.1. Use of lead simulates the hot

forging operation at room temperature. Because it shows hot forging characteristics at room temperatures, as explained detailed with Fig. B.1 in Appendix B.

# CHAPTER 6

## RESULTS AND DISCUSSION

### 6.1. INTRODUCTION

In this chapter, the experimental results and discussion are given. For flow modelling of specimens, the program Finite Element Simulation (FEM) are benefitted, and the modelling is compared with the actual results which reveals in the experiments.

### 6.2. RESULTS AND DISCUSSION

#### 6.2.1. U-Shape Aluminum Forging

The specimen U1-Al is upset to inner direction only. When the specimen U1-Al is forged, the inner flow starts upsetting (see Fig.6.1/Step 1). The motion of the meshes are more obvious in Step 2 and the meshes out of the inner surface gets larger as long as the forging is continued (see from Step 3 to 7), however, the meshes at lower side of the outer surface gets smaller. As seen in Fig.6.1, at the lower side of surface of finished work, cavity formation is observed. At step 1, the load is 2.4 tons and increases until the load 7.5 tons, Step 2 (see Fig. 6.2). After Step 2, it is seen that the inclination at the curve starts to increase, depending on the strain hardening and the friction effects. The inclination continues increasing until Step 7. In addition, between Step 6 and 7 the load-stroke curve increases rapidly, due to increasing friction and strain hardening effect.

As seen in Fig. 6.3., the inner surface of the guide hole does not fill completely, as well inner surface is too rough. This shows that the meshes gets longer along thickness while narrowed along the cross-section. Moreover, cavities are cared at outer surface as indicated in Fig.6.3. This case is due to the fact that the flow of metal is through inner direction.

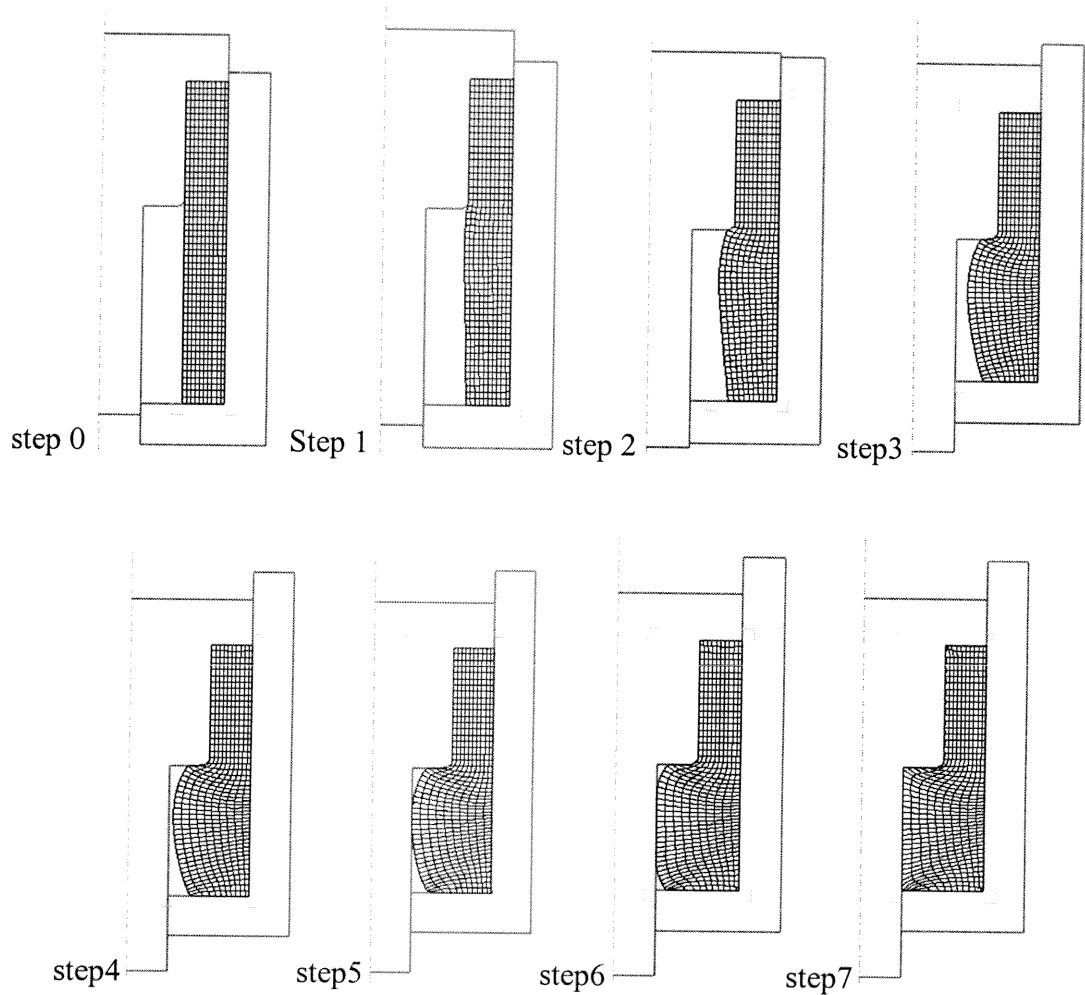


Figure 6.1. Flow Simulation of U1-Al Forging

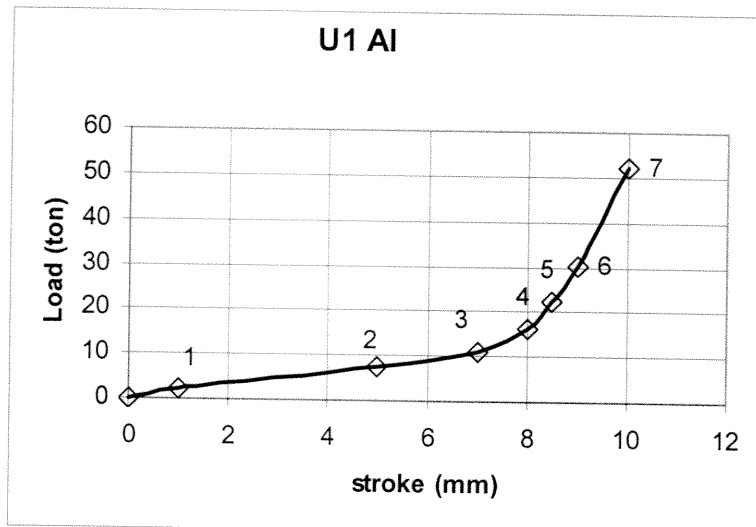
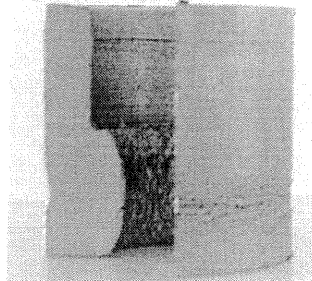


Figure 6.2. Experimental Load-Stroke characteristics of U1-Al forging



a. Preform



b. Product

Figure 6.3. Photo of U1-Al Forging

The specimen U2-Al fills the die by inner upsetting as well as extruding. While the punch moves downward, the flow starts to the centre beginning from the top of the material in Fig.6.4. With Step 1 the billet flows incrementally until Step 5. After Step 5 the inclination rises and with Step 6 the curve rises almost perpendicularly. The photo, Fig.6.6 shows the workpiece in Step 6. As seen in Fig.6.6, the lower part of the inner radius does not finish yet. Moreover, it is observed that the concentration of meshes rise as punch moves downwards, Fig.6.4. The load needed is 32 tons for finishing the process. And as seen in the photo the inner surface of the workpiece upper part is scraped as shown in Fig. 6.4.

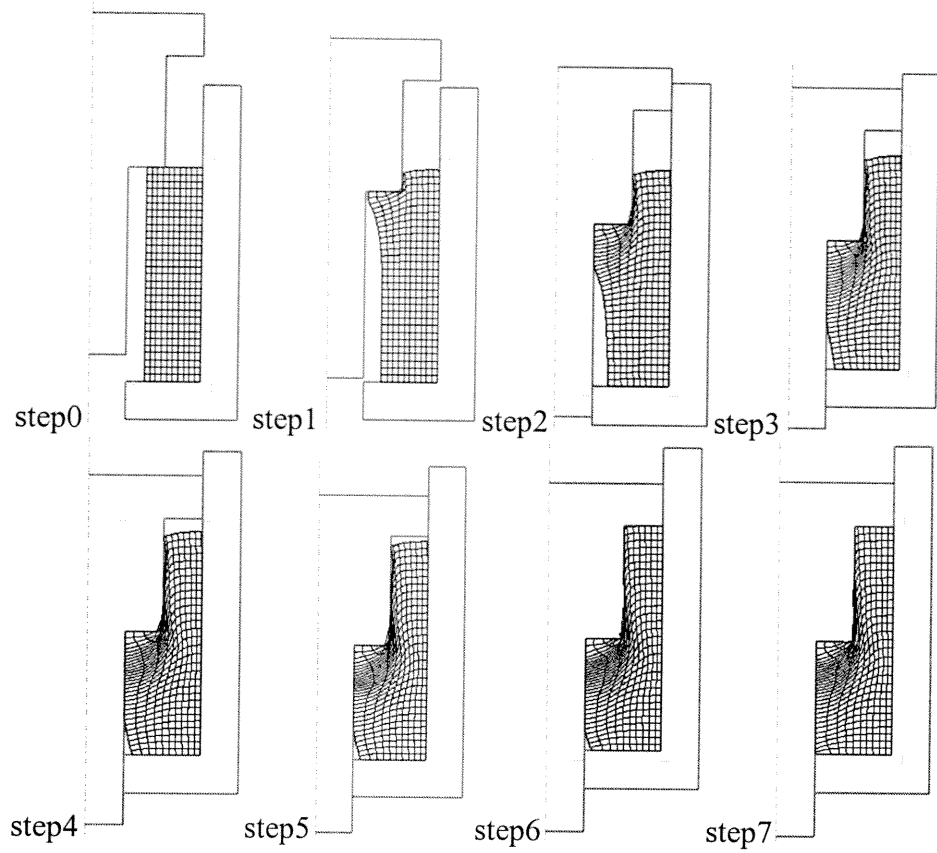


Figure 6.4. Flow Simulation of U2-Al Forging

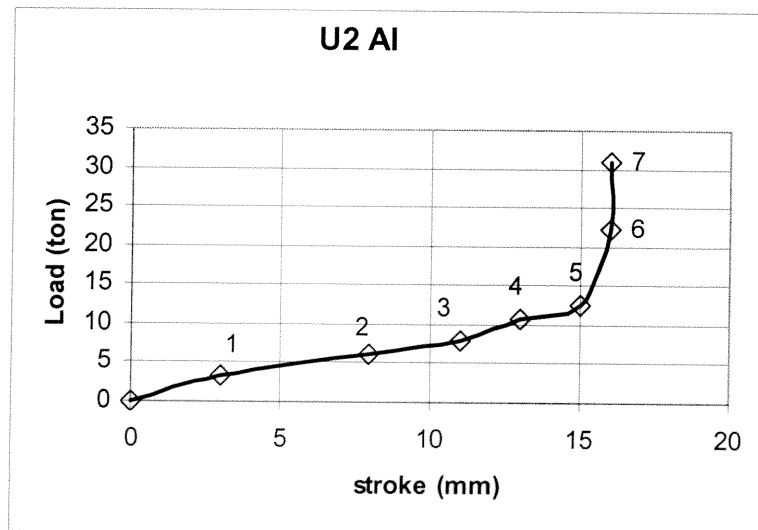


Figure 6.5. Experimental Load-Stroke characteristics of U2-Al Forging



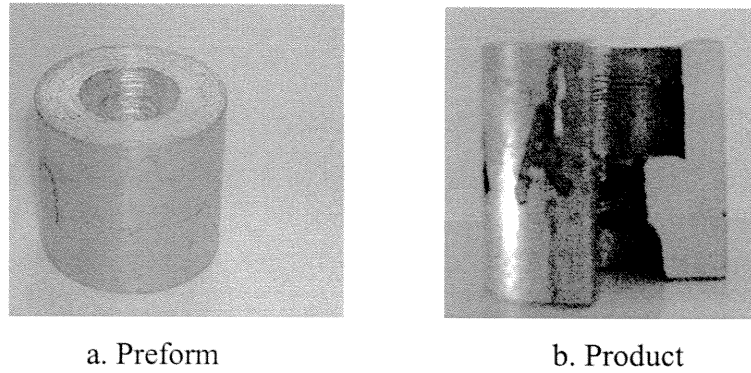
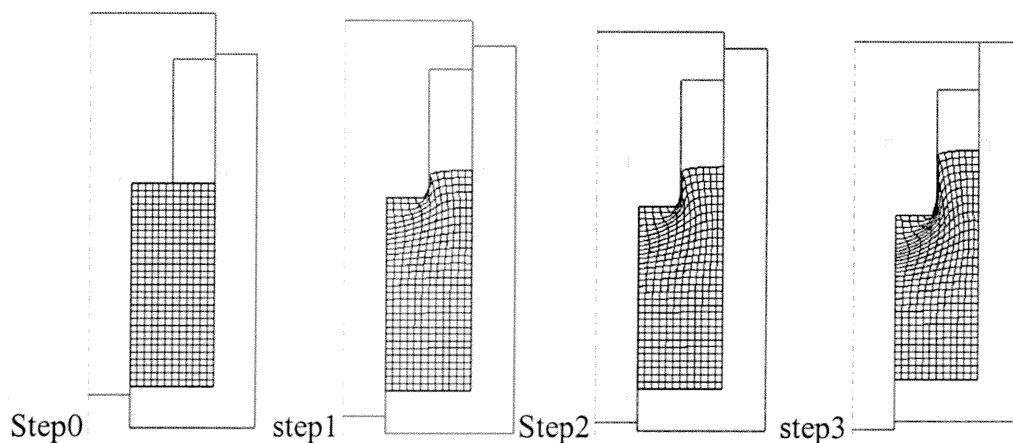


Figure 6.6. Photo of U2-Al Forging

The specimen U3-Al is extruded only. In step 1, the specimen is pressed with the load of 3.55 tons and punch moves downward 2 mm. In Step 2, punch movement is 3 mm and the load is 7.1 tons. The inclination of curve between Step 1 and 2 incrisis and decreases between Step 2 and 3. At Step 3, the punch movement is 5 mm with the load of 9.5 tons. By Step 3, the mesh concentration rises at the inner surface of the specimen. After Step3, the inclination of curve closes to zero until step 4, see Fig.6.7. With Step 4, the workpiece is deformed 11 mm with load 12.14 tons. The curve changes character after Step 4 and an increase in inclination is observed untill Step 5, see Fig. 5.8 and stroke is 12 mm with the load 14.8 tons. After Step 5, there is a sudden increase in load with a very small stroke of 1 mm until Step 6. The load at Step 6 is 28.7 tons. If a further deformation is continued, the die is filled with step 7. As seen in Fig. 6.9, the inner surface of the specimen is scraped and this case is observed in Fig. 6.7 too. Moreover, cavities are formed at the inner surface between mandrel and the workpiece.



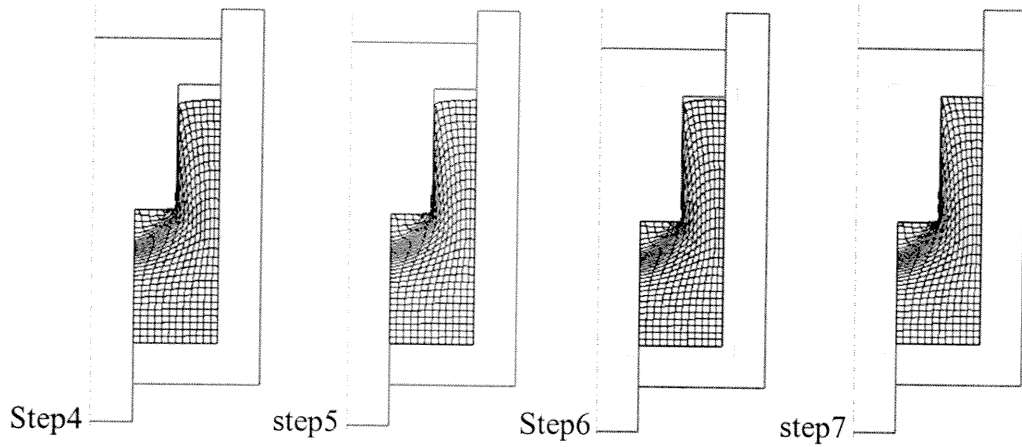


Figure 6.7. Flow Simulation of U3-Al Forging

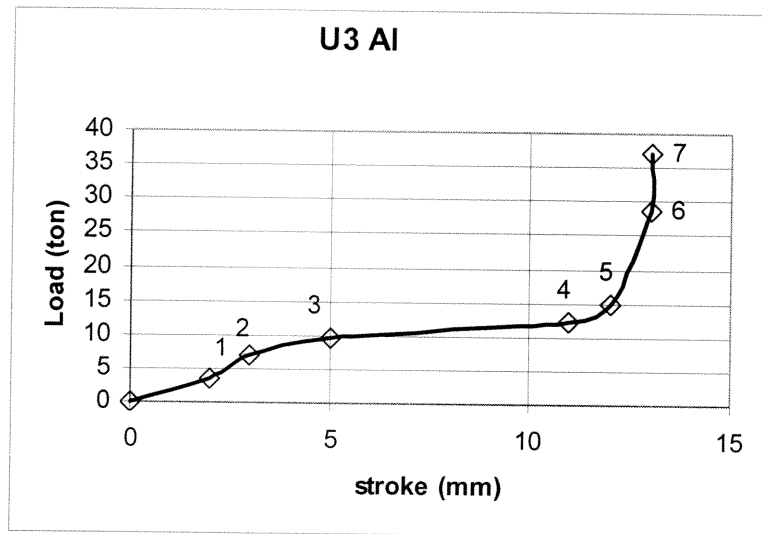
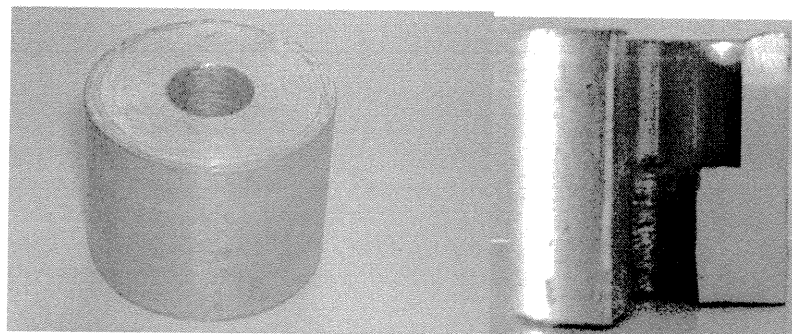


Figure 6.8. Experimental Load-Stroke characteristics of U3-Al Forging



a. Preform

b. Product

Figure 6.9. Photo of U3-Al Forging

The specimen U4-Al is extruded as well as upset. As the punch moves downward, it is observed that the tearing occurs at the top surface of the specimen, see Fig.6.10. With Step 1, the specimen is deformed 2 mm and the load is 1.8 tons. Between Step 1 and 3 the curve denotes a stable character. After Step 3, the inclination starts to rise. At Step 3, the deformation is 17 mm and the load is 3.05 tons. By Step 3, the tearing occurs, see Fig.6.12. At Step 4, the load and total deformation is 6.6 tons and 28 mm respectively. And the inclination of the curve rises more rapidly as the Step 7 is closed. As seen in Fig.6.11, with Step 6 the curve rises nearly perpendicularly. The finished load and stroke is 35 tons and 34 mm respectively. As seen in Fig.6.12, the punch cuts a piece of material, because there is a grazing at inner surface of specimen. And at the beginning of the forging process, the billet starts to buckle until touching to the inner surface of the die.

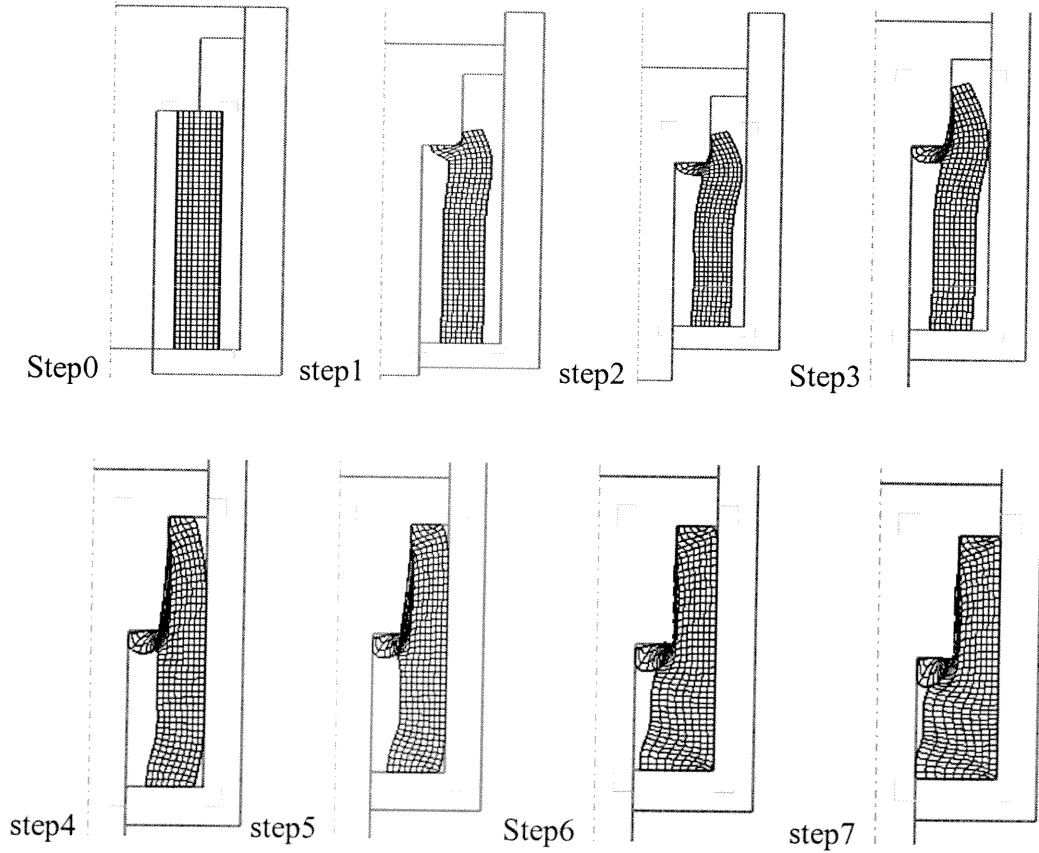


Figure 6.10. Flow Simulation of U4-Al Forging

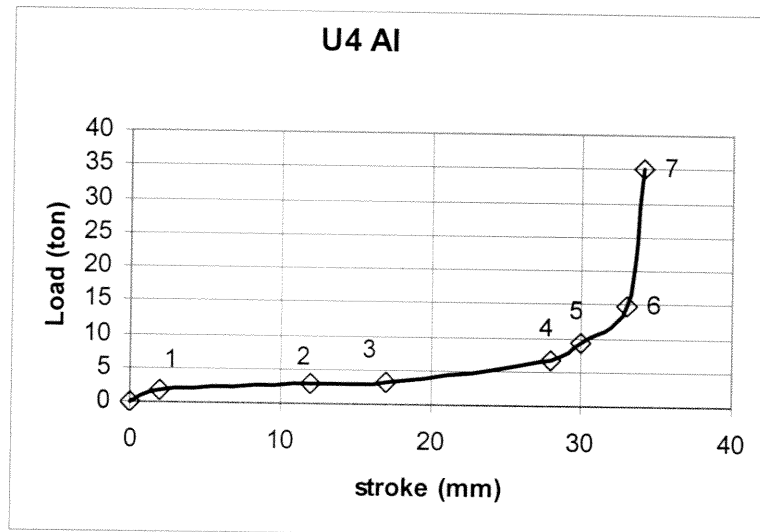


Figure 6.11. Experimental Load-Stroke characteristics of U4-Al Forging

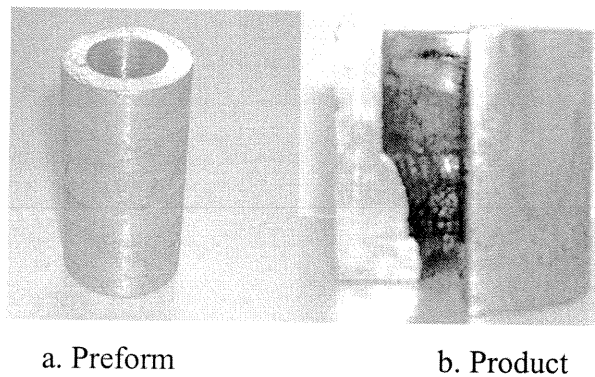


Figure 6.12. Photo of U4-Al Forging

As seen in Figs.6.13, the forging loads of U-shape for each preforms are different although, the finishing workpiece is same. So, if it is proposed to decrease the forging load, the billet U2-Al is ideal. But it has a folding problem at inner surface. So if surface smoothness is important, U3-Al is better. So for U-shape forging extrusion mode is ideal. Because the ideal filling is provided with lower load and the finish product has smooth surface. As well, the energy suffered for extrusion mode is lower than the other preform forging (see the area under curve U3-Al, Fig.6.13).

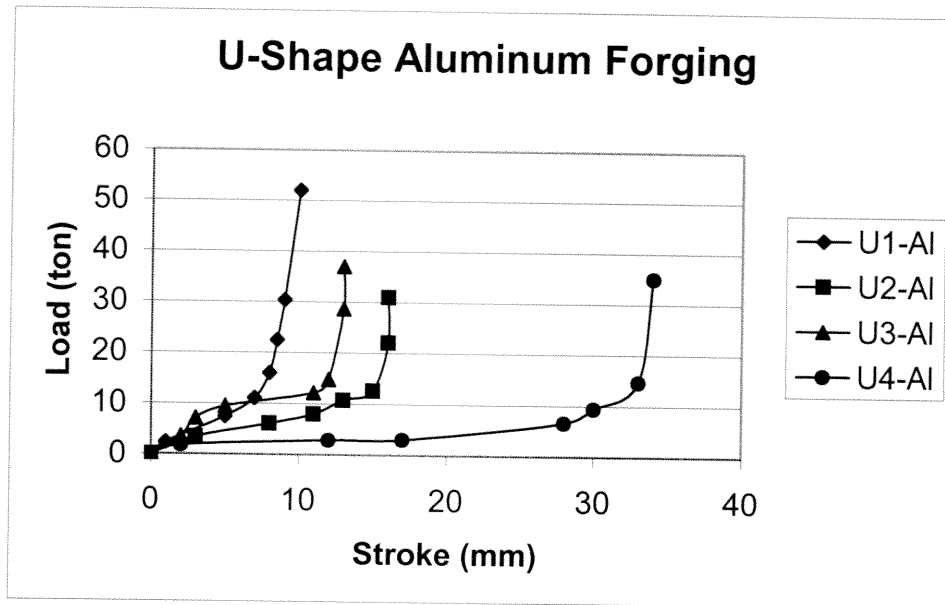


Figure 6.13 Experimental Load-Stroke Curve of U-Shape Aliminum

### 6.2.2. T-Shape Aluminum Forging

The specimen T1-Al flows through outward direction as forged. As seen in Fig.6.14, the meshes at outer surfaces get greater while the inner surface meshes get smaller. As seen in Step 3, the workpiece starts to separate from the guide of the die and folding occurs. The folding case is obviously seen in Fig.6.16. The lines are formed at the outer surface, due to the fact that lengthening of the meshes at the outer surfaces, see Fig.6.14, Step 0 to 7. The lines are along the circumference, see Fig.6.14. So, the specimen of this type has the problem of folding as well as outer surface quality.

The curve rises with a decreasing load until Step 1. Between Step 1 and Step 3 the curve increases incrementally, because the work piece is bending freely. Between Step 3 and Step 4 it is observed that the curve rises with an increasing load. The curve illustrates a steep increase by Step 5. As seen in Fig.6.14, Step 5 the billet begins to touch side surface of the die so the friction increases. On the other hand, the strain hardening of the material effects the load.

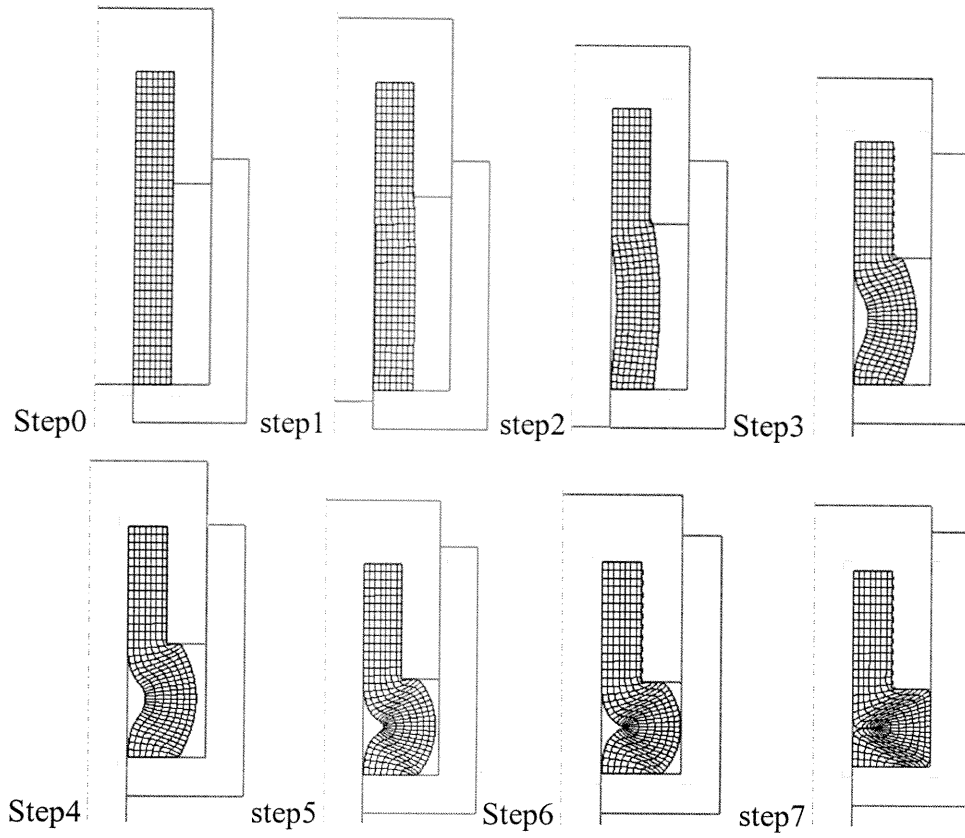


Figure 6.14. Flow Simulation of T1-Al Forging

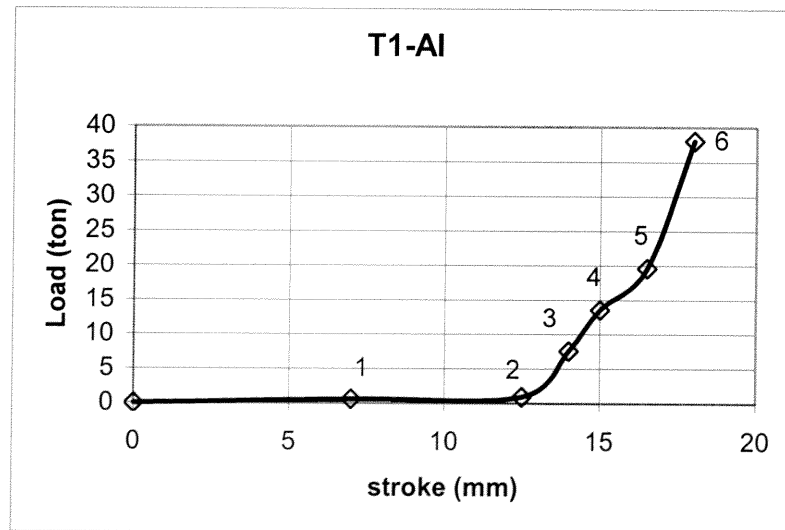


Figure 6.15. Experimental Load-Stroke characteristics of T1-Al Forging

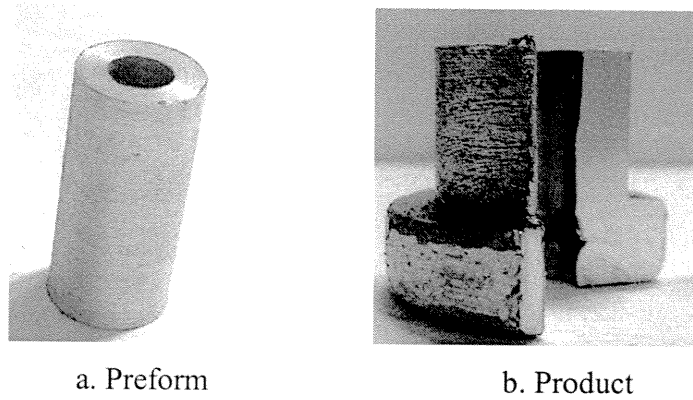
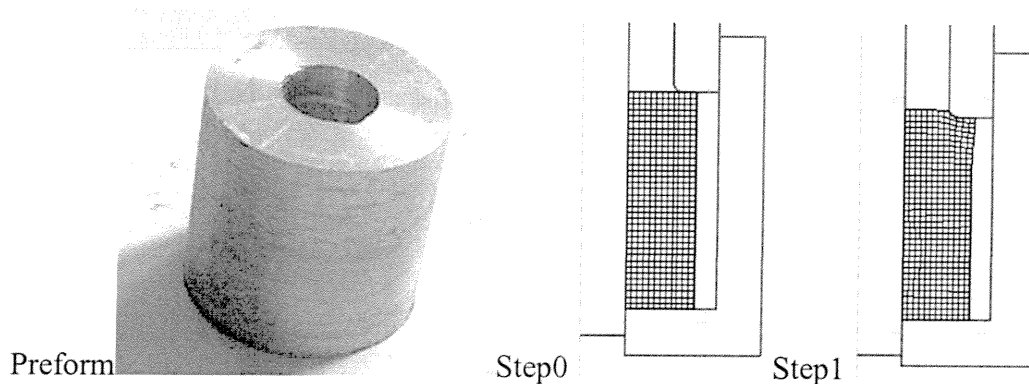


Figure 6.16. Photo of T1-Al Forging

The specimen T2-Al is extruded as well as outer upset, while the punch moves downward (see Fig.17/ from Step 0 to Step 5). The figure illustrates until step 5, because the modeling program can not go on after step 5 due to forming of fins at the interface of punch and the die. So the fin formation would be in high rates, as the flow continues to step 7. The experiment of T2-Al forging is completed until step 7 but the finished work piece can not be extracted due to being conqested in the die and punch. So the die and punch should be prepared in two pieces. But the size of punch's mandrel is too small to cut in two pieces. The sizes are small, due to the fact that the maximum capacity of the experimental press is low. So the design of parts are carried out with respect to press capacity. It is observed that cavity formation starts by step 4 (see Fig.6.17). According to load-stroke curve, the increase in load is uniform until step 3. But by step 3 the slope rises because of beginning contact between the work piece and the wall of die. So the work piece flows freely until step 3 and by step 3 the friction load increases with increasing contact area .By step 5, the load-stroke curve rises rapidly (see Fig.6.18). Because, probably, the extruding mode begins to be constrained due to interacting with lower surface of punch.



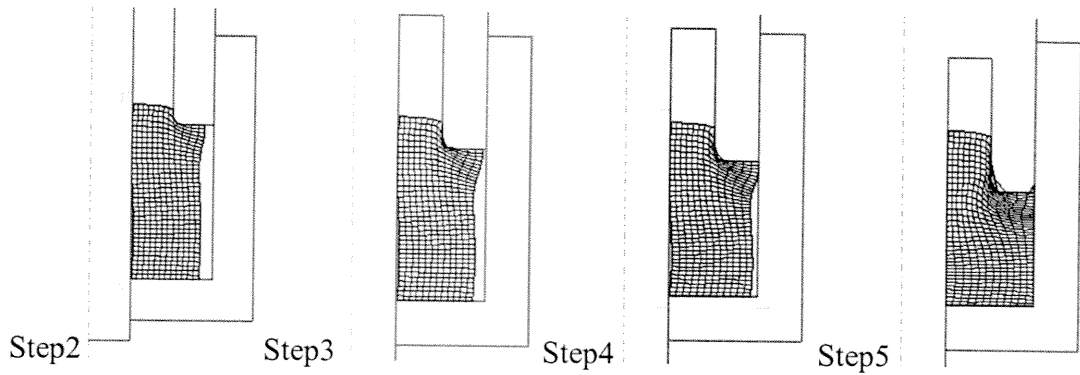


Figure 6.17. Flow Simulation of T2-Al Forging

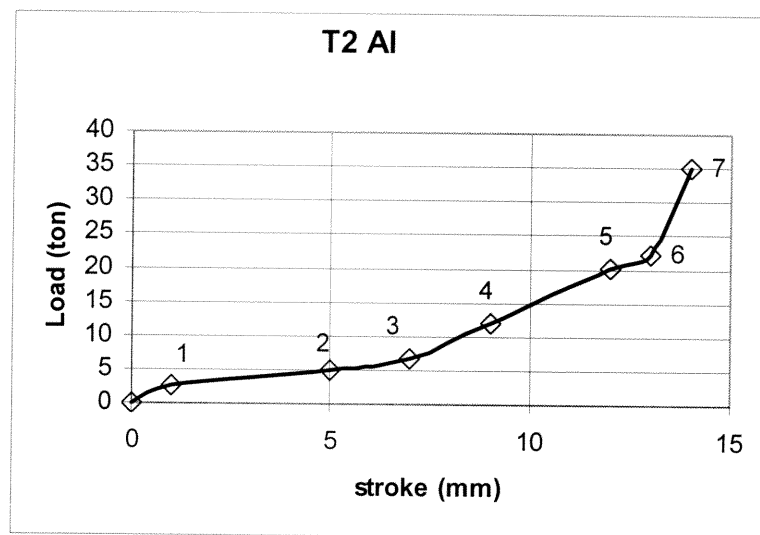


Figure 6.18. Experimental Load-Stroke characteristics of T2-Al Forging

In forging of T3-Al, the work piece is only extruding mode (see Fig.6.19). The Fig.6.19 illustrates until step 3, because modelling program can not continue the flow anymore, due to the formation of fins between punch and die surfaces in high-rates. So the data-base of the program can not solve the problem. The die problem exists for specimen T3-Al as in T2-Al. Because of high fin formations do not permit the extracting of finished work piece. Like T2-Al forging die, the die for T3-Al should be in two pieces. As seen in Fig.6.19, no cavity formation starts in extruding mode in T3-Al forging. Until step 2, the load-stroke curve incrementally increases but between step 2 and 5 more rapid increase is observed. Because increasing fin



formation results higher frictional load. By step 5, the curve rises steeply. Due to the fact that the interacting between lower surface of punch and work piece would begin.

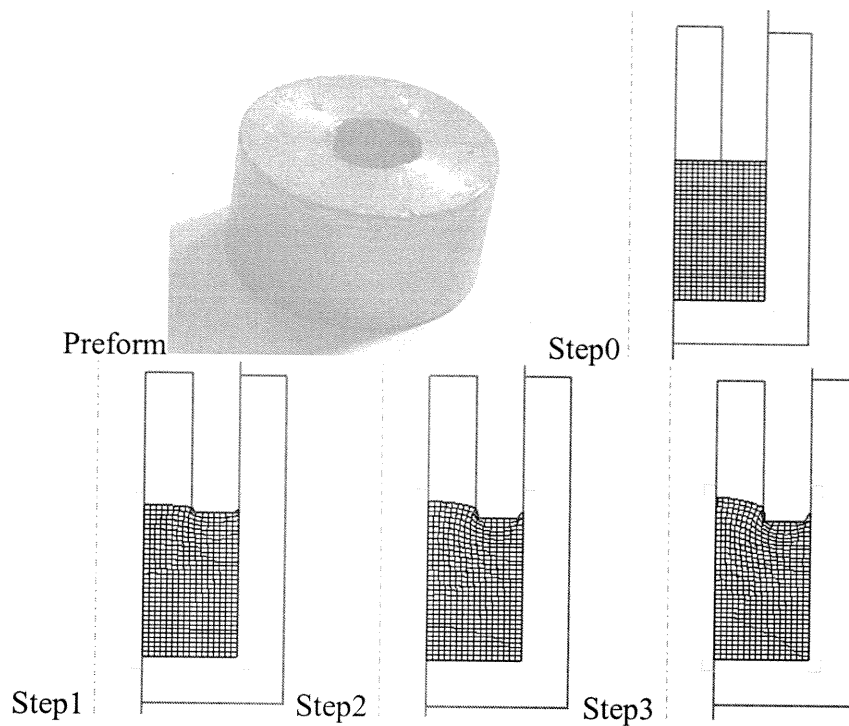


Figure 6.19. Flow Simulation of T3-Al Forging

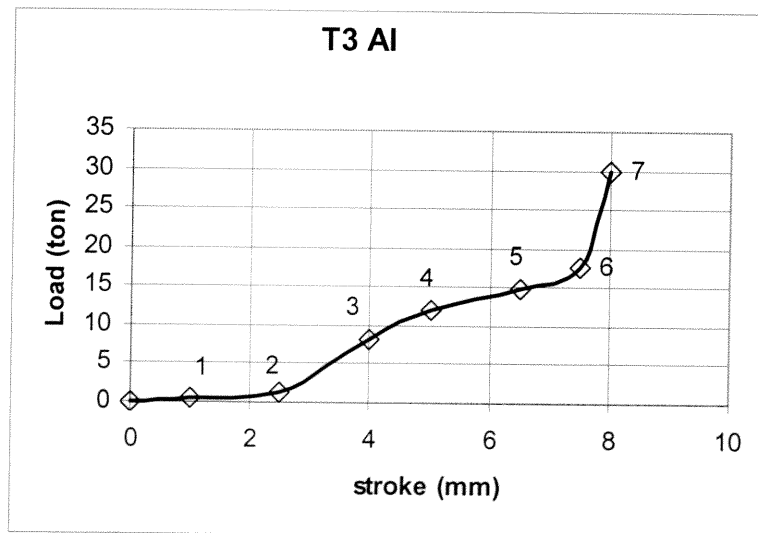
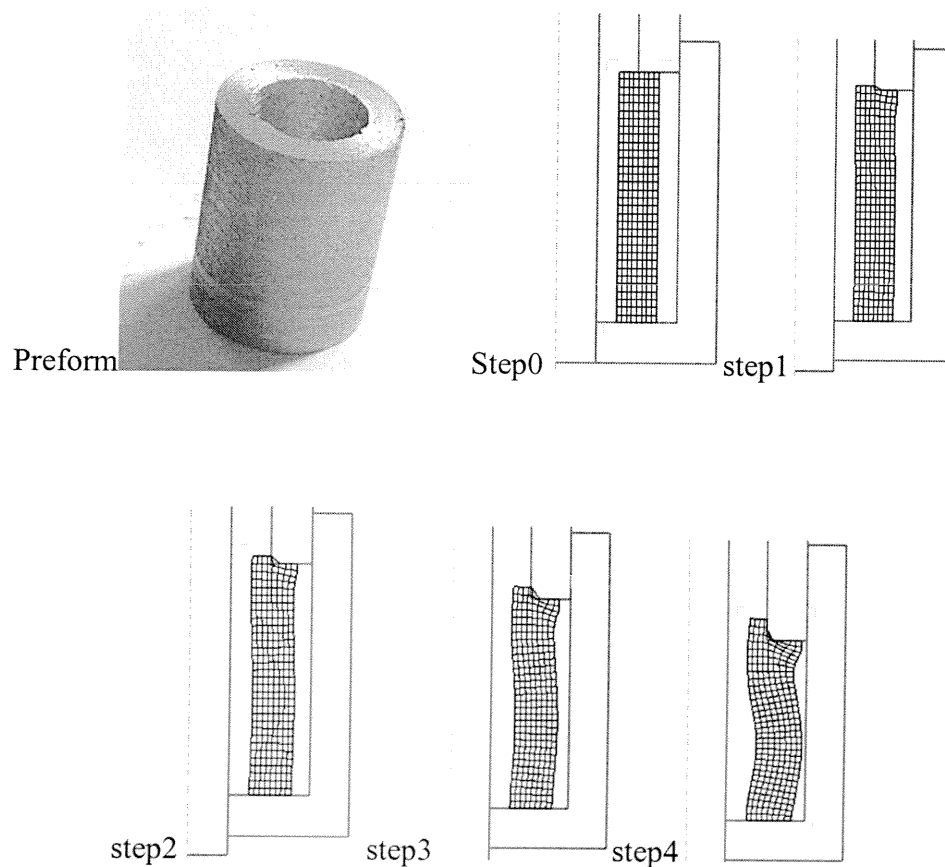


Figure 6.20. Experimental Load-Stroke characteristics of T3-Al Forging

The specimen T4-Al is forged to the central direction direction, at the same time, it flows through outward direction. As the forging is going on, concentration of the meshes at the outer surfaces rises, because as seen in the steps in Fig.6.21. As a result, folding is observed at the outer surface. Moreover, folding problem arises at the inner surface too.

The load-stroke curve rises incrementally between the steps of 1 and 4, see Fig. 6.22. By the Step 4, the inclination increases depending on the friction at the side walls which is the interface between the workpiece and the die. Because in Step 4 the workpiece starts to interact with the die wall. The curve rises nearly perpendicular between the Steps 7 and 9. This would be due to the fact that the increase in fin formation. As a result, frictional load increases.



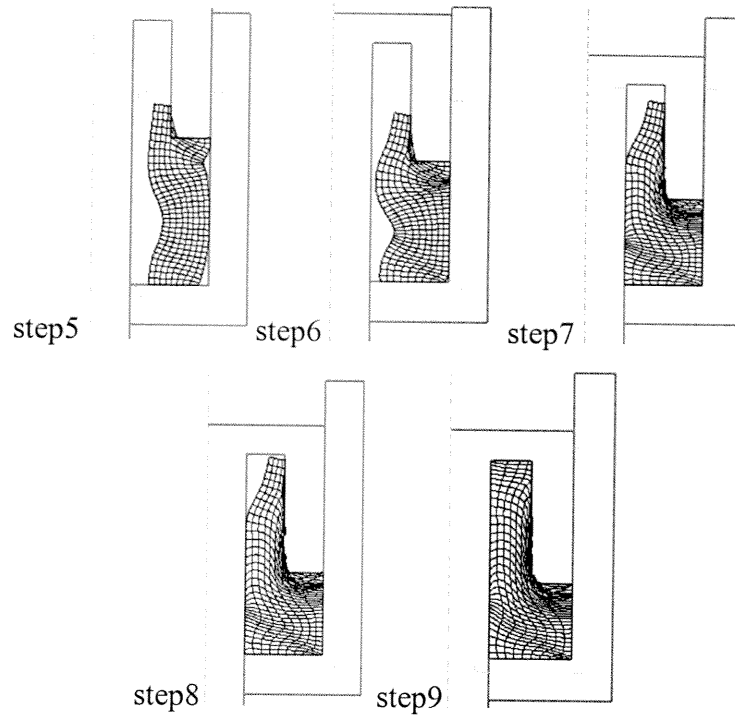


Figure 6.21. Flow Simulation of T4-Al Forging

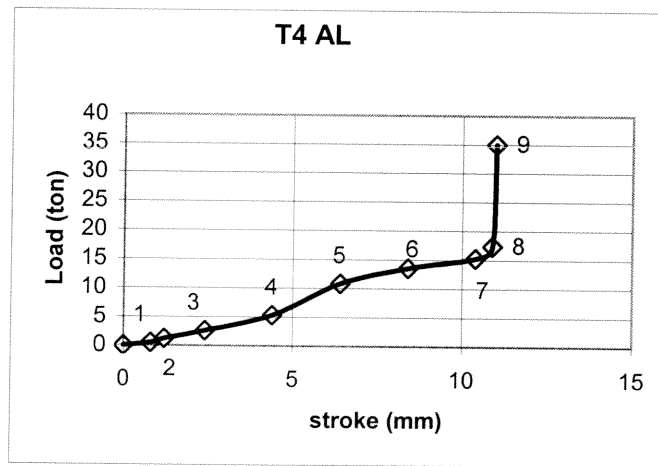


Figure 6.22. Experimental Load-Stroke characteristics of T4-Al Forging

The Fig.6.23 reveals the T-shape forgings of aluminum material. According to the curves, free forming of billet (T4-Al) is advantageous considering forging load in cold forming. But it has a folding problem at inner surface, due to non-homogenous flow. But this is achieved by using vibrating die. If the energy is considered under the curve, the extrusion mode is the best choice.

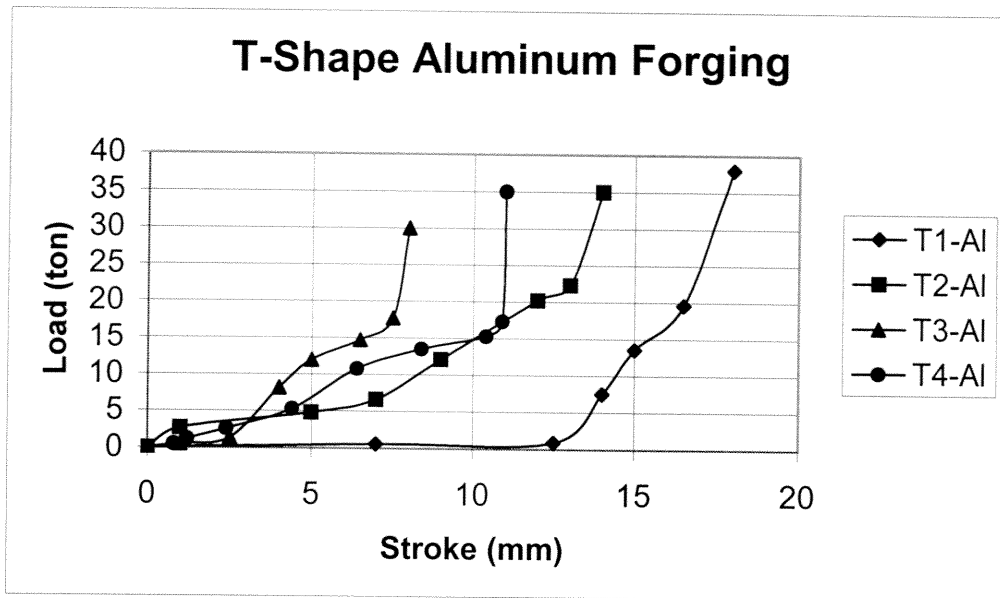


Figure 6.23 Experimental Load Stroke Curve of T-Shape Aluminum

### 6.2.3. H-Shape Aluminum Forging

The specimen H1-Al flows through central direction uniquely. The flow characteristic, load-stroke curve, is investigated at 7 steps, Fig.6.24. In Step 1, the punch moves 1 mm downward and the load is 3 tons. With Step 1 the curve changes more incremental zone until Step 2. In which the punch moves 2 mm with the load of 4-8 tons, see Fig.6.25. Between step 2 and 3 the curve inclination is lower. The load and total punch movement is 7.22 tons and 5 mm. After step 3, it is seen that the curve changes character and continues increasingly. This is due to the fact that material is strained hardened. As well as increasing friction. At Step 4, in which the load and deformation are 10.53 tons and 7 mm respectively. Step 5 has the load of 16.24 tons with 8 mm deformation. Step 6 and 7's load and deformations are 23.76 tons with 8.5 mm and 40 tons with 9 mm respectively.

As seen in Figs.6.26 while the inner surface meshes get greater, the meshes at the outer surface becomes pressed so cavities are formed at the outer surface, along circumference. However, the same type of lines are observed at the inner surface perpendicular to the circumference.

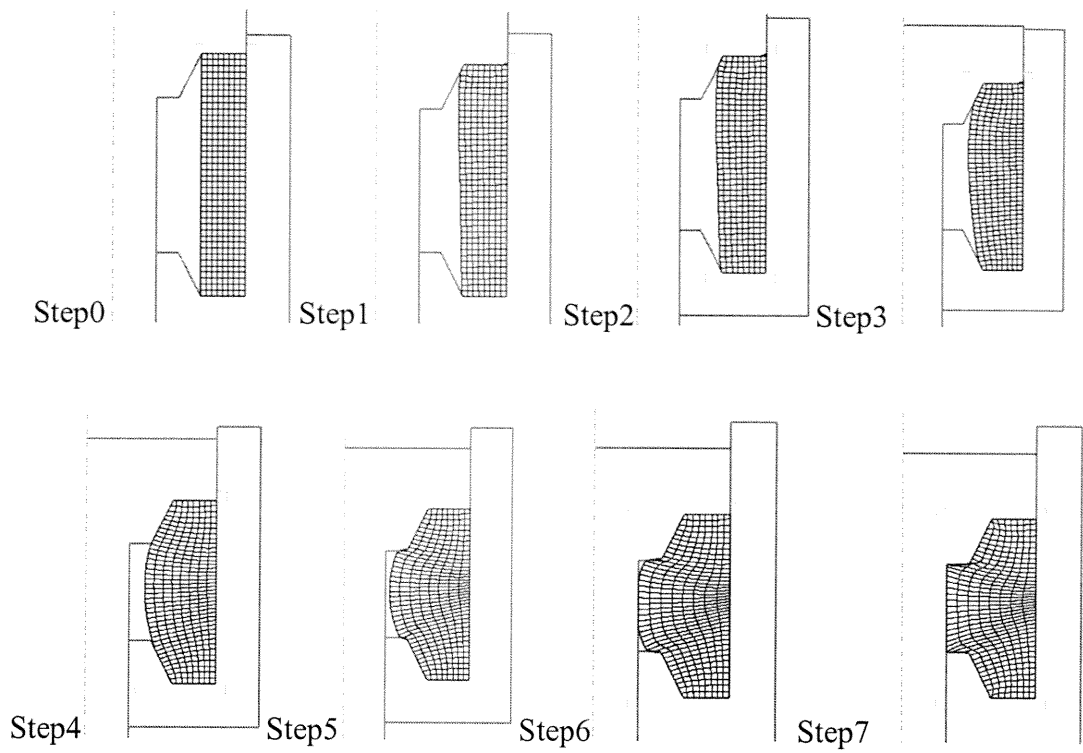


Figure 6.24. Flow Simulation of H1-AI Forging

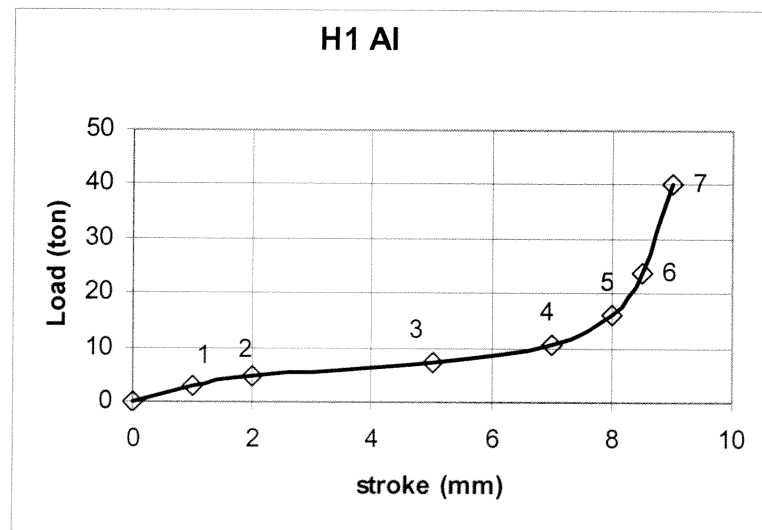


Figure 6.25. Experimental Load-Stroke characteristics of H1-AI Forging

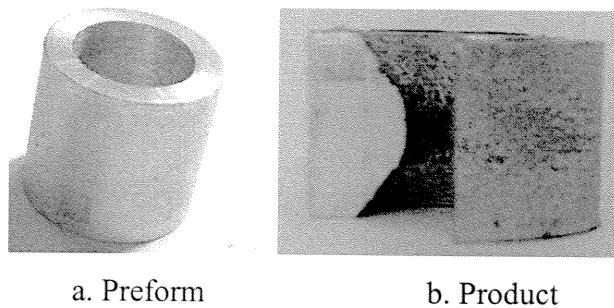


Figure 6.26. Photo of H1-Al Forging

The specimen H2-Al is extruded as well upset to the inner direction (see Fig. 6.27). The flow curve is investigated at 7 points (see Fig.6.28). At point 1, the load is 2.1 tons and the stroke is 0.5 mm. And step 2, the billet is deformed 1.5 mm with the load of 3.61 tons. The step 3 denotes that the deformation and load is 2.5 mm and 5.41 tons respectively at step 4 the load and stroke are 13.1 tons and 4 mm. Step 5 shows that the load of 20.75 tons is applied to the billet and deformed 6.5 mm totally. At the step 6 and 7, the applied loads are 29.77 tons and 40 tons respectively and the total deformations are 7 mm and 8mm.

As seen in Fig.6.28, the load-stroke curve propagates incrementally between step 1 and 3. However, there is an increase in inclination between step 3 and 4. But the inclination decreases between step 4 and 5. After step 5 the curve rises rapidly until step 6 and this rise lowers between step 6 and 7, due to increasing frictional load and strain hardening of material. The rapid increase in step 5 may be due to the fact that the lower die just completes the filling.

The inner and outer surfaces are in different characters (see Fig.6.29). It is observed that the cavities at outer surface are along circumference but the cavities at inner surface run along circumference and thickness. Due to the fact that upsetting and extruding modes occur at the same time.

Moreover, the flow is non-uniform. Because the lower die is filled after the upper die is filled. This shows that the filling of moving parts completes filling sooner than stationary pieces.

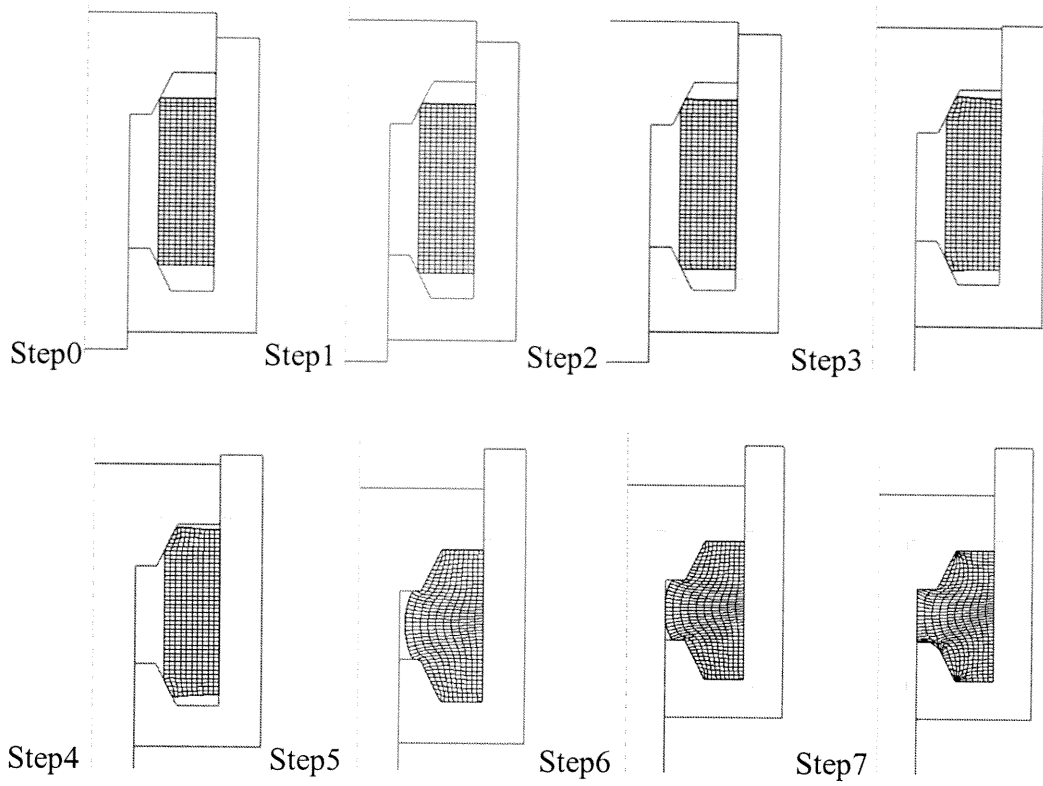


Figure 6.27. Flow Simulation of H2-Al Forging

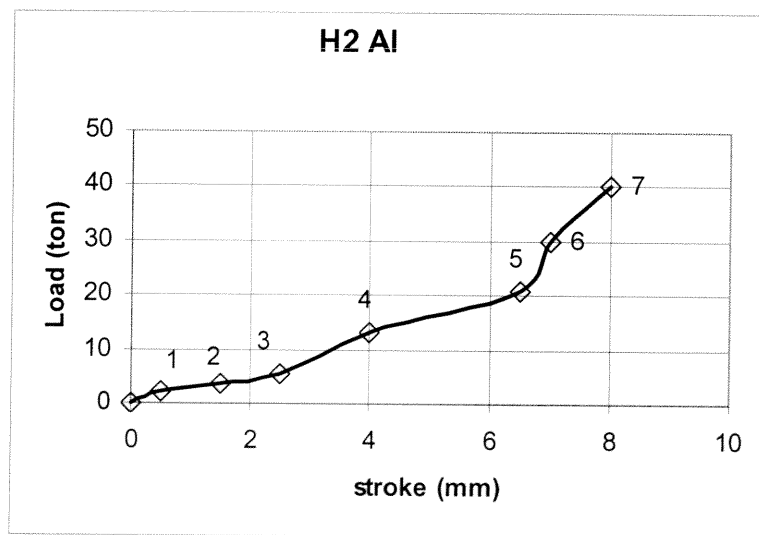


Figure 6.28. Experimental Load-Stroke characteristics of H2-Al Forging

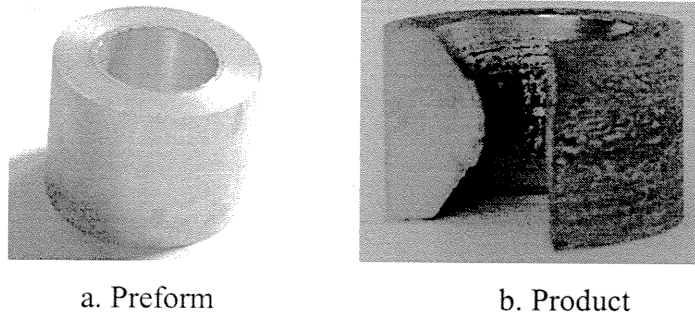


Figure 6.29. Photo of H2-Al Forging

The curve increases to step 4 incrementally (Fig. 6.31). By step 4 the curve continues smaller interval of stroke with respect to higher increase in load until step 5. Between step 5 and 7, load-stroke curve rises more rapidly. The increase in inclination by step 4 to 7 is because of the fact that the strain hardening of material and friction. As seen in flow figures, Fig.6.30, except lower die, other parts are nearly full filled, so a hardening effect and friction factor would be started. The outer surface of the finished work piece is smooth (see Fig.6.32). However, a folding problem is observed at the inner surface (see Fig.6.32). So, there is an increase in mesh concentration at the inner surface.

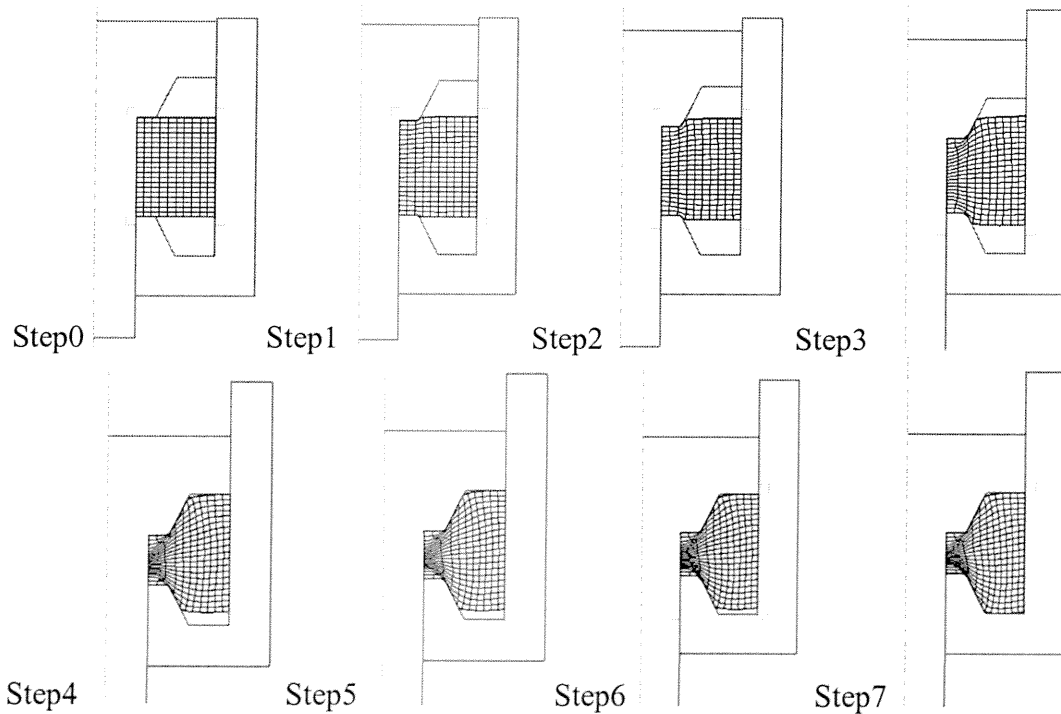


Figure 6.30. Flow Simulation of H3-Al Forging



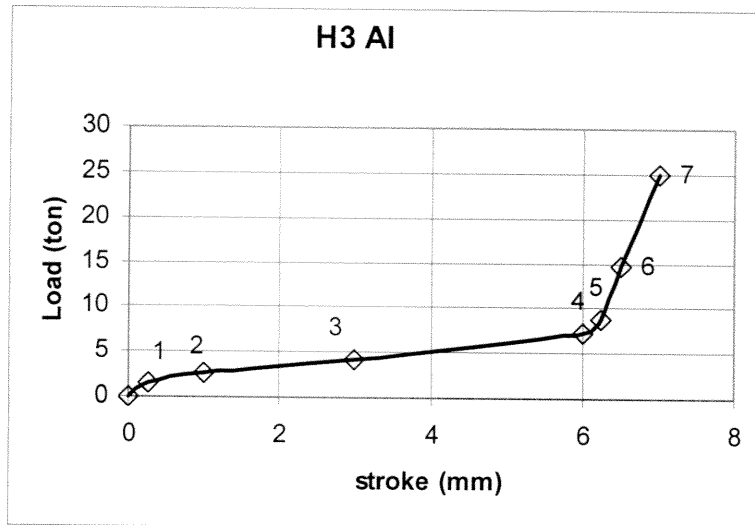
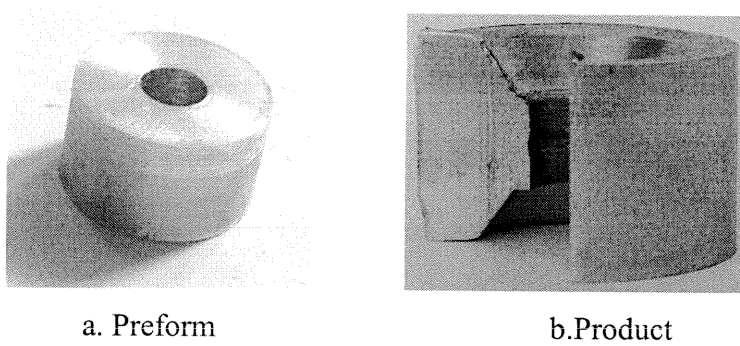


Figure 6.31. Experimental Load-Stroke characteristics of H3-Al Forging Specimen



a. Preform

b. Product

Figure 6.32. Photo of H3-Al Forging

The flow of specimen H4-Al is investigated in 7 steps. As seen in Fig.6.33, there is an incremental increase until step 3. But it is observed that a steep decrease from step 3 to 4. Because, the shearing strength of the material is overcome before the material flows to the wall of the cover die. As a result, the specimen cracks (see Fig.6.34). But as the flow of metal is lasted, it is observed that the crack disappears and finished work piece is extracted. After shearing, step 4, the incremental increase in the load-stroke curve is observed. And the crack is not seen in the finished product due to cold-shot (see Fig.6.35).

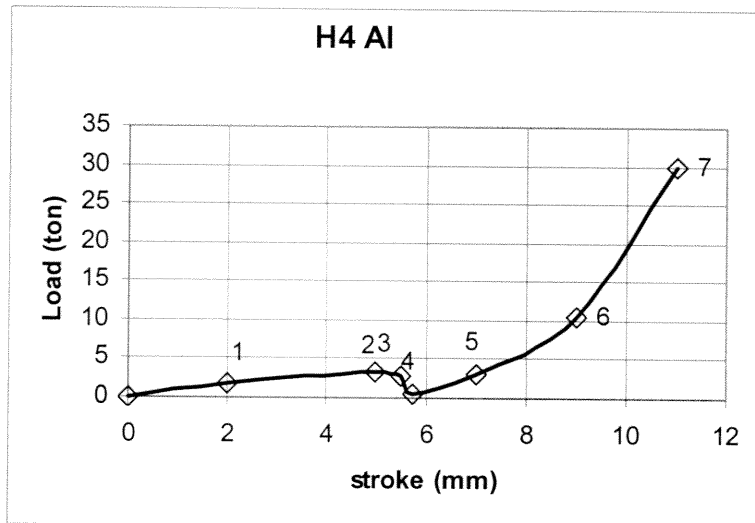
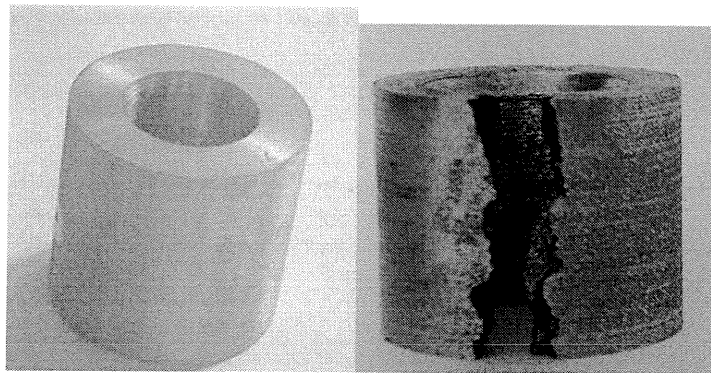


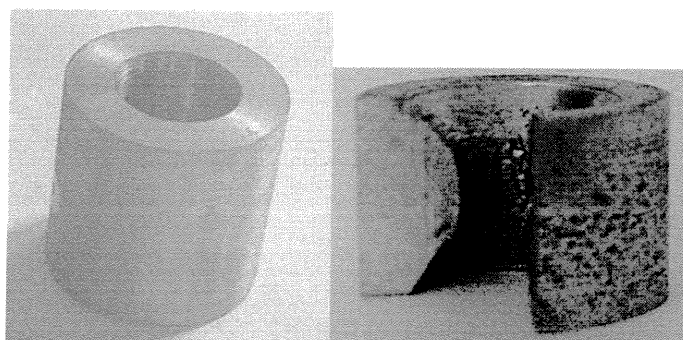
Figure 6.33. Experimental Load-Stroke characteristics of H4-Al Forging



a. Preform

b. Product

Figure 6.34. Photo of H4-Al Forging (Failed Specimen)



a. Preform

b. Product

Figure 6.35. Photo of H4-Al Forging

But if the specimen H4-Al is fit to the guide diameter of the punch tightly, namely the inner flow is restricted, there would not be shearing problem. But at this time, a folding problem would occur at the inner surface, as seen in fig. Step 4 and 5 obviously, see Fig.6.36.

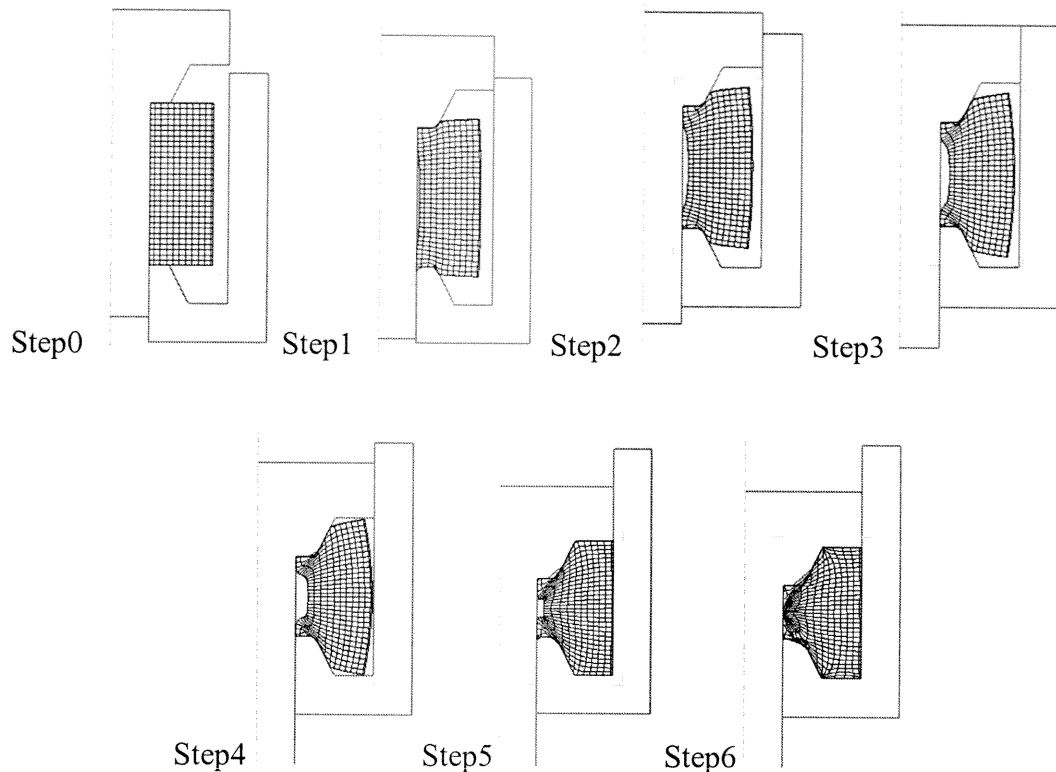


Figure 6.36. Flow Simulation of H4-Al Forging,  
if the specimen would be fit to the die guide diameter

The Fig.6.37 illustrates the H-shape of aluminum forging load-stroke curve. According to the Fig.6.37, extrusion mode of specimen (H3-Al) is more suitable than the others with respect to amount of loads. But when investigating the Figure 6.30, the extruding mode has a folding problem. The best surface finish is extracted by upsetting mode uniquely but the loading increases. So the problem of non-homogeneity in extruding mode is removed by using vibrating die and as well the load is decreased by benefitting the step wise forging.

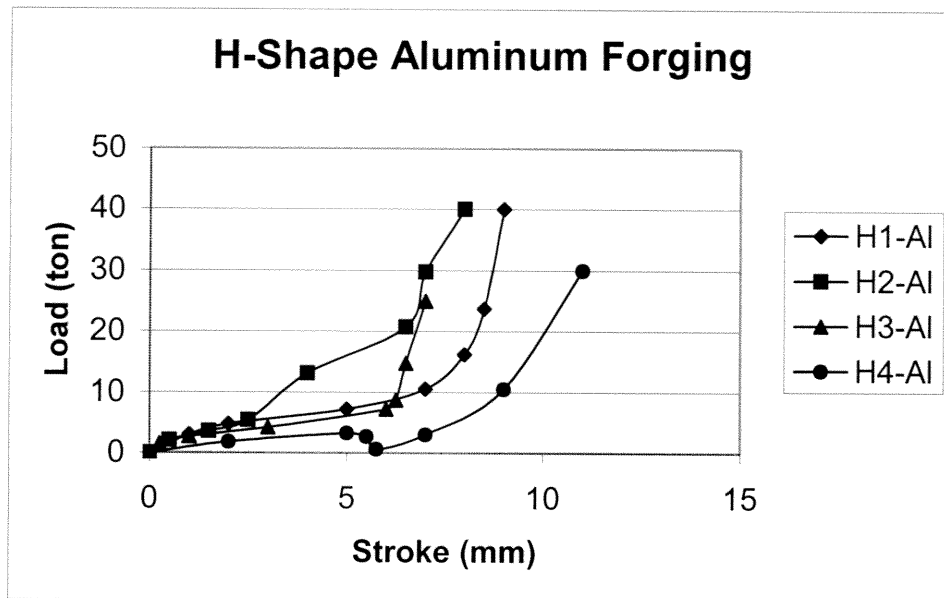


Figure 6.37. Experimental Load Stroke Curve of H-Shape Aluminum

#### 6.2.4. U-Shape Lead Forging

In U1-Pb forging the material flow is inner direction. As seen in Fig.6.38, the flow is uniform or the mesh flows continuously. Investigating Step 0 to 8, the top part of the workpiece is the deadzone, namely no change in mesh sizes. Fig. 6.39 denotes a circumferential cavity at the outer surface of the lower part of the specimen. Fig. 6.38/Step 7 shows that at the zone of line formation the meshes narrow. The metal is more uniform than the same billet of aluminum. The bottom part of billet slides to central direction uniformly due to low friction between Step 4 and Step 8. In load-stroke diagram, Fig.6.39, the load increases with small intervals until step 4. Because of friction effect. By Step 4 it is observed that the inclination increases, because as seen in Fig.6.38, the billet begins to interact with the guide surface of the die so an increase in friction exists.

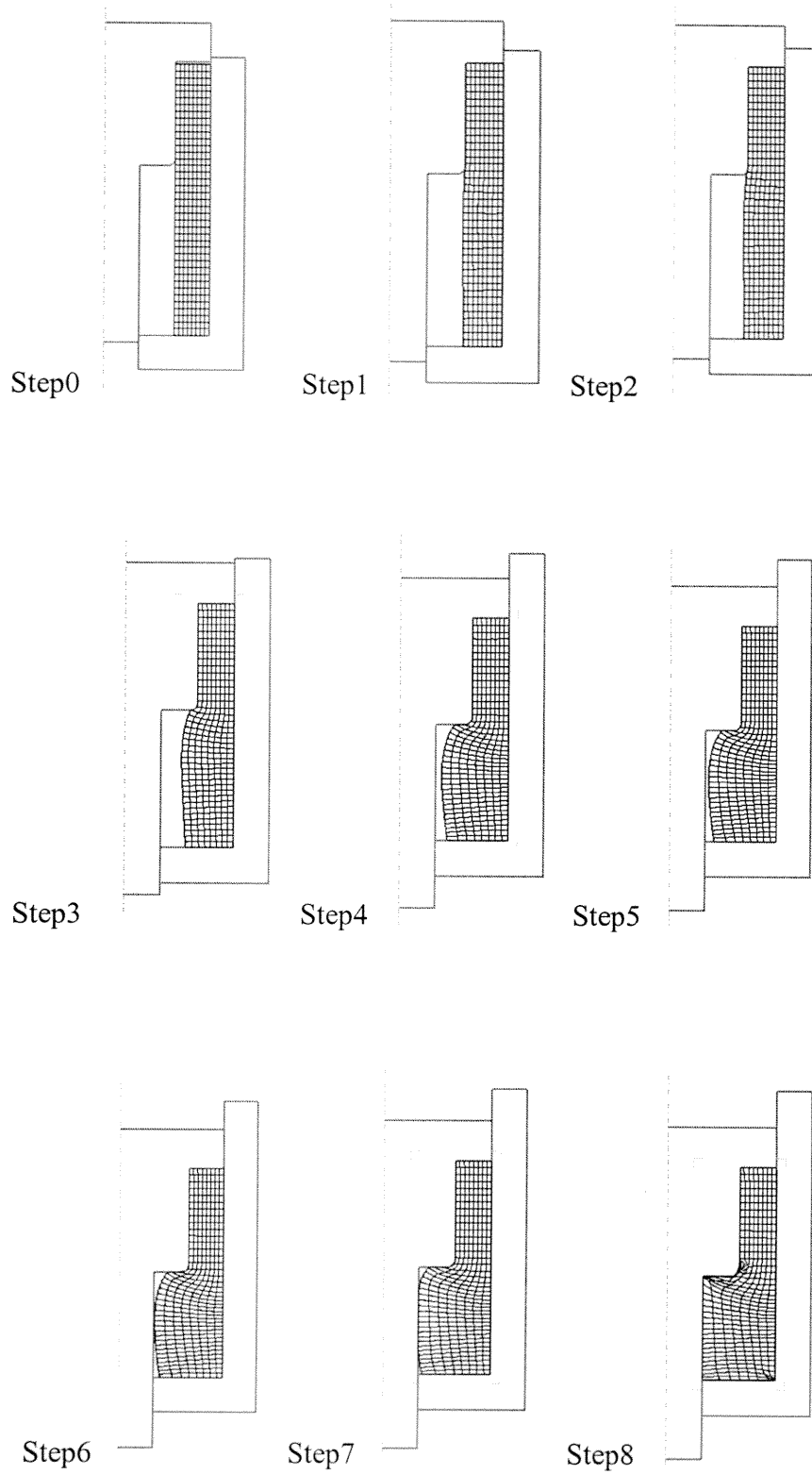


Figure 6.38. Flow Simulation of U1-Pb Forging

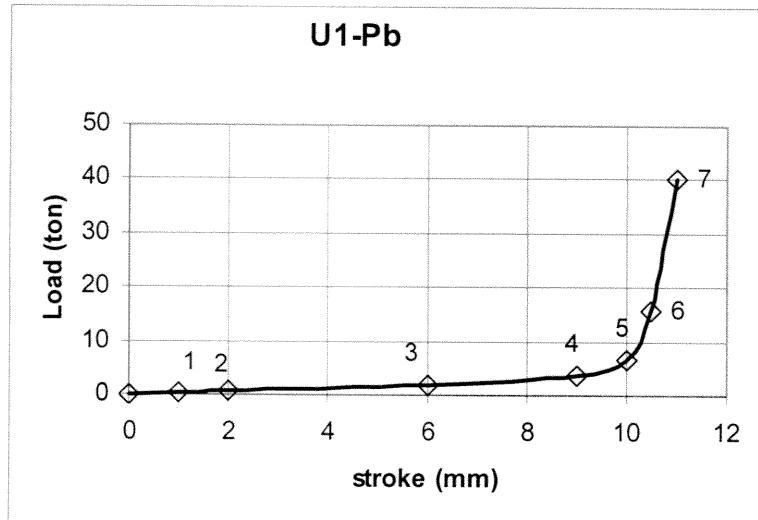
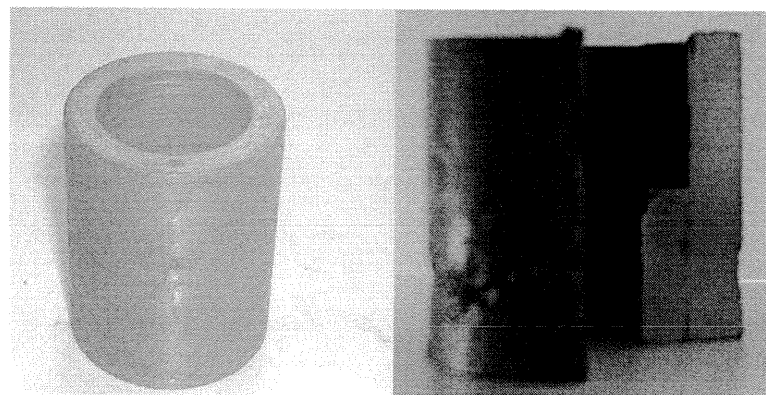


Figure 6.39. Experimental Load-Stroke characteristics of U1-Pb Forging



a. Preform

b. Product

Figure 6.40. Photo of U1-Pb Forging

In forging of U2-Pb billet both upsetting and extrusion take place. However, in this forging the tearing of billet is observed (see step 2 to 8). As well, at the tearing zone, folding starts (step 4). The load-stroke characteristic is the same as U1-Pb forging. After step 4, the curve rises more steeply, because with step 5, the bottom surface of the billet starts to slide over die surface so the friction load increases. As seen in Fig.6.40 , the die can not be filled completely. In this photo, the folding, starting eith step 4, can not be observed. Because a cold welding happens.

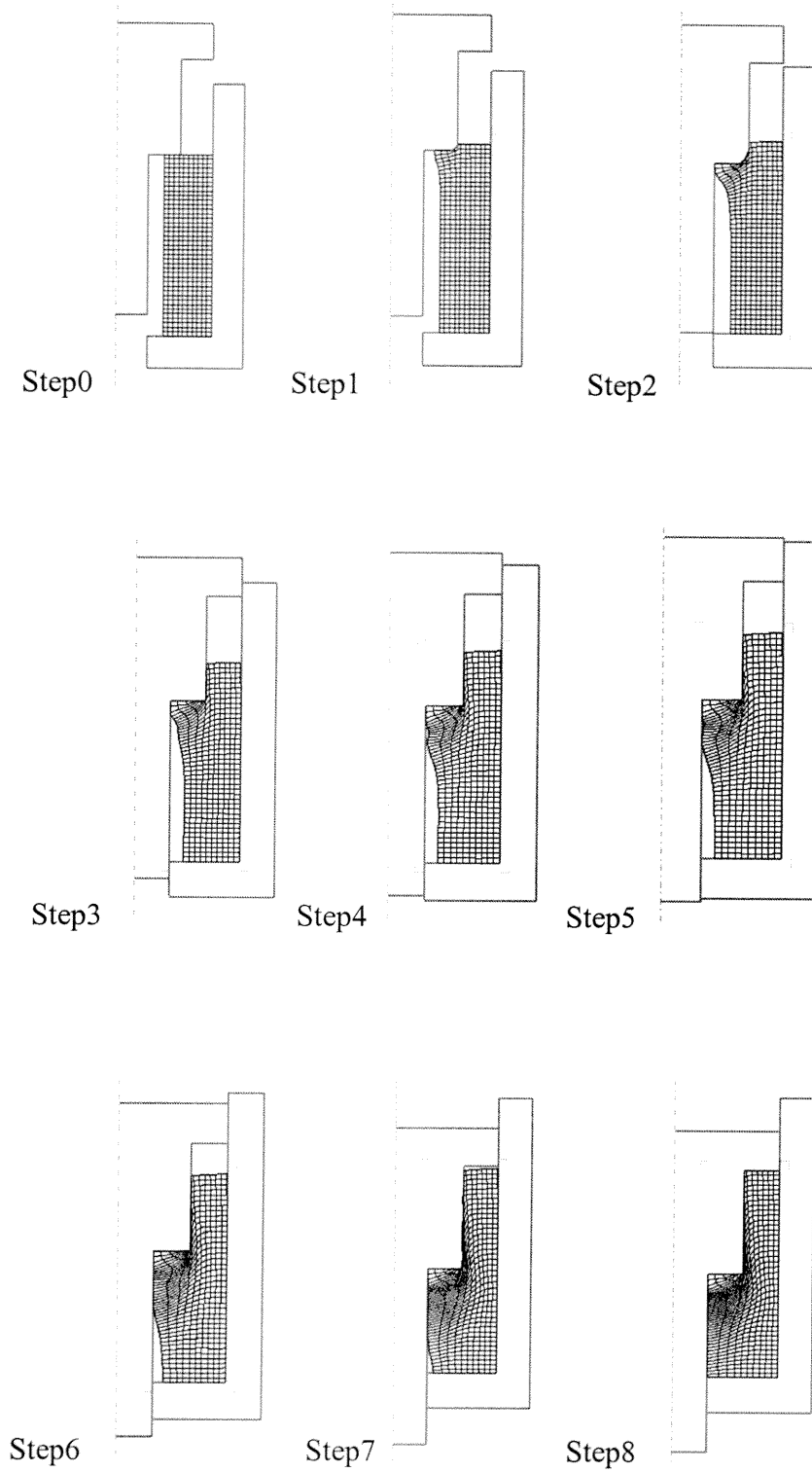


Figure 6.41. Flow Simulation of U2-Pb Forging

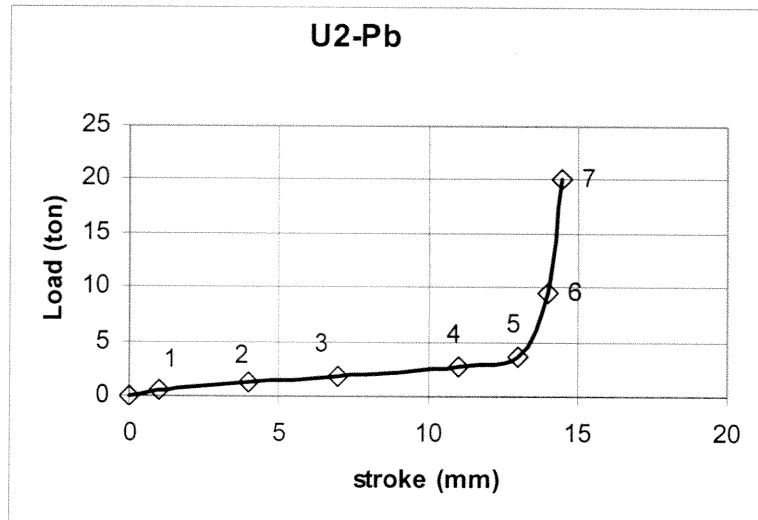
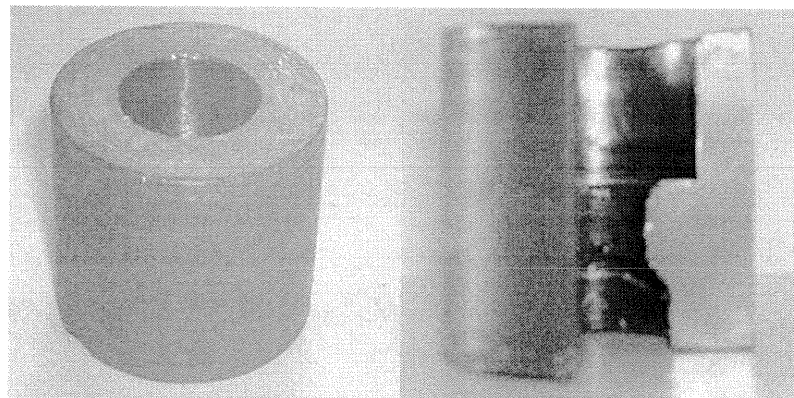


Figure 6.42. Experimental Load-Stroke characteristics of U2-Pb Forging



a. Preform

b. Product

Figure 6.43. Photo of U2-Pb Forging

The deformation mode of specimen U3-Pb is only extrusion. As the billet is forged, tearing is observed at the corner of the workpiece which is in contact with punch (see Fig. 6.44/step 2 to 7). The load stroke diagram characteristic changes after step 1, because step 1 and 2 tearing begins. The tearing is achieved in step 2, then, the diagram changes a more stable zone between step 2 and 5. But after step 5, a steep rise is observed, due to increase in interface contact. The surface is smooth (see Fig. 6.45).



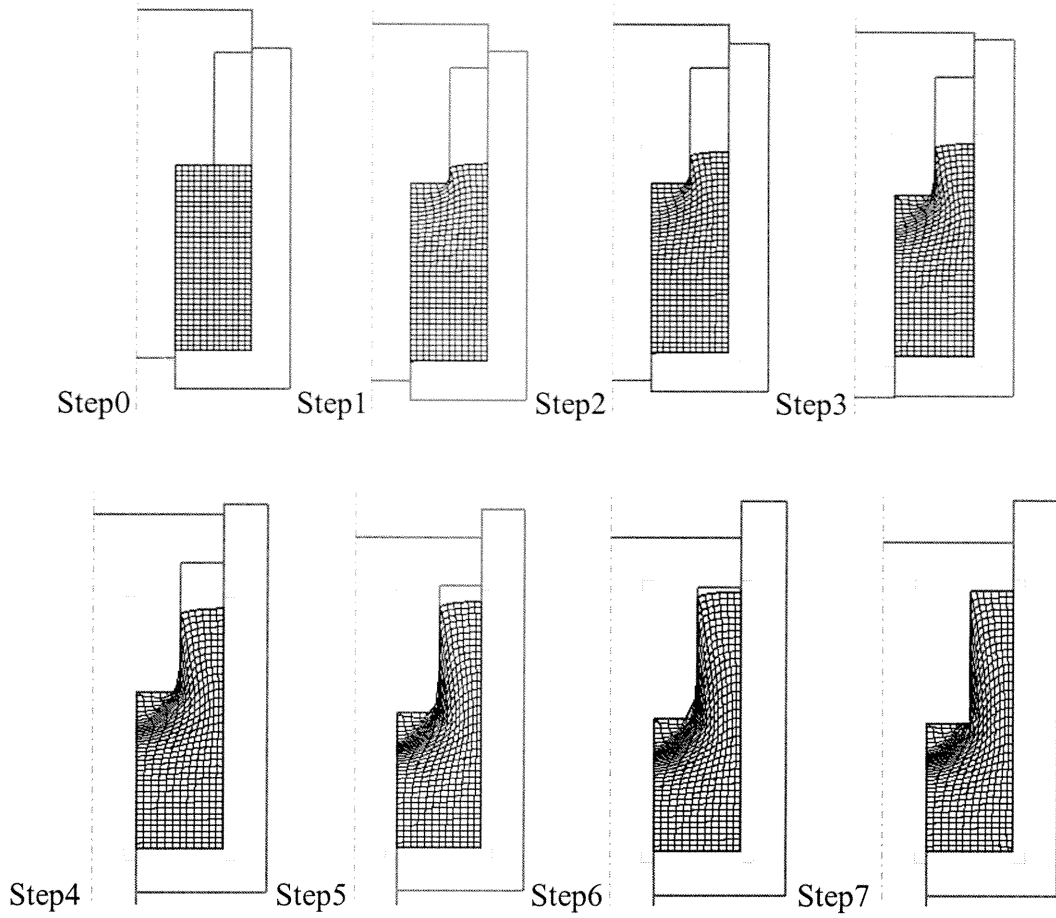


Figure 6.44. Flow Simulation of U3-Pb Forging

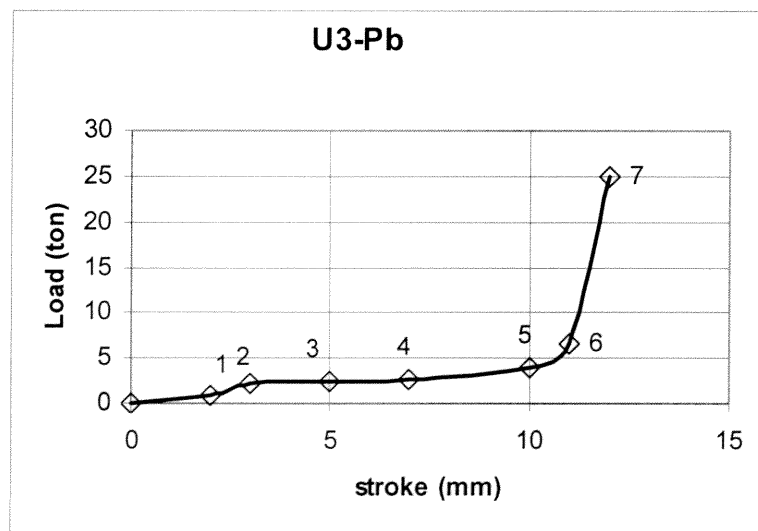
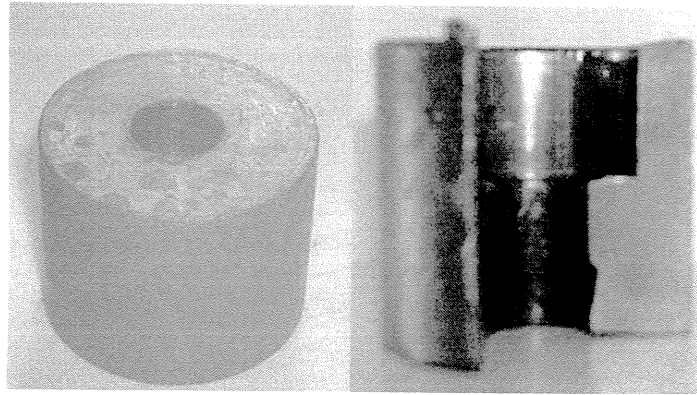


Figure 6.45. Experimental Load-Stroke Characteristics of U3-Pb Forging

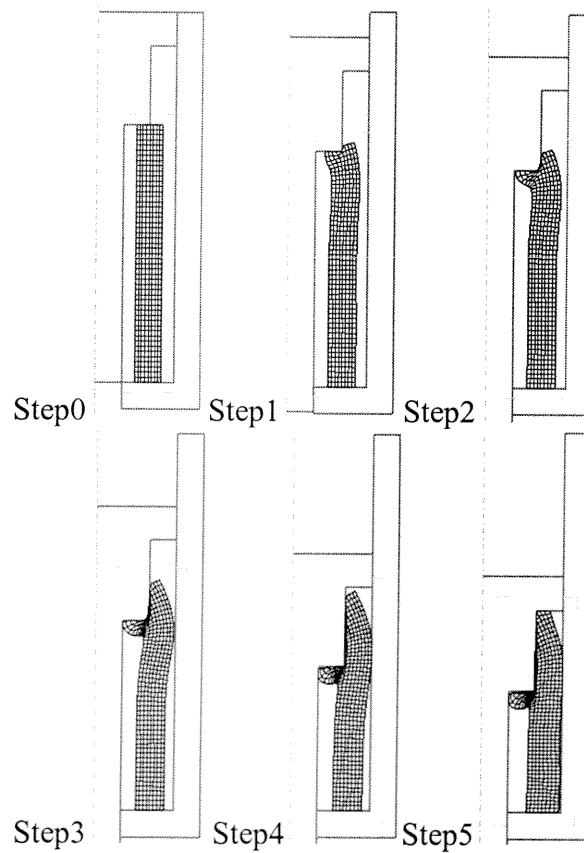


a. Preform

b. Product

Figure 6.46. Photo of U3-Pb Forging

U4-Pb billet is chosen for inspecting the flow characteristic if there is no side contact at the die and the specimen. As the punch moves downward, a piece of material is torn (see Fig.6.47./step3). Tearing is obviously seen.



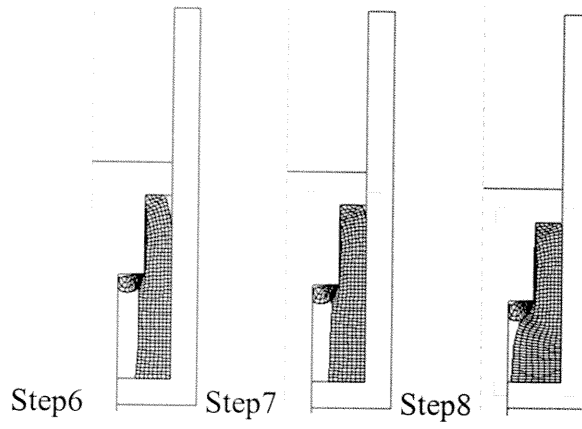


Figure 6.47. Flow Simulation of U4-Pb Forging Specimen

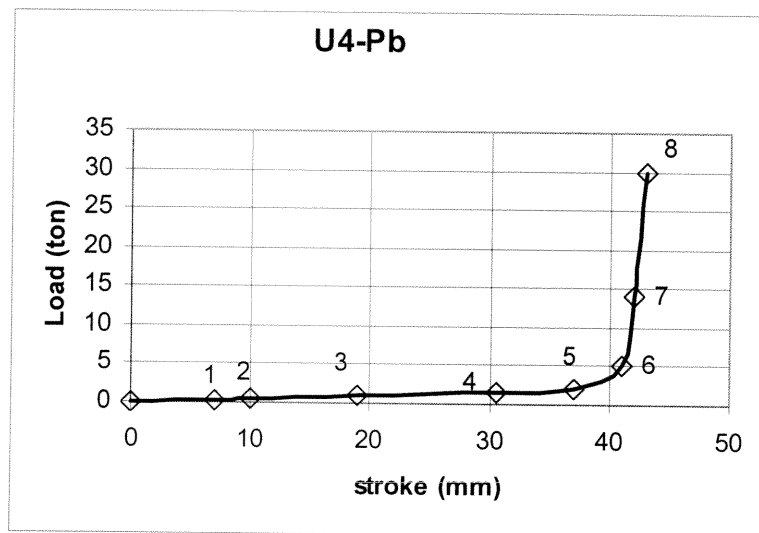
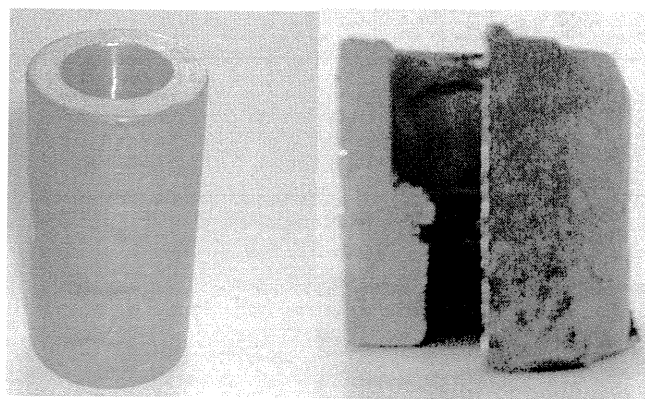


Figure 6.48. Experimental Load-Stroke characteristics of U4-Pb Forging



a. Preform

b. Product

Figure 6.49. Photo of U4-Pb Forging

Fig.6.50 shows the U-shape forging of lead. If the load is considered, the U2 preform is ideal. Namely, the upsetting as well as extruding mode is to be chosen. But it has a problem of tearing at the zone of punch contacting to the work piece . All extruding modes have the problem of tearing so the uniquely upsetting mode should be best choice. But the load is highest with respect to the others. The forging load decreases by using vibrating tool and stepwise forging. And the energy needed for upsetting mode is the most suitable.

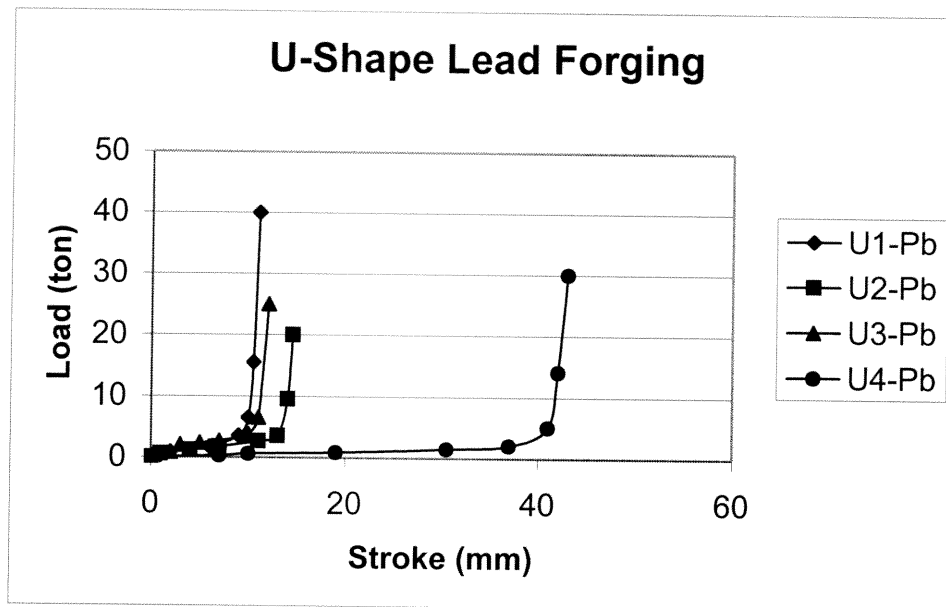


Figure 6.50 Experimental Load Stroke Curve of U-Shape Lead

### 6.2.5. T-Shape Lead Forging

T1-Pb specimen flows away from central direction as being forged. The workpiece is bended while forging is carried out until Step 6, due to low load capacity of the press. But simulation is carried out until Step 7, completely filling of the die. A folding line occurs at the inner surface of the workpiece. Until step 2, the increase in load is very low. But after step 2, an increase in slope is observed, because the material begins to flow at the bottom as well as being bended, so friction load increases with increasing surface area until step 5. After step 5, the load rises rapidly. As seen in Fig 6.51/step 5 the workpiece begins to interact with the side walls of die. So increasing interface area rises the friction load.

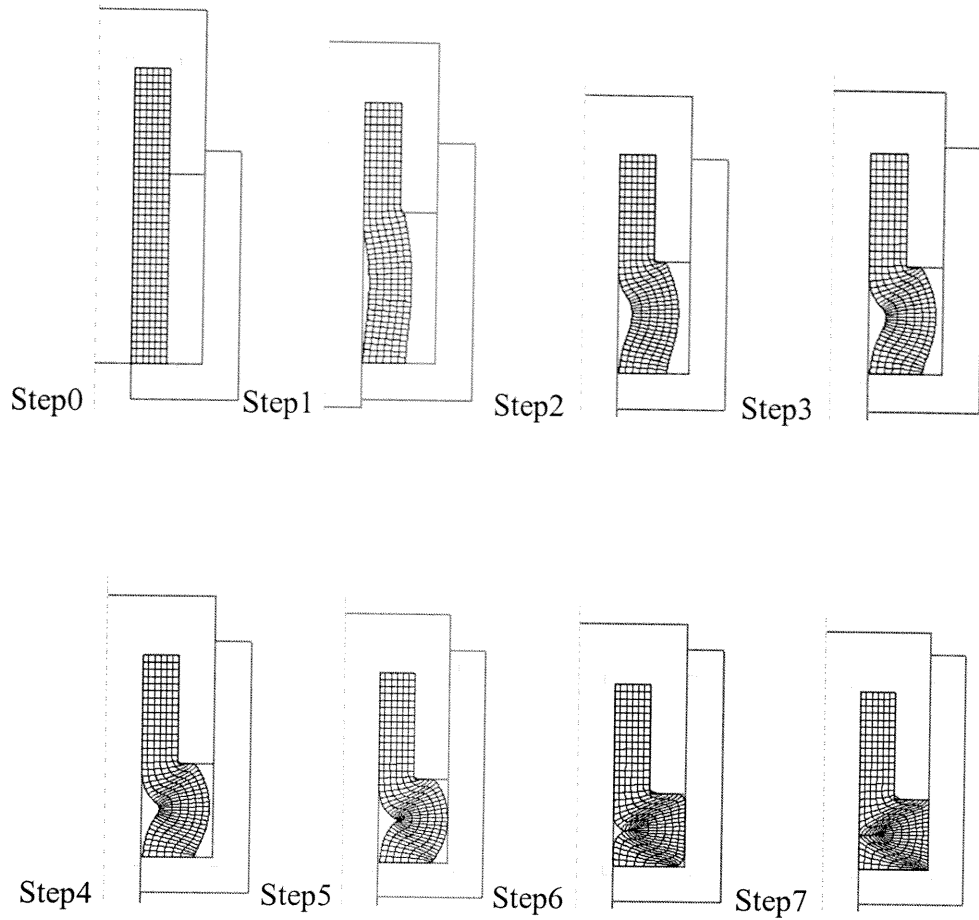


Figure 6.51. Flow Simulation of T1-Pb Forging

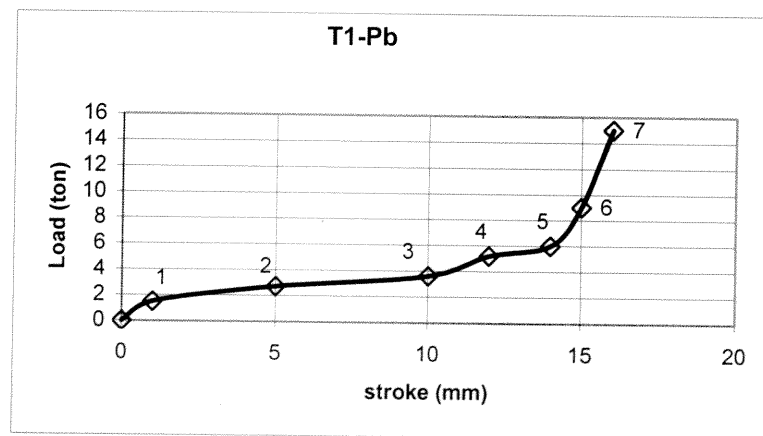


Figure 6.52. Experimental Load-Stroke characteristics of T1-Pb Forging



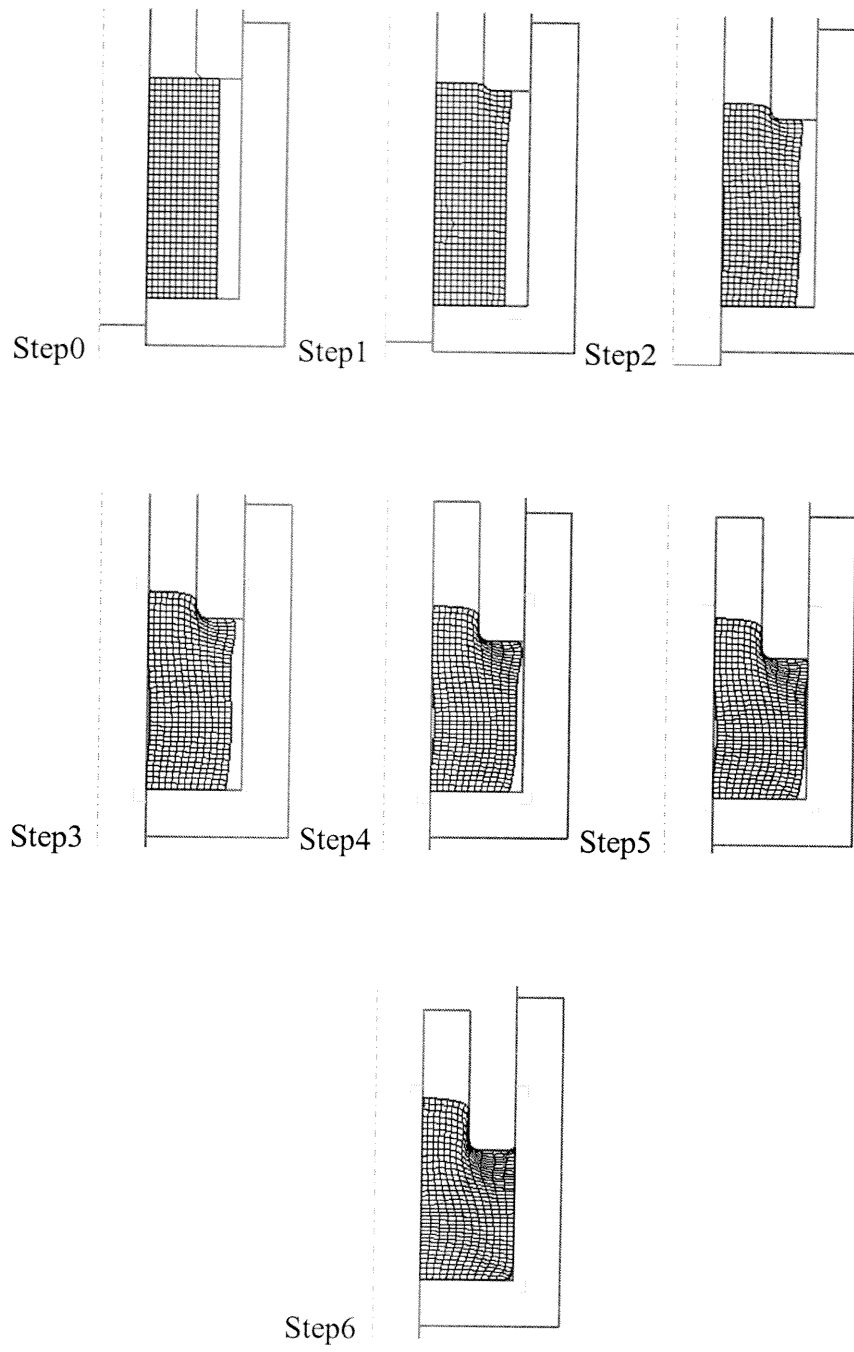


Figure 6.54. Flow Simulation of T2-Pb Forging

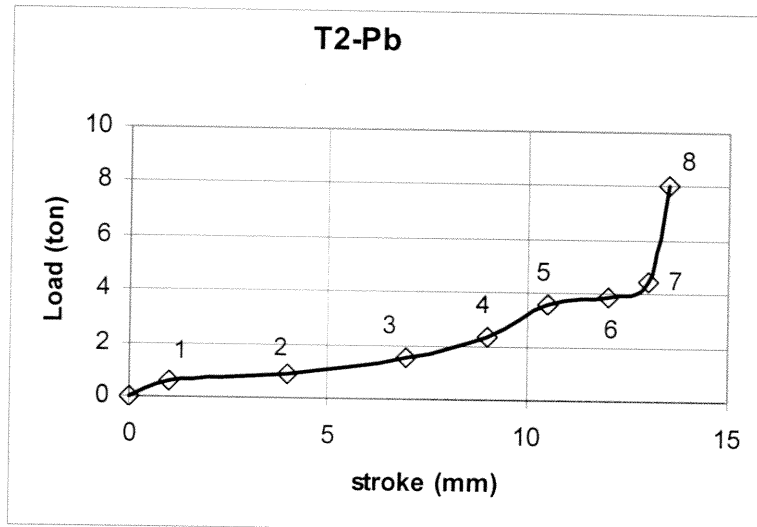
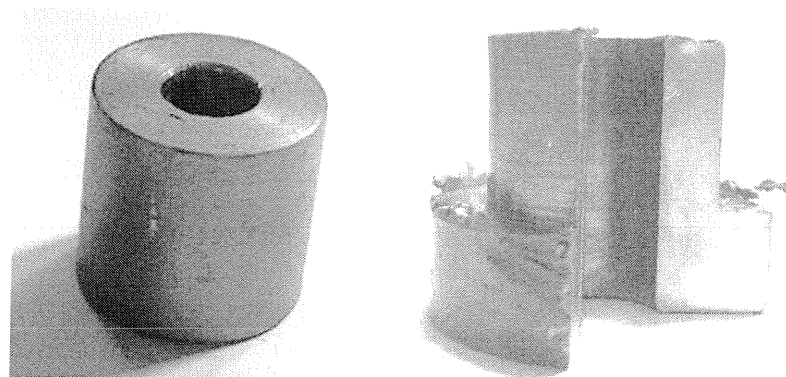


Figure 6.55. Experimental Load-Stroke characteristics of T2-Pb Forging



a. Preform

b. Product

Figure 6.56. Photo of T2-Pb Forging

The specimen T3-Pb is extruded only (see Fig.6.57/step 0 to 4). The figure illustrates the flow until step 4, because the modelling program has the same problem as in forging of T2-Al, T3-Al and T2-Pb. But the extracting of finished work piece from die is overcome due to softness of lead material. After load is released at the end of experiment, the friction rate lowers enough for taking out the finished work piece. As seen in Fig.6.59, the fin formation is very low and the finished surface is as smooth as T2-Pb forging. But the die is not completely filled. The load rises rapidly between step 0 and 3, because the fin formation between punch and the die wall increases the frictional load. But with step 3 the fin formation would be completed and the work



piece extruded uniquely so the inclination drops between step 3 and 5. After step 5, the load increases steep against small deformation period. This load steep increase depends on the formation of contact between lower surface of punch and the top surface of work piece, so frictional load increases rapidly.

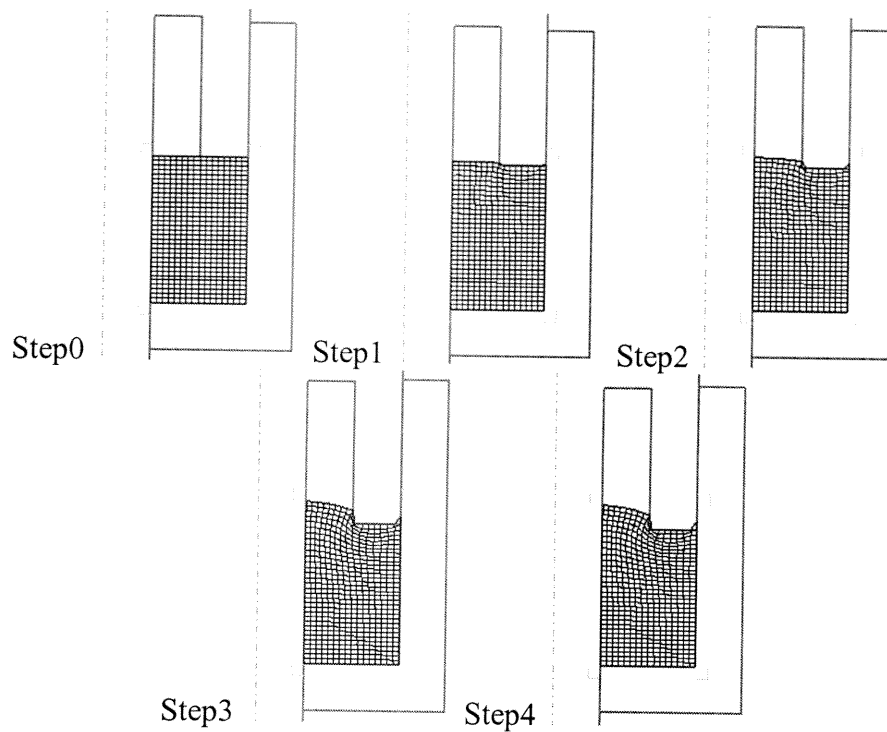


Figure 6.57. Flow Simulation of T3-Pb Forging Specimen

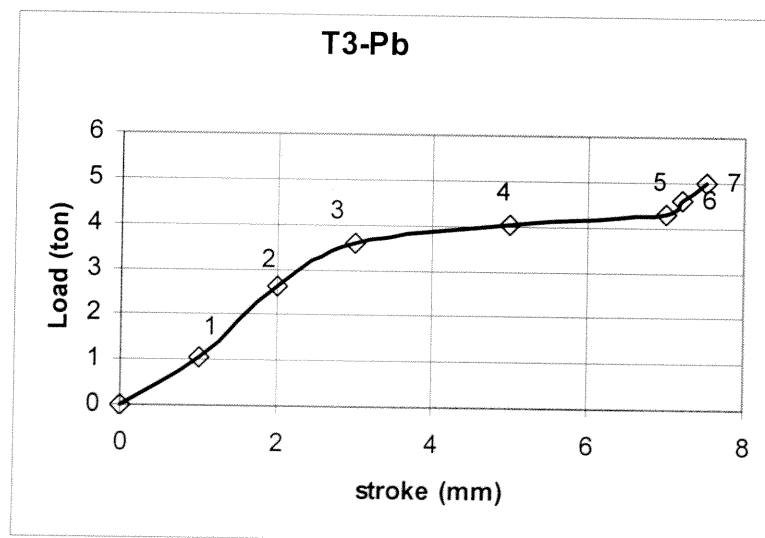


Figure 6.58. Experimental Load-Stroke characteristics of T3-Pb Forging

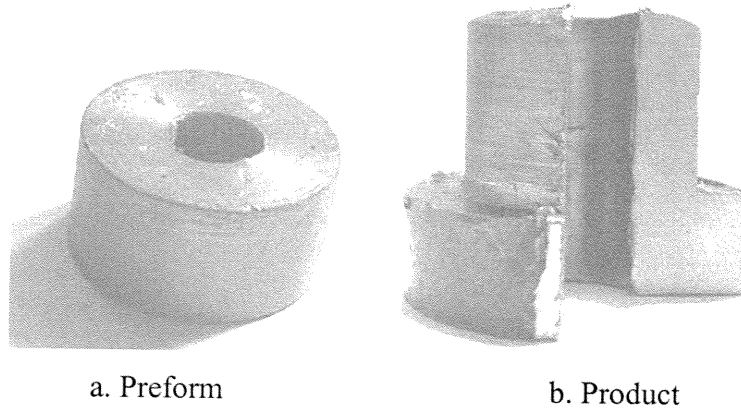
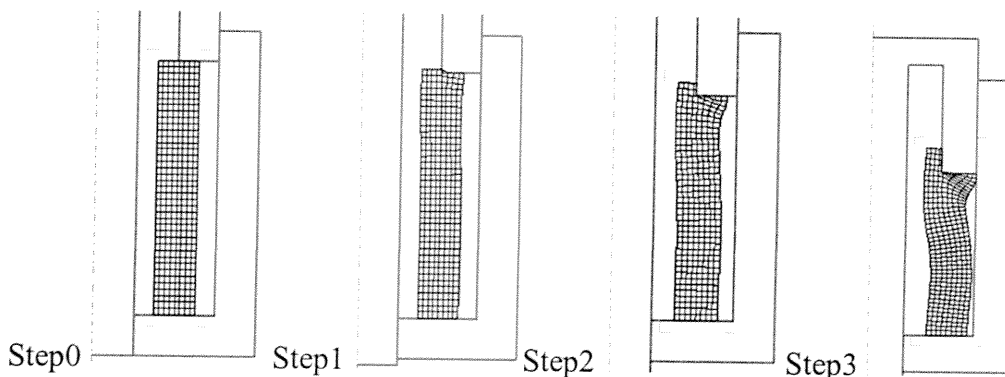


Figure 6.59 Photo of T3-Pb Forging

T4-Pb billet flows inner and outer directions while extruding. The flow is not uniform. The workpiece is bended until touching side wall of the die. So, firstly outer upsetting occurs then the inner flow starts. This point of crossing is step 4. So the stroke-load curve slope increases as the billet starts inner upsetting. This character of load-stroke curve goes on step 6. So this shows the inner upsetting needs higher loads than the outer upsetting. In Fig.6.62, a folding line at the outer surface is observed but in the photo of the finished workpiece no folding line is shown. So the folding line could be cold shut. But a folding line is seen at the inner surface of the finished workpiece in the photo. The load-stroke graph changes character between step 6 and step 7. Because with step 6 the upsetting mode is finished and extruding mode begins. But after step 7, a rapid rise in load is observed. The top surface of the extruded part of billet starts to contact with lower surface of the punch. So friction load increases with increasing area and the top surface begins inner upsetting. As a result the load increases. Moreover, the fin formation very high.



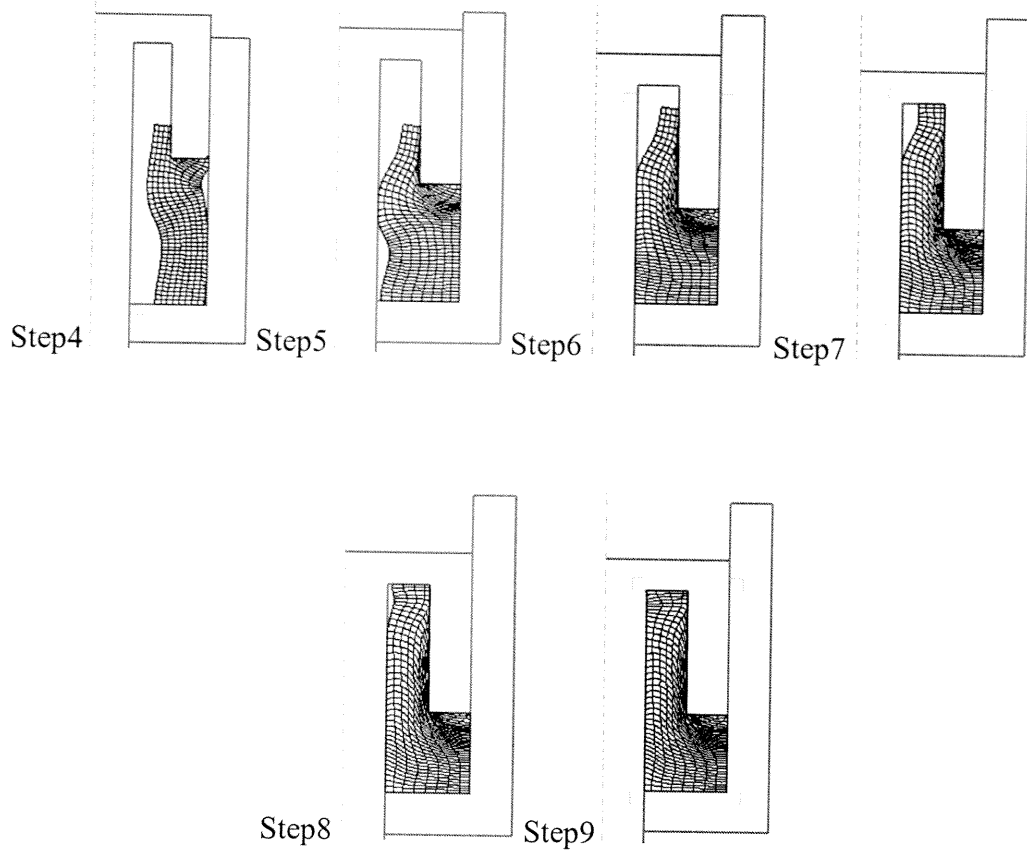


Figure 6.60. Flow Simulation of T4-Pb Forging

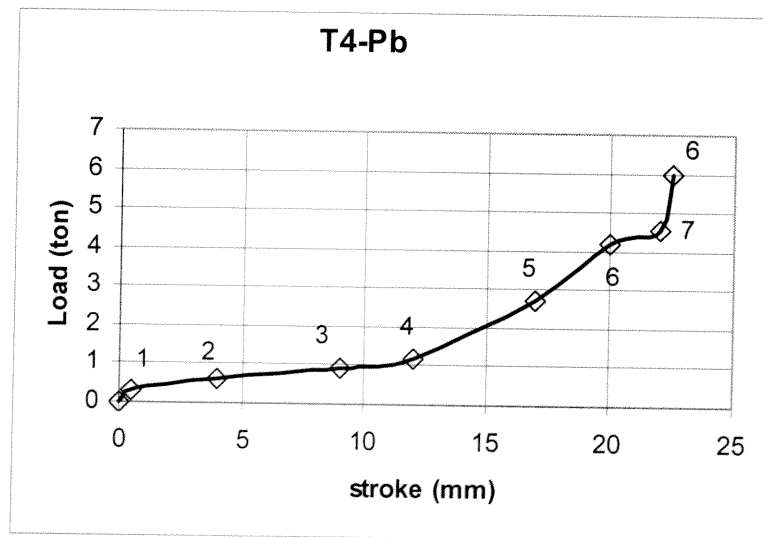
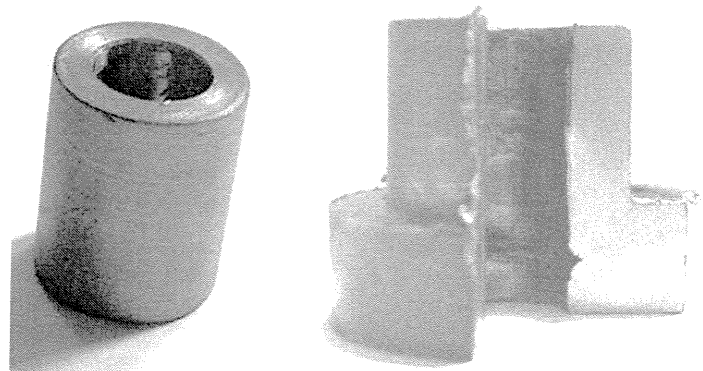


Figure 6.61. Experimental Load-Stroke characteristics of T4-Pb Forging



a. Preform

b. Product

Figure 6.62. Photo of T4-Pb Forging

The load-stroke curve denotes that the extruding mode (T3-Pb) has the lowest forging load of hot working. As well, extruding needs the lowest energy with respect to the other modes. But investigating Fig. 6.58, the die is not filled completely, so the filling problem is solved with vibrated die. As the die vibrates, more uniform flow is obtained and the filling problem will be solved. Moreover, the energy suffered for upsetting mode is most suitable with respect to the other flow modes (Fig. 6.63).

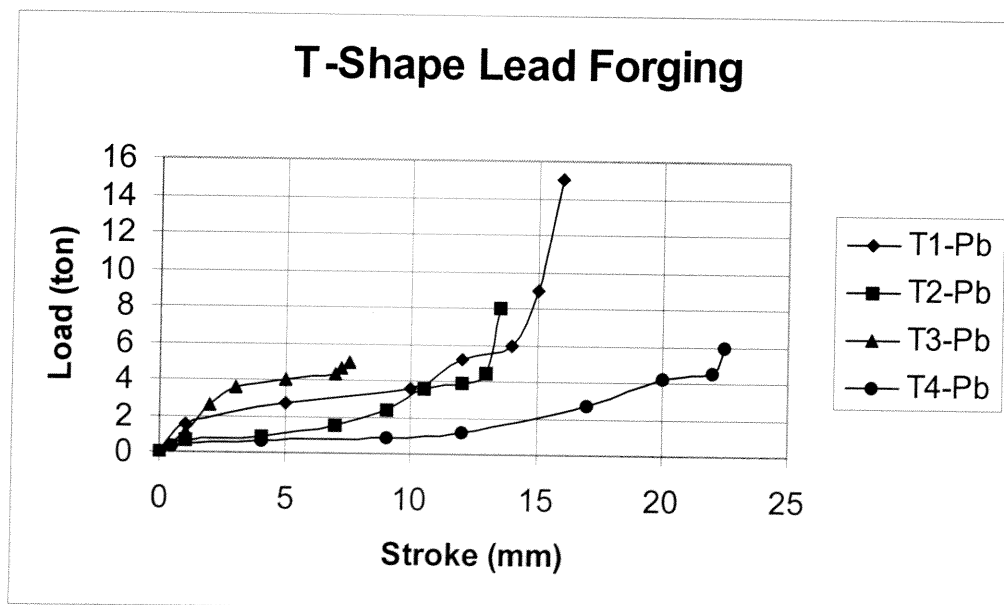
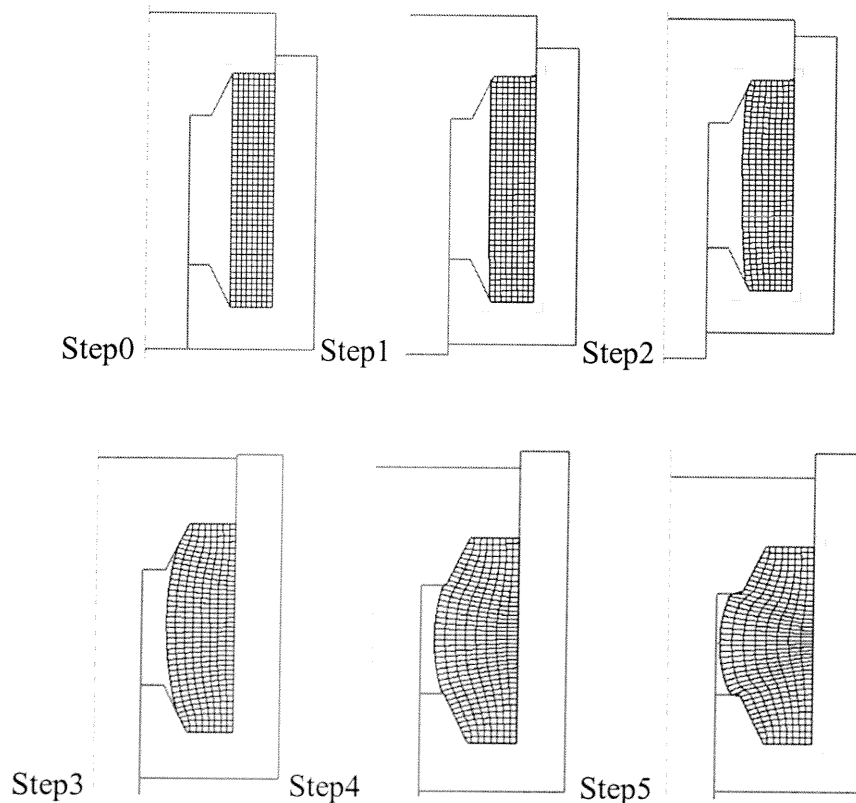


Figure 6.63. Experimental Load Stroke Curve of T-Shape Lead

### 6.2.6. H-Shape Lead Forging

The billet H1-Pb denotes inner upsetting mode. As the punch moves downward, the workpiece upsets to the inner direction. As seen in Fig. 6.64/ step1 to 7, the flow is more uniform than the flow of H1-Al. Remembering that the aluminum flow is not uniform, firstly the upper part is filled. Later the lower die is completely filled. But here, lead specimen fills the top and bottom die cavities at the same time. As seen in Fig.6.66, lines are formed at the outer surface due to the fact that the flow lines are through central direction. Investigating the load-stroke curve, the increase in load between steps 1 and 4 is uniform the increase rises more rapidly with step 4. Because the material fills the narrow part of the die between punch and lower die. Moreover, after step 5 the load-stroke curve runs steeply, because the workpiece touches the mandrel surface of the die with step 5. So friction load increases.



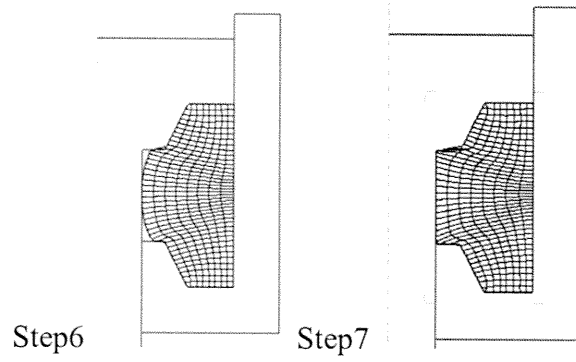


Figure 6.64. Flow Simulation of H1-Pb Forging

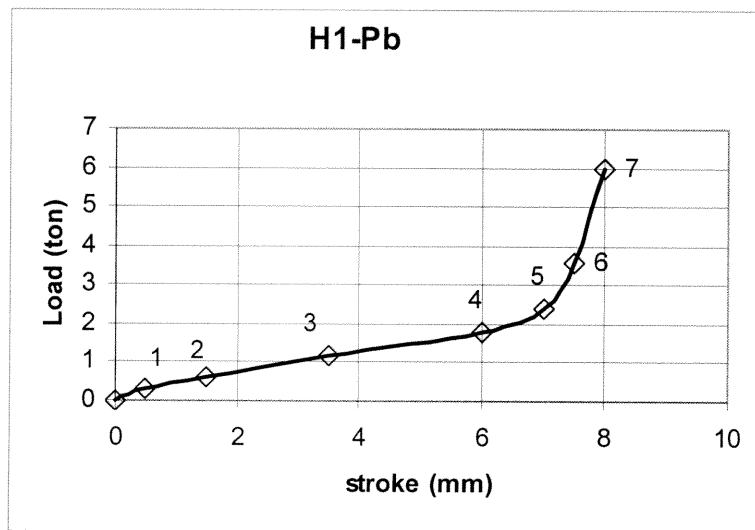
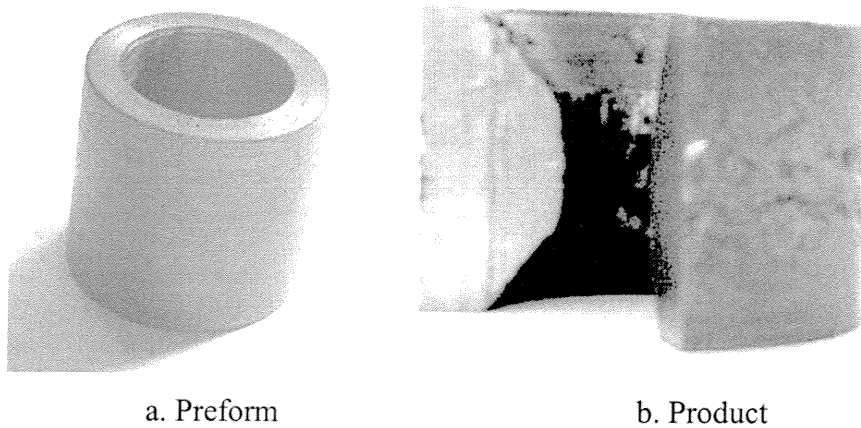


Figure 6.65. Experimental Load-Stroke characteristics of H1-Pb Forging



a. Preform

b. Product

Figure 6.66. Photo of H1-Pb Forging

Specimen H2-Pb flows inner upsetting at the same time extrudes. As the punch goes down, the extruding and upsetting exist uniformly. The material fills the cavities equally. Flow occurs with a stable increase in load until step 2. After step 2, the inclination of the curve rises with step 3 until step 5. Because extruding mode finishes and the workpiece starts to touch punch and lower die surfaces. After that, the material flows to the narrow zone between punch and lower die by upsetting. So the inclination increases between step 5 and 6. With step 6 the load rises steeply. The material interacts with mandrel so the flow is constrained and the friction load increases. The inner surface covers cavities in the form of lines, due to contraction of workpiece while forging.

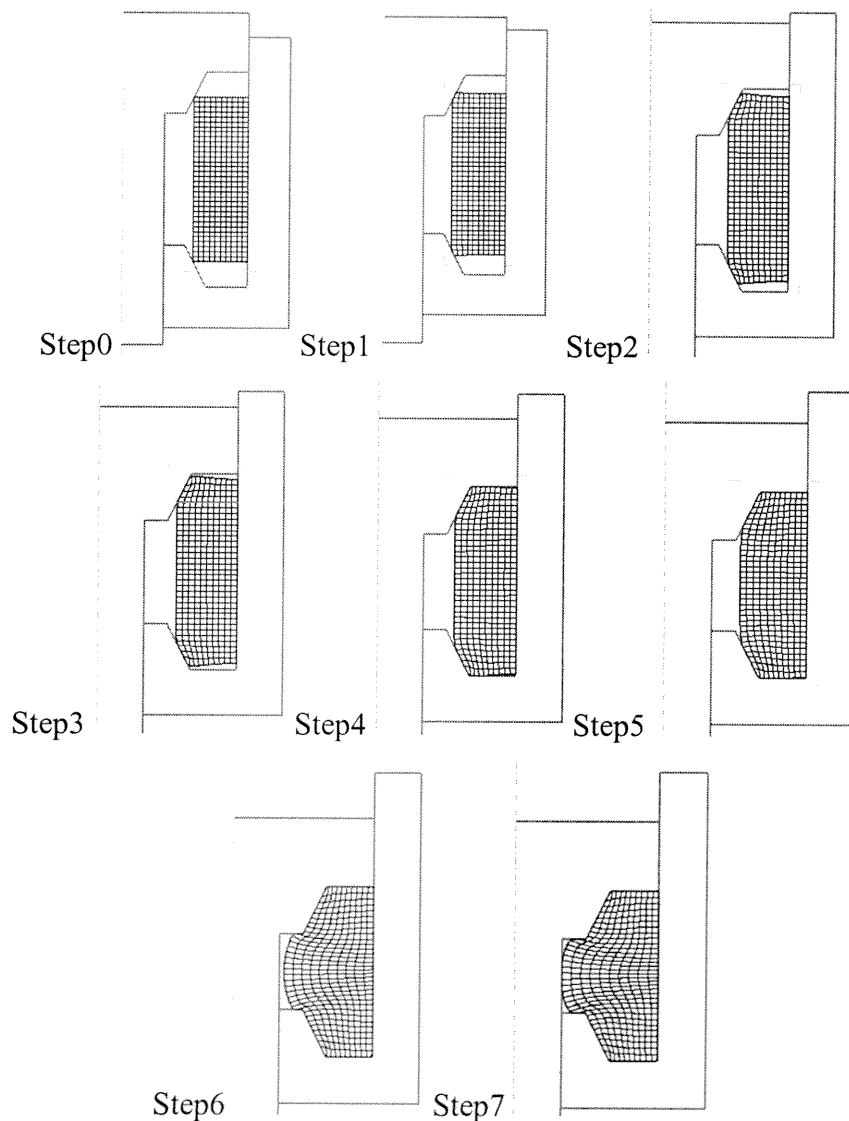


Figure 6.67. Flow Simulation of H2-Pb Forging

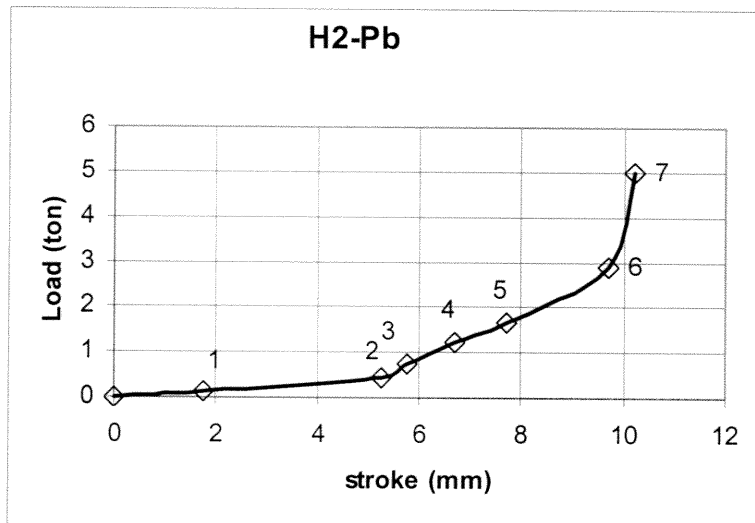
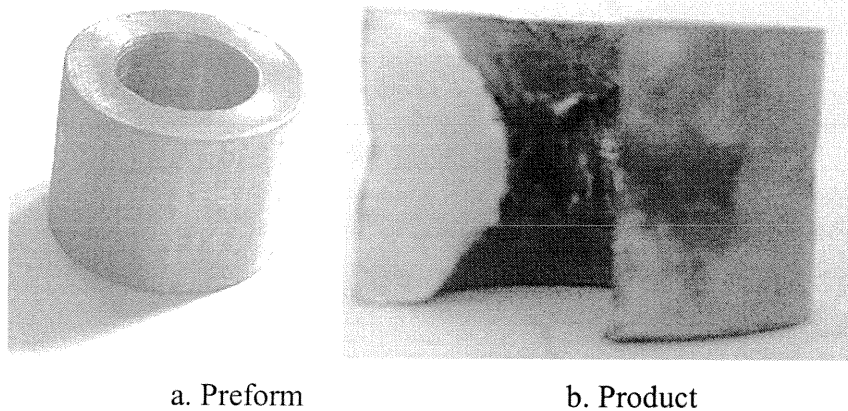


Figure 6.68. Experimental Load-Stroke characteristics of H2-Pb Forging



a. Preform

b. Product

Figure 6.69. Photo of H2-Pb Forging

While punch moves downward, H3-Pb flows inner upsetting. The upper cavity is filled more quickly than the lower cavity, see Fig.6.70/step 1 to 7. So filling of die is not uniform. The load stroke curve changes character with step 2 and continues stable inclination until step 4. However, it is observed that the load rises more rapidly until step 6. Between step 6 and 7 load rises steeply. At the inner surface a folding line exists (see Fig. 6.71). However, the other surfaces are smooth and the fin



formation is very low. Fig. 6.72 illustrates from Step 5 to Step 7. As seen in the photos, the folding line gets smaller while the die is filling completely. And the simulation (Fig. 6.70) shows the same character of the die filling and surface with the photos illustrating from Step 5 to Step 7.

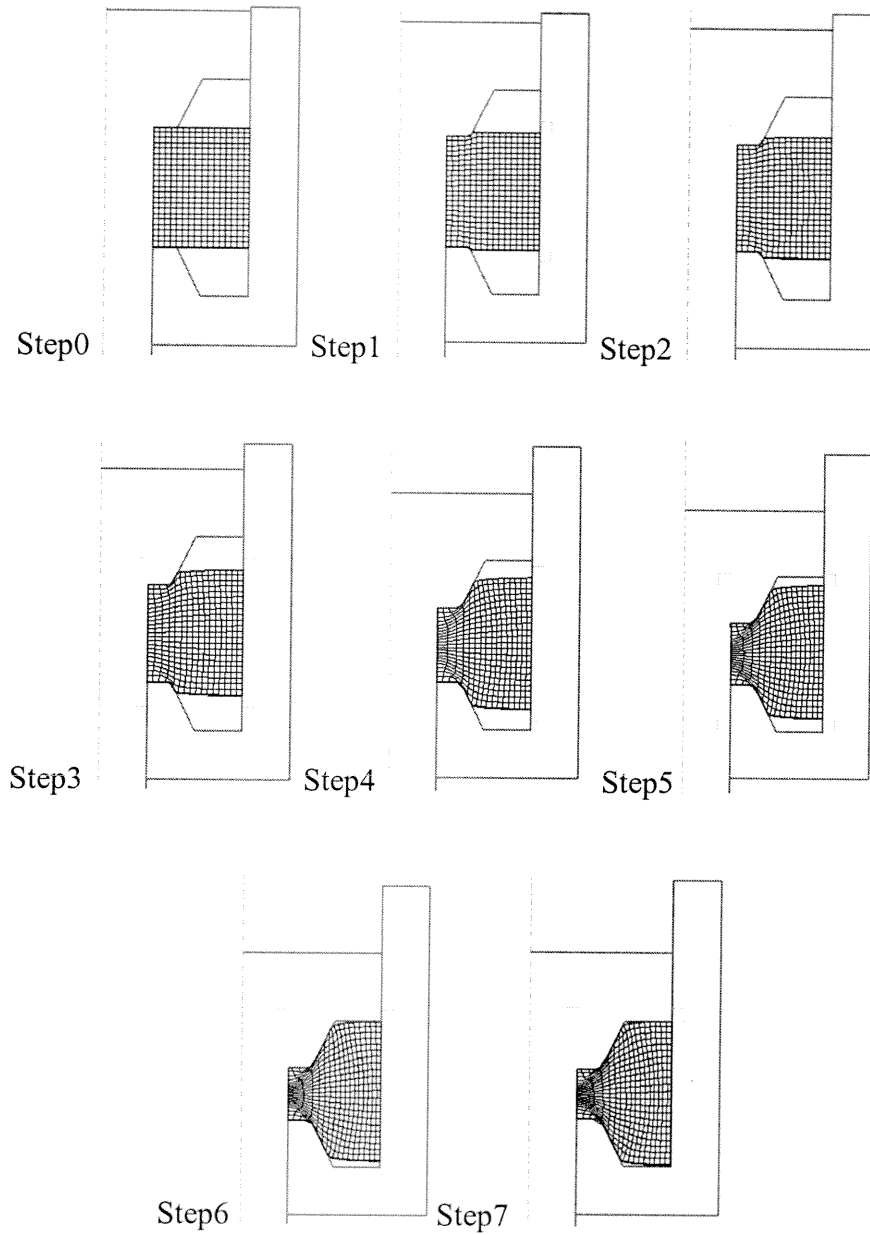


Figure 6.70. Flow Simulation of H3-Pb Forging

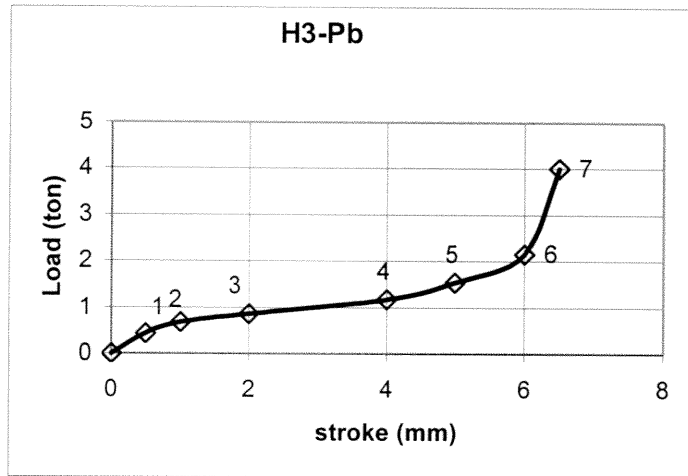


Figure 6.71. Experimental Load-Stroke characteristics of H3-Pb Forging

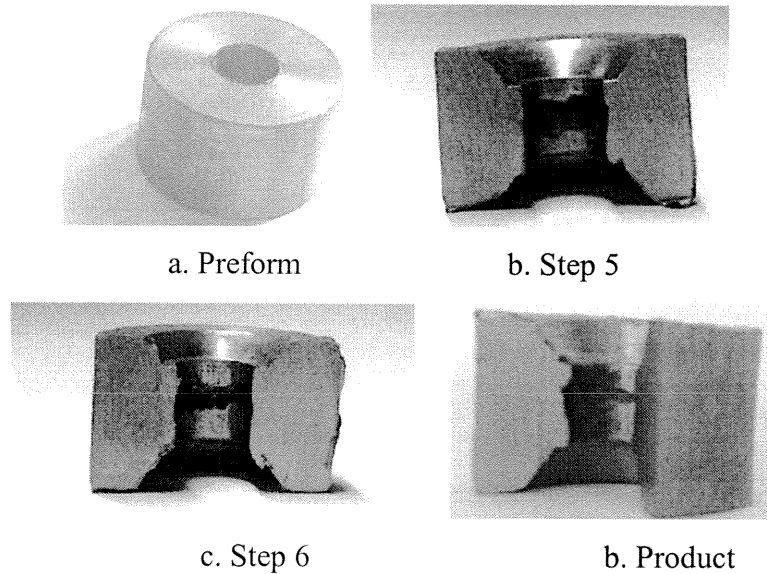


Figure 6.72. Photo of H3-Pb Forging

H4-Pb forging is carried by providing inner and outer upsetting as well as extruding modes. The load-stroke curve rises constantly until step 4. But after step 4, the load increases more rapidly until step 6. The billet flows outer direction and interacts with the walls of the die. So friction load increases as well forging load rises. The load increases steeply between step 6 and 7, due to interacting of workpiece with all surfaces. The finished workpiece has tearings, but no obvious cracking occurs while forging. If cracking is happened, the steep decreasing of load is observed. But small tearings which does not cause decreasing of forging load can be cold welded due to high pressure.

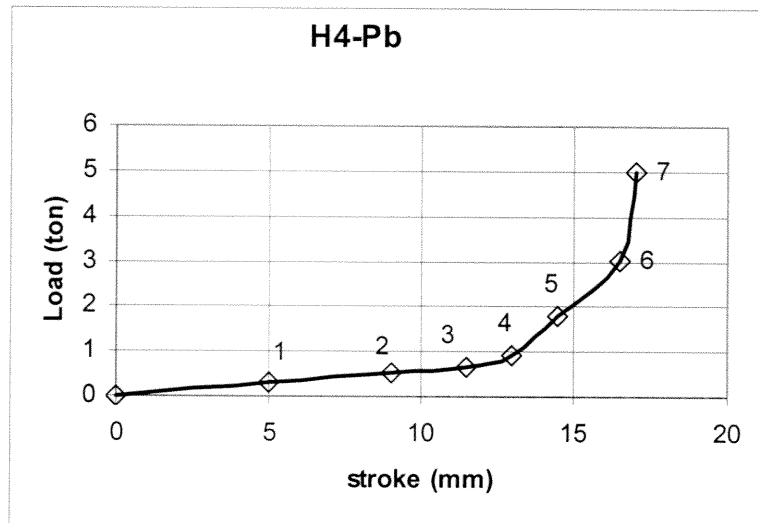
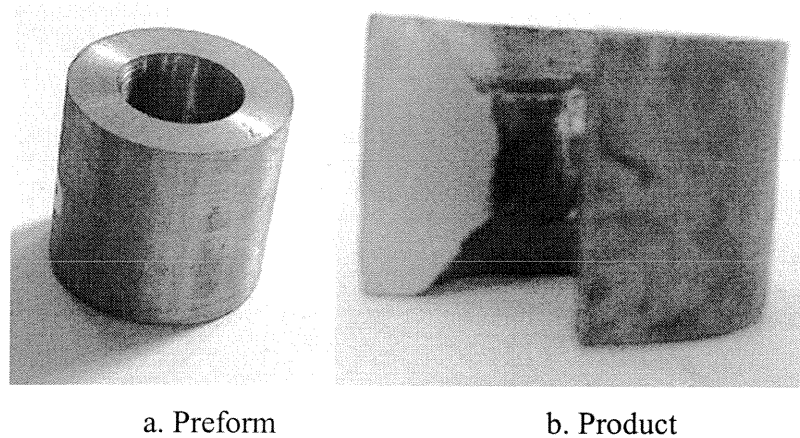


Figure 6.73. Experimental Load-Stroke characteristics of H4-Pb Forging



a. Preform

b. Product

Figure 6.74. Photo of H4-Pb Forging

The Fig.6.75 illustrates the H-shape forging load-stroke curve of lead specimens. According to the curve uniquely extruding mode seems advantageous but the preform has a folding problem. So the free flow, inner and outer flow as well extrusion, is the best solution. The required forging load is decreased by step-wise forging operation as well as using vibrating die.

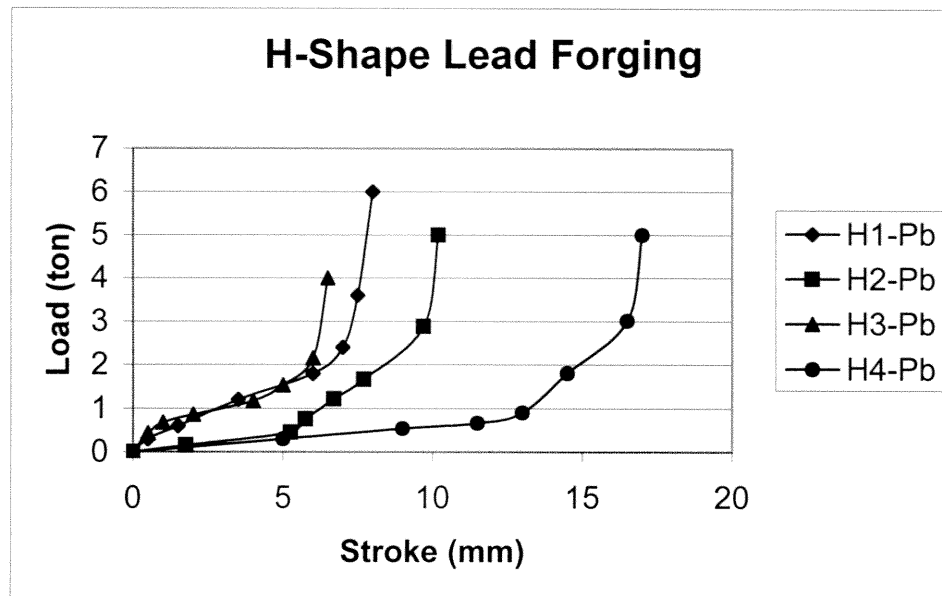


Figure 6.75. Experimental Load Stroke Curve of H-Shape Lead

### 6.2.7. Reducing Forging Load and Energy

As stated experiments of U-Shape, T-Shape and H-Shape of aluminum and lead, the rise of load is caused especially by frictional load and non-homogenous flow. Namely, the forging load has the components of ideal deformation load, frictional load and non-homogenous flow. So, if the frictional load or redundant load due to non-homogenous flow is overcome, the ideal deformation load can be obtained, at the same time the working load is to be decreased. In our study, to reduce the frictional load and/or overcome non-homogenous flow, additional experiments are carried out by vibrating the die.

Also forging is done in two steps as a roughing and finishing operations using the same die to change the lubrication condition. These experiments are carried out by using the rings which have the dimensions  $\varnothing 30$  outer,  $\varnothing 15$  inner diameters with 10 mm height ( $\varnothing 30 \times \varnothing 15 \times 10$  mm), for simplicity of the process.

Firstly, the stepwise forging experiments is carried out. As seen as in load-stroke curve (Fig.6.76), the maximum load for 2 mm upsetting of cylinder is 37 tons in one step. In the second experiment, the ring is upset in two steps (see Fig. 6.77). In first step the stroke is 1 mm with the finishing load of 23 tons then the ring is ejected and

relubricated before second step is carried out. In second step the ring is upset 1 mm more with finishing load of 27 tons. So it is observed that we gain 10 tons due to the relubrication. The relubrication provides a decrease in the frictional load. As a result, it is investigated that during deformation the lubricant is removed or highly pressurized.

The load-stroke curve in Fig.6.78 shows the upsetting characteristics of the rings in vibrating-die. The die is vibrated by means of a motor which is fixed to the die and adjusted to the rotation of 2400 rpm. The shaft of the motor rotates eccentrically, so this eccentricity gives the die vibration roughly. As seen in Fig.6.78, the ring is upset 2.3 mm with the finishing load of 40 tons. Again, the curve shows that if the ring is upset 2 mm, the finishing load would be 32 tons. So it is concluded 5 tons difference between the direct upsetting of the ring and upsetting of ring in vibrated die. Therefore, vibration reduces sticking of the workpiece to the die surface and reduces highly pressurized liquid film.

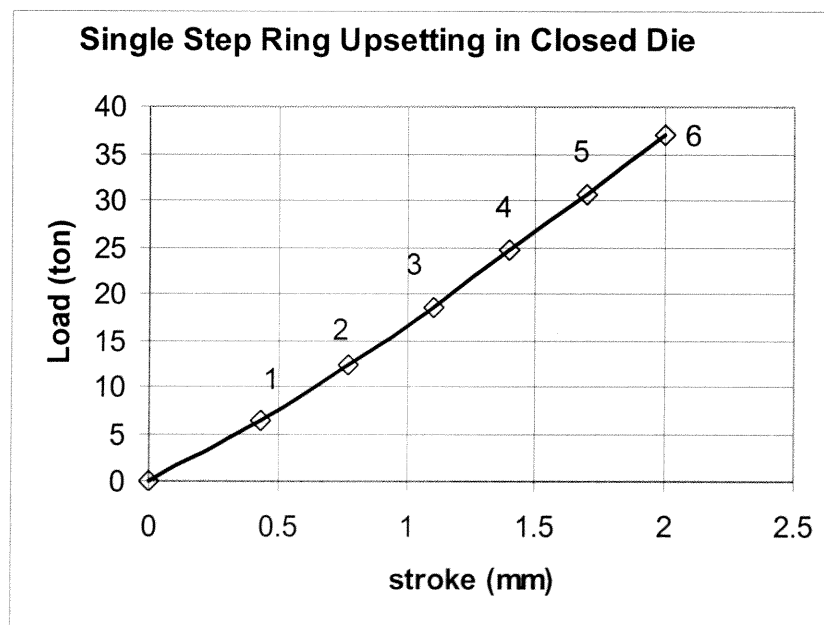


Figure 6.76. Experimental Load-Stroke characteristics of Single Step Ring Upsetting

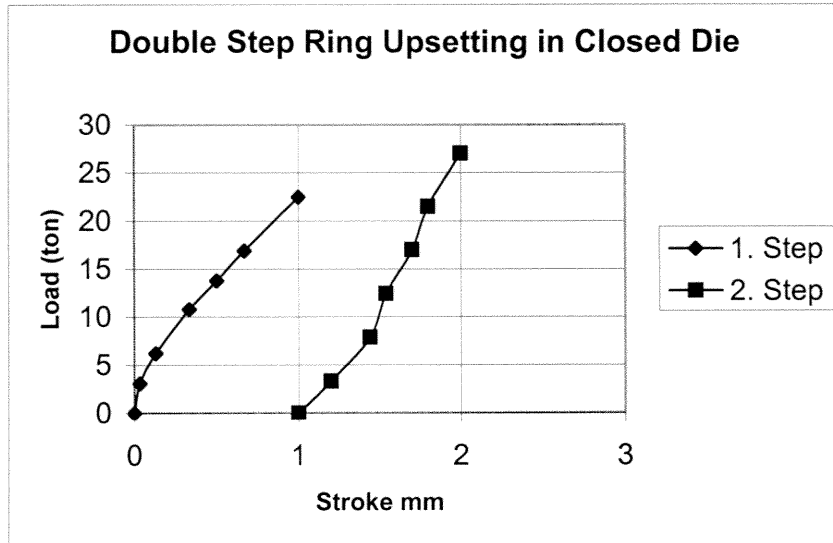


Figure 6.77. Experimental Load-Stroke characteristics of Double Step Ring Upsetting

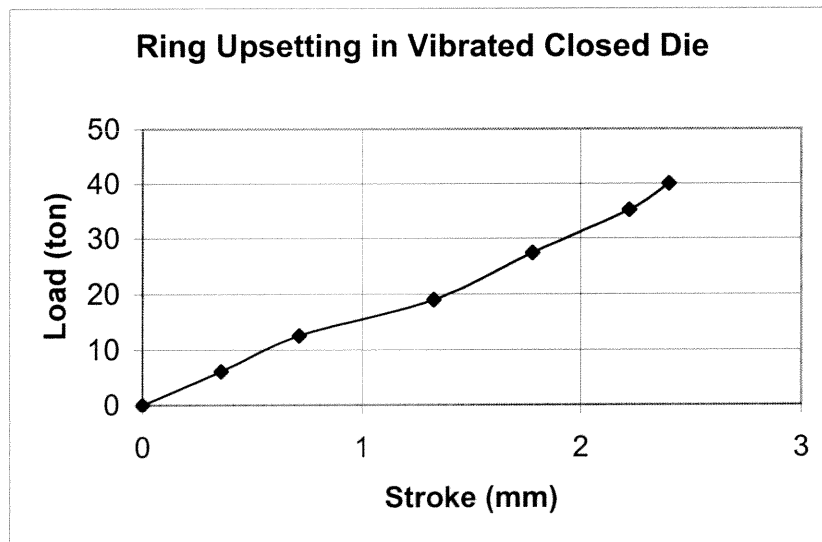


Figure 6.78. Experimental Load-Stroke characteristics of Ring Upsetting in Vibrated Die

## **CHAPTER 7**

### **CONCLUSIONS AND RECOMMENDATIONS FOR FUTURE STUDIES**

#### **7.1. INTRODUCTION**

The results of the experimental studies are concluded in this chapter to assess to what extent the objectives have been met.

#### **7.2. CONCLUSION**

##### **7.2.1. U-Shape Forgings**

1. Experimental results show that the forging load is different, although the forging workpiece is the same for different preforms.
2. The load required for the preform deforming only by upsetting is higher than the extrusion one.
3. Non-contacting preforms causing non-homogenous flow and may fold or buckle, although reducing frictional load.
4. For U-Shape forging, the preform whose outer surface is touching the die wall and flowing inside by upsetting, results very uniform metal flow lines (i.e. high strength) but higher forging loads.

### **7.2.2. T-Shape Forgings**

1. Forging load of each preform is different for the same workpiece.
2. However forging load required for upsetting is smaller than the extrusion one, folding problem arises in upsetting process.
3. Free flowing preforms exhibits non-uniform metal flow lines and resulting in folding and buckling problems.
4. For T-Shape forging, the preform, being extruded, are constrained being upset. So, uniform metal flow lines are obtained, although the forging loads are high.

### **7.2.3. H-Shape Forgings**

1. Different forging loads are obtained for different preforms, although the finishing workpiece is the same.
2. Extrusion of the preforms requires lower forging loads than the upsetting modes preforms.
3. Though the flow in extrusion mode requires lower forging load, upsetting flow results more uniform flow lines.
4. The outer upsetting requires lower forging load than the inner upsetting. But preforms fails while outer upsetting, due to passing shearing strength of metal.
5. So, the preforms of inner upsetting as well as extruding have uniform flow, although the forging loads are high.

### **7.2.4. Vibrating Tool**

1. Tool vibration provides more uniform flow by preventing sticking. So more smooth finishing surface is obtained.
2. Because of the decrease in frictional load and sticking between die surface and the workpiece, the wear is lower than the forging carried without vibrating tool. So longer die life increases.
3. Forging load decreases when using the vibrating-tool.



### **7.2.5. Two-Step Forging**

1. Relubrication in two-step forging process lowers the frictional load between the die surface and the workpiece. So, the forging load is decreased.
2. Two step forging results very uniform flow lines, which increases the strength and surface quality of the finished work.

### **7.3. RECOMMENDATION FOR FUTURE STUDIES**

For the future study, the vibration of the die should be improved to overcome the frictional loads and non-homogenous flow. On the other hand, by benefitting the simple shapes studied here, the forging loads of more complex axisymmetric shapes can be extracted and a modelling would be formed. And self-relubricating of tools will be improved for overcoming the forging loads.

## LIST OF REFERENCES

1. Johnson W. and Sowerby, R. Metal Forming Processes, Analyses and Technolgy, ASME, AMD, vol 28, p1, 1978.
2. Lange K. Handbook of Metal Forming, vol I, II, and III, Springer-Verlag, Berlin 1985.
3. Altan, T, Oh S. I, and Gegel H, Metal Forming: Fundamentals and Applications, ASM International, Metals Park, OH, 1983.
4. Tuncer, M.N. Precison Forging of Hollow Parts, PhD Thesis, The University of Birmingham, 1985.
5. Skipley, R. J, Precision Forging, ASM Metals Handbook-Forming and Forging, v14, ASM International 1988.
6. Metals Hand Book, Forging and Casting, American Society for Metals, 1974, vol.5, pp.1-142
7. Eyercioglu Ö, Developments and Performance Analyses of Precision Forged Spur Gears, PhD Thesis, The University of Birmingham,1995.
8. Akaram Srikanth, Nicholas Zabarar, Shape Optimisation and Preform Desing in Metal Forming Process, Computer Methods in Applied Mechanics and Engineering, 190, 1859-1901, 2000

9. Xinhai Zhao, Guoqun Zhao, Guangchun Wang, Tonghai Wang, Preform Die Shape Design for Uniformity of Deformation in Forging Based on Preform Sensitivity Analysis, *J of Material Processing Technology*, 128, 25-32, 2002.
10. Ibadode, A. O. A . and Dean ,T. A, Corner Filling Characteristics in Precision Forging, *Machine Tools and Manufacture*, vol 28, n2, 103-122, 1988.
11. A. N. Bramley, UBET and TEUBA: Fast Methods of Forging Simulation and Preform Design, *Journal of Materials Processing Technology*, 116, 62-66 2001.
12. S. R. Lee, C. H. Park, D. Y. Yang, A New Method of Preform Design in Hot Forging By Using Electric Field Theory, *International Journal of Mechanical Sciences*, 44 773-792, 2002.
13. D. Y. Yang, D. Y. Ahn, C. H. Lee, C.H Park, T.J. Kim, Integration of CAD/CAM/CAE/RP for the Development of the Metal Forming Process, *Journal of Material Processing Technology*, 125-126, 26-34, 2002.
14. Hyunbo Shim, Optimum Preform Design for the Free Forging of 3-D Shapes By The Sensitivity Analysis, *J of Material Processing Technology*, 134, 99-107, 2003.
15. Guogun Zhao, Guangchun Wang, Ramana V. Grandhi, Die Cavity Design of Near Flashless Forging Process Using FEM-Based Backward Simulation ,*Journal of Materials Processing Technology*, 121, 173-181, 2002
16. Victor Vazquez, Taylan Atlan, Die Design for Flashless Forging of Complex Parts, *Journal of Materials Processing Technology*, 98, 81-89, 2002.

17. H. H. Jo, S. K. Lee ,D. C. Ko, B. M. Kim, A Study on the Optimal Tool Shape Desing in A Hot Forming Process, Journal of Materials Processing Techonology, 111, 127-131, 2001.
18. Parikh, H. And Bhavin, M. Forging Process Analysis and Preform Design, Queen City Forging Company, [www.qforge.com](http://www.qforge.com)
19. Badrinarayanan S, Constantinescu A. and Zabarar N, Preform Design in Metal Forming, Journal of Material Processing Technology, Sibley School of Mechanical and Aerospace Engineering, Cornell University, Ithaca, NY 14853
20. Qingbin L, Shichun W. And Sheng S. Preform Design in Axisymmetric Forging by a New FEM-UBET Method, Journal of Materials Processing Technology, 74, 218-222
21. Yilmaz, N. F. An Expert System for Near Net Shape Axisymmetric Forging Die Design, Ph. D. in Mechanical Engineering, University of Gaziantep, 2002
22. Almohaileb M., Gunasekera J. S, Backward Simulation Using Upper Bound Elemental Techique for Preform Design in Forging Process
23. Li Q, Hu Z, Srikanth A. and Zabarar N, Towards the Development of Robust Computational Design Simulator for Metal Forming Process, [www.mae.cornell.edu/zabarar/](http://www.mae.cornell.edu/zabarar/)
24. Balendra R. and Qin Y, Research Dedicated to the Development of Advanged Metal Forming Technologies, Journal of Material Processing Technologies, 145 (2004) 144-152

25. Rasgado M. T. A. and Davey K, The Effect of Vibration on Surface Finish for Semisolid and Cast Components, Journal of Material Processing Technologies, 125-126 (2002) 543-548
26. Huang Z, Lucas M. and Adams M. J, Modelling Wall Boundary Conditions in an elasto-viscoplastic Material Forming Process, Journal of Material Processing Technologies, 107 (2000) 267-275
27. Hung J. C. and Hung C, The Influence of Ultrasonic Vibration on hot upsetting of Aluminum Alloy, Journal of Material Processing Technologies, Ultrasonic (2005)
28. Materials Forming Handbook, Schuler Press, II. Title, pp. 405-543, 1998
29. Introduction to Manufacturing Processes, John A. Schey, Third Edition, pp. 305-480
30. Introduction to Materials Science For Engineers, James F. Shackelford, 1998, SI Edition
31. Mechanics of Materials, Ferdinand P. Beer, E. Russell Johnston, 1992, II. Edition
32. Metal Deformation Processes / Friction and Lubrication, Schey J. A, Publication: Marcell Dekker Inc., 1970
33. Key to Steel , C. Wegst and M. Wegst, 3-922599-20-6, 2004
34. MatWeb Material Property Data, [www.matweb.com/search/specificmaterial](http://www.matweb.com/search/specificmaterial)

## APPENDIX A

The yield stress of aluminum specimen is about 102.42 Mpa and ultimate elongation is %16. The strength coefficient,  $K$ , is about 216.126 and strength exponent,  $n$ , is 0.448 (see Fig. A.1).

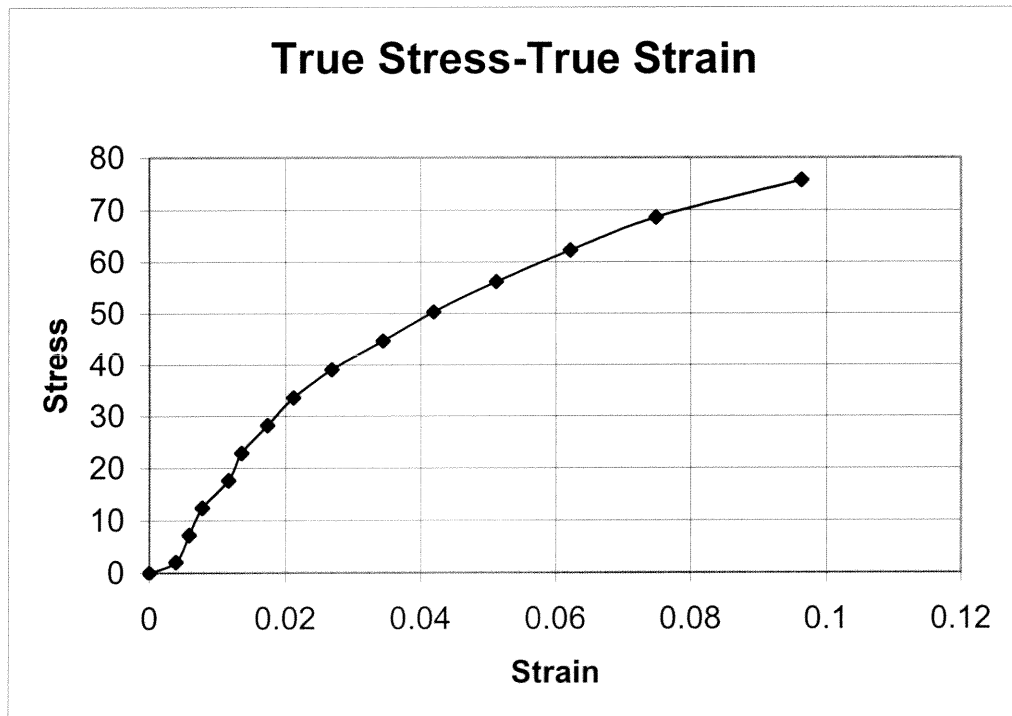


Figure A.1. True Stress-True Strain Diagram of Aliminum Billets

## APPENDIX B

The yield stress of lead specimen is 15 Mpa and ultimate elongation is %80. The strength coefficient,  $K$ , is about 29.1 and strength exponent,  $n$ , is 0.296 (see Fig. B.1).

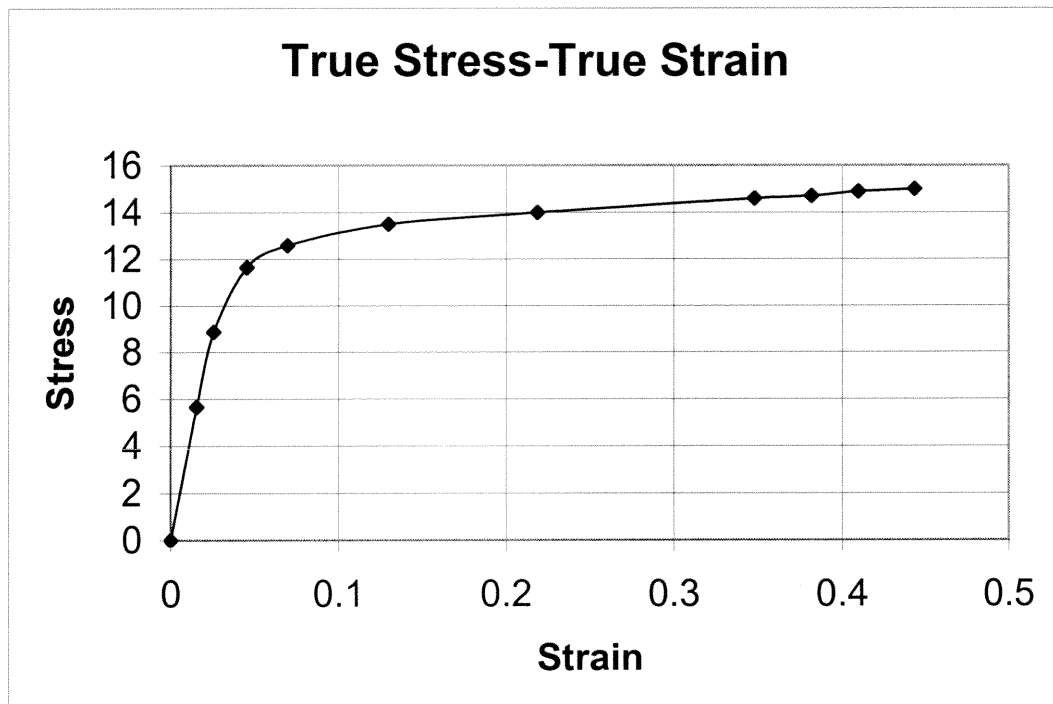


Figure B.1. True Stress-True Strain Diagram of Lead Billets

## APPENDIX C

For measuring the frictional factor between the die surface and aluminum specimen, the aluminum ring, which has the dimensions of  $\varnothing 30 * \varnothing 15 * 10$  is upset between two plates. The surfaces of plates are machined in same conditions with the forging dies. The load-stroke curve is as seen in Fig.C.1. The ring is upset 4 mm with the finishing load of 25 tons. The finished inner diameter is measured at eight different points, and the measured diameters are 14.2 mm, 13.0 mm, 14.0 mm, 14.8 mm, 13.5 mm, 13.5 mm, 13.6 mm, and 13.9 mm respectively. The mean diameter is 13.81 mm. So decrease in diameter is %8.

In Fig.C.1, the upsetting height is 4mm but after measuring finished ring, the measured value is 3.75 mm. So the material spring backs 0.25 mm. Reduction in height is %37.5. Benefitting the curve in Fig. C.2, the value of friction coefficient is 0.125.



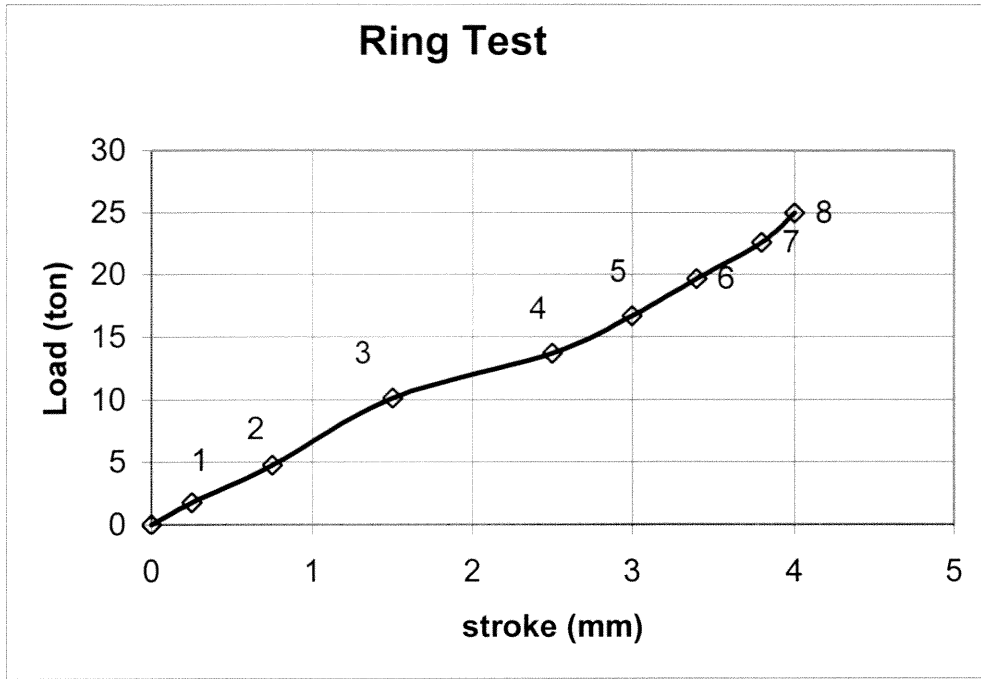


Figure C.1. Load-Stroke Curve of Ring Test

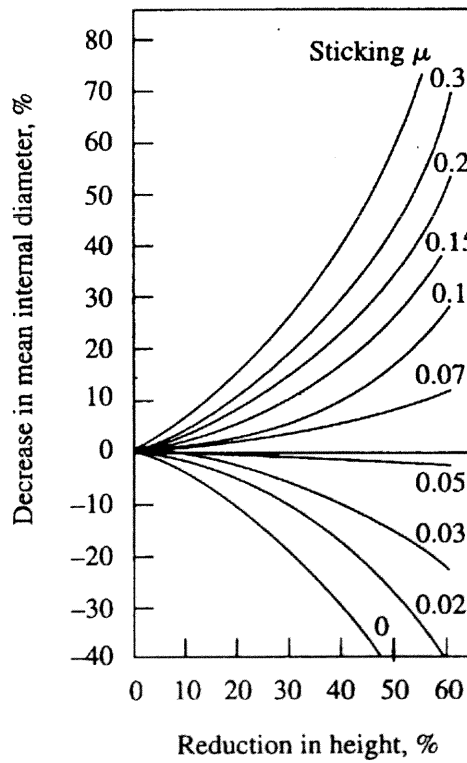


Fig. C.2. Coefficient of Friction in Ring Upsetting [29]

## APPENDIX D

Hardness Brinell	30
Tensile Strength, Ultimate	110 Mpa
Tensile Strength, Yield	103 Mpa
Elongation at Break	%10
Modulus of Elasticity	69 Gpa
Poisson`s Ratio	0.33
Shear Modulus	26 Gpa
Shear Strength	69 MPa

Table D.1. Mechanical Properties of Al 1050 [34]

Hardness Brinell	4.2
Tensile Strength, Ultimate	18 Mpa
Tensile Strength, Yield	-----
Elongation at Break	-----
Modulus of Elasticity	14 Gpa
Poisson`s Ratio	0.42
Shear Modulus	-----
Shear Strength	-----

Table D.2. Mechanical Properties of Pure Lead [34]

# APPENDIX E

Designation and Composition, %	Liquids/Solidus, °C	Usual Temp., °C	Hot Working				Cold Working							
			Flow Stress, † MPa		Workability †	Flow stress, † MPa		Elongation, %	RA, %	Annealing Temp., § °C				
			at °C	C		m	K				n	σ <sub>0.2</sub> , MPa	TS, MPa	
<b>Steels:</b>														
1008 (0.08C), sheet		<1250	1000	100	0.1	A	600	0.25	180	320	40	70	850-900 (F)	
1015 (0.15C), bar		<1250	800	150	0.1	A	620	0.18	300	450	35	70	850-900 (F)	
			1000	120	0.1									
			1200	50	0.17									
1045 (0.45C)		<1150	800	180	0.07	A	950	0.12	410	700	22	45	790-870 (F)	
			1000	120	0.13									
			1000	120	0.1	A			350	620	30	60		
~8620 (0.2C, 1Mn, 0.4Ni, 0.5Cr, 0.4Mo)		900-1080	1000	190	0.13	B	1300	0.3					880 (F)	
D2 tool steel (1.5C, 12Cr, 1Mo)			1000	80	0.26	B								
H13 tool steel (0.4C, 5Cr 1.5Mo, IV)			1000	80	0.26	B								
302 SS (18Cr, 9Ni) (austenitic)	1420/1400	930-1200	1000	170	0.1	B	1300	0.3	250	600	55	65	1010-1120 (Q)	
410 SS (13Cr) (martensitic)	1530/1480	870-1150	1000	140	0.08	C	960	0.1	280	520	30	65	650-800	
<b>Copper-Base Alloys:</b>														
Cu (99.94%)	1083/1065	750-950	600	130	0.06	A	450	0.33	70	220	50	78	375-650	
			(48)	(0.17)										
Cartridge brass (30Zn)	955/915	725-850	900	41	0.2	A	500	0.41	100	310	65	75	425-750	
			600	100	0.24									
			800	48	0.15									
Muntz metal (40Zn)	905/900	625-800	600	38	0.3	A	800	0.5	120	380	45	70	425-600	
			800	20	0.24									
Leaded brass (1Pb, 39Zn)	900/855	625-800	600	58	0.14	A	800	0.33	130	340	50	55	425-600	
			800	14	0.20									
Phosphor bronze (5Sn)	1050/950		700	160	0.35	C	720	0.46	150	340	57		480-675	
Aluminum bronze (5Al)	1060/1050	815-870				A			170	400	65		425-750	

Designation and Composition, %	Hot Working				Cold Working							
	Liquidus/ Solidus, °C	Usual Temp., °C	Flow Stress, <sup>b</sup> MPa		Work- ability <sup>f</sup>	Flow stress <sup>c</sup> MPa		TS, <sup>d</sup> MPa	Elonga- tion, <sup>d</sup> %	RA, <sup>e</sup> %	Annealing Temp., <sup>e</sup> °C	
			at °C	C		m	K					n
<b>Light Metals:</b>												
1050 Al (99%)	657/643	250-550	300	60	0.08	A	140	0.25	35	90	35	340
~3003 Al (1Mn)	649/648	290-540	500	14	0.22	A				40	30	370
~2017 Al (3.5Cu, 0.5Mg, 0.5Mn)	635/510	260-480	400	90	0.12	B	380	0.15	70	180	20	415 (F)
5052 Al(2.5Mg)	650/590	260-510	480	35	0.13	A	210	0.13	90	190	25	340
6061-O(1Mg, 0.6Si, 0.3Cu)	652/582	300-550	400	50	0.16	A	220	0.16	55	125	25	415 (F)
6061-T6	NA <sup>g</sup>	NA	NA	NA	NA	NA	450	0.03	275	310	8	45
~7075 Al(6Zn, 2Mg, 1Cu)	640/475	260-455	450	40	0.13	B	400	0.17	100	230	16	415
<b>Low-Melting Metals:</b>												
Sn (99.8%)	232	100-200				A				15	45	150
Pb (99.7%)	327	20-200	100	10	0.1	A				12	35	20-200
Zn (0.08% Pb)	417	120-275	75	260	0.1	A				130/170	65/50	100
			225	40	0.1							
<b>High-Temperature Alloys:</b>												
Ni (99.4Ni + Co)	1446/1435	650-1250				A				140	440	65
Hastelloy X (47Ni, 9Mo, 22Cr, 18Fe, 1.5Co, 0.6W)	1290	980-1200	1150~	140	0.2	C				360	770	42
Ti (99%)	1660	750-1000	600	200	0.11	C				480	620	20
Ti-6Al-4V	1660/1600	790-1000	900	38	0.25	A				900	950	12
Zirconium	1852	600-1000	900	50	0.25	A				210	340	35
Uranium (99.8%)	1132	~700	700	110	0.1	A				190	380	4

Table E.2. Manufacturing Properties of Various Non-Ferrous Alloys (ASME Ser. B, 95:1009 (1973)) [29]

## APPENDIX F

Workpiece Material	Working	Forging		Extrusion <sup>†</sup>		Wire Drawing		Rolling		Sheet Metalworking	
		Lubricant	$\mu$	Lubricant	$\mu$	Lubricant	$\mu$	Lubricant	$\mu$	Lubricant	$\mu$
Sn, Pb, Zn alloys	Hot	FO-MO	0.05	FO or soap	FO	FA-MO or MO-EM	0.05	FA-MO or MO-EM	0.05	FO-MO	0.05
	Hot or warm	GR and/or MoS <sub>2</sub>	0.1-0.2	None		MO-FA-EM	0.2	GR in MO or dry soap	0.1-0.2		
Al alloys	Hot	GR or MoS <sub>2</sub>	0.1-0.2	None		MO-FA-EM	0.2				
	Cold	FA-MO or dry soap	0.1	Lanolin or soap on PH	FA-MO-EM, FA-MO	1-5% FA in MO(1-3)	0.1	FO, lanolin, or FA-MO-EM	0.05-0.1		
Cu alloys	Hot	GR	0.1-0.2	None (or GR)	FO-soap-EM, MO	MO-EM	0.2				
	Cold	Dry soap, wax, or tallow	0.1	Dry soap or wax or tallow		MO-EM	0.1	FO-soap-EM or FO-soap	0.05-0.1		
Steels	Hot	GR	0.1-0.2	GL (100-300), GR		None or GR-EM	ST <sup>‡</sup>	GR	0.2		
	Cold	EP-MO or soap on PH	0.1	Soap on PH	Dry soap or soap on PH	10% FO-EM	0.05	EP-MO, EM, soap, or polymer	0.05-0.1		
Stainless steel, Ni and alloys	Hot	GR	0.1-0.2	GL (100-300)		None	ST <sup>‡</sup>	GR	0.2		
	Cold	CL-MO or soap on PH	0.1	CL-MO or soap on PH	Soap on PH or CL-MO	FO-CL-EM or CL-MO	0.1	CL-MO, soap, or polymer	0.1		
Ti alloys	Hot	GL or GR	0.2	GL (100-300)			0.05	GR, GL,	0.2		
	Cold	Soap or MO	0.1	Soap on PH	Polymer	MO	0.1	Soap, or	0.1		

Table F.1. Typical Lubricants and Friction in Plastic Deformation (ASM (1983)) [29]

## APPENDIX G

Forging Shape	$Q_c$	$Q_{fe}$
Simple, no flash	3-5	2.0-2.5
Simple, with flash	5-8	3
Complex (tall ribs, thin webs), with flash	8-12	1-4

Table G.1. Multiplying Factors for estimating Forces  $Q_c$  and energy requirements  $Q_{fe}$  in Impression Die Forging [29]